

**JIMMA UNIVERSITY**

**SCHOOL OF GRADUATE STUDIES**

**JIMMA INSTITUTE OF TECHNOLOGY**

**FACULTY OF CIVIL AND ENVIRONMENTAL ENGINEERING**

**STRUCTURAL ENGINEERING STREAM**

**Investigation on Effect of Different Steel Section on the Performance of Encased Composite Column**

A Thesis Submitted to the School of Graduate Studies of Jimma University in Partial Fulfillment of the Requirements for the Degree of Master of Science in Civil Engineering (Structural Engineering)

By: Mulgeta Mersha

January, 2020

Jimma, Ethiopia

**JIMMA UNIVERSITY**  
**SCHOOL OF GRADUATE STUDIES**  
**JIMMA INSTITUTE OF TECHNOLOGY**  
**FACULTY OF CIVIL AND ENVIRONMENTAL ENGINEERING**  
**STRUCTURAL ENGINEERING STREAM**

**Investigation on Effect of Different Steel Section on the Performance of Encased  
Composite Column**

A Thesis Submitted to the School of Graduate Studies of Jimma University in Partial  
Fulfillment of the Requirements for the Degree of Master of Science in Civil Engineering  
(Structural Engineering)

By: Mulgeta Mersha

Advisor: Eng. Elmer C. Agon (Asso.Prof)

Co-Advisor: Eng. Kefyalew Zerfu (MSc)

January, 2020  
Jimma, Ethiopia




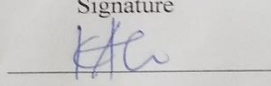
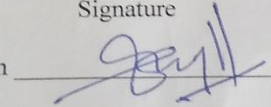
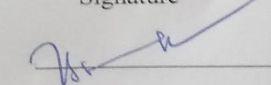
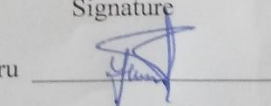
CAMON 11  
16M AI Clear Selfie

JIMMA UNIVERSITY  
SCHOOL OF GRADUATE STUDIES  
JIMMA INSTITUTE OF TECHNOLOGY  
FACULTY OF CIVIL AND ENVIRONMENTAL ENGINEERING  
STRUCTURAL ENGINEERING CHAIR

INVESTIGATION ON THE EFFECTS OF DIFFERENT STEEL SECTIONS ON THE  
PERFORMANCE OF ENCASED COMPOSITE COLUMN

MULUGETA MERSHA

APPROVED BY BOARD OF EXAMINERS

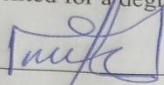
1. Engr. Elmer C. Agon		03 / 02 / 2020
Main advisor	Signature	Date
2. Engr. Kefiyalew Zerfu		03 / 02 / 2020
Co-advisor	Signature	Date
3. Dr. S. Moses Aranganathan		03 / 02 / 2020
External Examiner	Signature	Date
4. Engr. V. S. Ravi Kumar		03 / 02 / 2020
Internal Examiner	Signature	Date
5. Engr. Yehamleshet Menberu		03 / 02 / 2020
Chairperson	Signature	Date

An Investigation on the Effect of Different Steel Section on the Axial and Cyclic Load Resistance Performance of Encased Rectangular Composite Column | 2019

DECLARATION

This thesis entitled "An Investigation on the Effect of Different Steel Section on the Axial and Cyclic Load Resistance Performance of Encased Rectangular Composite Column" is my original work and has not been presented for a degree in any other university.

Mulgeta Mersha


  
Signature

03/02/2020  
Date

Name

Date

Eng. Elmer C. Agon (Asso.Prof)

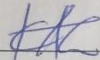
  
Signature

03/02/2020  
Date

Advisor

Date

Eng. Kefiyalew Zerfu (M.Eng.)

  
Signature

03/02/2020  
Date

Co-Advisor

Signature

Date

MSc Thesis By Mulgetaa Mersha

i



CAMON 11  
16M AI Clear Selfie

### DECLARATION

This thesis entitled “An Investigation on the Effect of Different Steel Section on the Axial and Cyclic Load Resistance Performance of Encased Rectangular Composite Column” is my original work and has not been presented for a degree in any other university.

Mulgeta Mersha \_\_\_\_\_

Name

Signature

Date

Eng. Elmer C. Agon (Asso.Prof ) \_\_\_\_\_

Advisor

Signature

Date

Eng. Kefiyalew Zerfu (M.Eng.) \_\_\_\_\_

Co-Advisor

Signature

Date

### **ABSTRACT**

*Composite columns are constructed by providing structural steel inside concrete or concrete inside the structural steel. These columns are being used worldwide for the construction of high rise buildings since it can reduce the size of the columns in the building and increase the usable space of the floor plan. In addition, composite column enhances the overall rigidity of the building and provides significant shear resistance to strong earthquakes and other lateral loads.*

*This study presents the behavior and performance of fully encased composite column subjected to axial load and horizontal cyclic load. In order to achieve the goal of the study, a parametric investigation procedure is undertaken, on a series of eighteen (18) sample column with different study parameters. A parametric study was conducted using the numerical model to investigate the influences of geometric properties of fully encased composite (FEC) columns. The geometric variables were shape of structural steel, column slenderness ratio ( $L/D$ ) / the ratio of length of column ( $L$ ), to the depth of the column cross-section, ( $D$ ) and ties spacing ratio ( $s/D$ )/the ratio of transverse tie spacing, ( $s$ ), to the depth of the column cross-section, ( $D$ ). The column specimens were modeled as fixed cantilever columns with concentric axial load level of 50% of their axial load capacity as well as cyclic loading similar to that suggested by Applied Technology Council guidelines (ATC 1992 ATC 24). The material quality used for all composite column are the same grade. The nonlinear combined hardening and the concrete damage plasticity (CDP) model were used to define properties of steel and concrete respectively. In the Finite Element Analysis (FEA) C3D8R was used for solid elements and T3D2 was used for reinforcement. Nonlinear 3-D finite element output was then examined to know the response of column. The finite element analysis results demonstrate that the profile of encased section affect the performance of fully encased composite columns. Encased Tube Section (ETS) columns had good performance than Encased Circular Section (ECS) and Encased H- Section (EHS) due to its high stiffness. Increasing slenderness ratio of column from 7.5 to 11.25 and 15 reduce the lateral resisting capacity by 6.74% and 15.83% respectively. Spacing of tie also have a significant effects on axial and lateral resistance capacity of composite column. The effect is more observed on the buckling effects: as the spacing of lateral tie increases longitudinal reinforcement fail in buckling failure followed by crushing of concrete material before they reach their yielding stress.*

**Key words:** Axial Load Capacity, Cyclic Load Capacity, Failure Mode, Composite Column, slenderness ratio, tie spacing.

## ACKNOWLEDGEMENT

First and at most, greatest thanks from the depth of my heart is to Almighty GOD for endowing me with the courage, strength as well as health throughout my school time and the full help provided by him for the successful accomplishment of my MSc class and preparation of this MSc thesis.

My deepest gratitude goes to my advisor **Mr. Elmer C Agon (Associate Professor)** and my co-advisor **Eng. Kefiylew Zerfu (M.Eng)** for all their limitless efforts in guiding me through my work and appreciation of my efforts and for providing me useful reference material needed to achieve my goal. I also would like to extend my thanks and appreciation to Jimma University, School of Graduate Studies, Jimma Institute of Technology, Civil and Environmental Engineering Department, Structural Engineering chair holder and all academic staffs of civil engineering department, librarians and administrative workers of the Institute.

Next, I would like to say thanks a lot to all my friends who shared their unselfish help and kind support in preparing this thesis. Finally, my special thanks go to my parents who are always been there in times of difficulties and giving me moral support.

## TABLE OF CONTENTS

DECLARATION .....	iv
ABSTRACT.....	v
ACKNOWLEDGEMENT .....	vi
TABLE OF CONTENTS.....	vii
LIST OF TABLES .....	x
LIST OF FIGURES .....	xi
ACRONYMS AND ABBREVIATIONS .....	xiv
CHAPTER ONE .....	91
INTRODUCTION .....	91
1.1 Background of the Study .....	91
1.2 Statement of the Problem.....	92
1.3 Objective of the Study .....	93
1.3.1 General objective .....	93
1.3.2 Specific Objectives .....	93
1.4 Research Questions.....	93
1.5 Significance of the Study .....	94
1.6 Scope of the study.....	94
CHAPTER TWO .....	95
RELATED LITERATURE REVIEW .....	95
2.1 General.....	95
2.2 Theoretical review of composite column.....	95
2.2.1 Concrete-Filled Composite Column .....	97
2.2.2 Concrete Encased Composite Column.....	97
2.3 Research on Steel-Encased Concrete Columns.....	100
2.3.1 Experimental investigations.....	100
2.3.2 Numerical and analytical investigations .....	102
2.4 Review of Effect of Confinement and stirrup.....	105
2.5 Review of Design code .....	106
2.6 Review of cyclic testing.....	107



2.6.1 Quasi-static cyclic loading protocols .....	109
CHAPTER THREE .....	114
RESEARCH METHODOLOGY .....	114
3.1 General .....	114
3.2 Research Methodology .....	114
3.3 Study Variables .....	114
3.3.1 Dependent Variables .....	114
3.3.2 Independent Variables .....	115
3.4 Population and Data Collection Process .....	115
3.4.1 Model samples and cross sections used in this study .....	116
3.5 Finite element method .....	118
3.6 Data Processing and Analysis .....	119
3.7 An overview of ABAQUS© .....	120
3.7.1 Linear analysis .....	120
3.7.2 None linear analysis .....	120
3.8 Finite Element Modelling of encased composite column .....	121
3.8.1 Element type and selection .....	123
3.8.2 Meshing .....	124
3.8.3 Interactions and Kinematic Constraints between Components .....	125
3.8.4 Boundary Conditions and Loading .....	127
3.9 Material Modeling .....	128
3.9.1 Compression properties of concrete .....	128
3.9.2 Tension properties of concrete .....	131
3.9.3 Damage plasticity modeling of concrete .....	132
3.9.4 Structural Steel and Reinforcement material modeling .....	135
3.10 PARAMATRIC STUDY .....	138
CHAPTER FOUR .....	140
RESULTS AND DISCUSSION .....	140
4.1 General .....	140
4.2 Effect of overall column slenderness ratio .....	140
4.2.1 Axial Load versus axial deformation response .....	141
4.2.2 Modes of failure .....	143
4.2.3 Lateral Load versus lateral displacement response (Hysteretic behavior) .....	147

4.3 Effect of transverse reinforcement spacing.....	150
4.3.1 Axial Load versus axial deformation response .....	151
4.3.2 Modes of failure .....	153
4.4 MODEL VERIFICATION .....	157
4.4.1 Verification of FEM of the Encased Composite Columns.....	157
CHAPTER FIVE .....	161
CONCLUSIONS AND RECOMMENDATIONS .....	161
5.1 CONCLUSIONS.....	161
5.2 RECOMMENDATIONS .....	161
REFERENCES .....	163
APIINDEX .....	168
A . MATERIAL INPUT DATA SHEET FOR ANALYSIS .....	168
B. SEISMIC LOADING PROTOCL USED FOR THIS STUDY .....	172
C. MODEL OF COLUMN UNDER STUDY .....	174
D. OUT PUT OF ANALYSIS .....	178
E.ANALIYSIS OUT PUT FROM ABAQUS PROGRAM.....	182

**LIST OF TABLES**

Table 2.1 Sequence of loading of ATC-24 cyclic loading protocol	20
Table 2.2 Sequence of loading of ISO cyclic loading protocol (Filiatrault et al., 2018)	111
Table 2.3 Sequence of loading of SAC standard protocol	113
Table 3.1 Geometric properties of t specimens under the study	118
Table 3.2: Various Elements Used in ABAQUS© (ABAQUS, 2014)	124
Table 3.3 Default parameters of CDP model under compound stress	135
Table 3.4: Mechanical Properties of the Steel, Reinforcement and concrete used for this study	137
Table 3.5 Columns for investigating the effect of slenderness ratio (L/D)	138
Table 3.6 Columns for investigating the effect of transverse reinforcement spacing, (s/D)	139
Table 4.1 Effect of slenderness ratio (L/D) on peak axial load and axial deformation	141
Table 4.2 Effect of slenderness ratio (L/D) on peak lateral load and lateral deformation	148
Table 4.3 Effect of transverse reinforcement spacing on peak axial load and axial deformation	152
Table 4.4 Effect of transverse reinforcement spacing on lateral load and lateral deformation	157
Table 4.5: Specimen dimension and materials properties (Campian et al., 2011)	158
Table 4.6 Values for axial force N and lateral force H	159
Table.A.1 compressive behavior	168
Table A.2 Tensile behavior	80
Table.A.3 Abaqus compression input	171
Table.A.4 Abaqus Tension input	171
Table A, 4 Input values for plastic behaviour of longitudinal reinforcement	172
Table B.1 step time versus amplitude	172

### LIST OF FIGURES

Figure 2.1: Typical Cross-Section of Composite Columns with Fully or Partially Concrete-Encased H-Section (Source: ETHIOPIAN STANDARDS, ES EN 1994-1-1:2015)	96
Figure 2.2: Typical Cross-Section of Composite Columns with Concrete-Filled Hollow Section (Source: ETHIOPIAN STANDARDS, ES EN 1994-1-1:2015)	96
Figure 2.3 construction sequence of concrete filled encased column (source: Han and An 2014)	98
Figure 2.4 Encased composite column with different steel profile. (Source: Han et al.,2007).	99
Figure 2.5 Encased composite column with I-profile. (Source: Chen and Lin, 2006)	99
Figure 2.6 a) Spatial frame and Plane frame sub-assembly of the structure b) Testing setup outline for Horizontal T and inverted T specimens (Castiglioni and Drei, 2016).	108
Figure 2.7 loading protocol of ATC-24 (ATC-24, 1992)	20
Figure 2.8 ISO cyclic loading protocol (Filiatrault et al., 2018).	111
Fig. 2.9 SAC (Clark et al., 1997) loading protocol	112
Figure 3.1 Cross-section taken for the analysis (a ,b ,c)	117
Figure 3.2 3D-view taken for the analysis	117
Figure 3.3 Modeling of circular tube incased composite Components in Abaqus©CAE	121
Figure 3.4 Modeling of H profile incased composite Components in Abaqus©CAE	122
Figure 3.5 Modeling of square tube incased composite Components in Abaqus©CAE	122
Figure3.6 Finite element mesh for FEC columns	125
Figure 3.7 Kinematic Constraints between Components	127
Figure 3.8 End boundary conditions in FE model for concentric load	127

Figure 3.9 Stress-strain relation for non-linear structural analysis (EBCS EN1992, 2015).	40
Figure 3.10 Stress-strain relationship for Confined Concrete (EBCS EN1992, 2015).	131
Figure 3.11 Post failure stress-fracture energy curve. (Abaqus user Manual, 2014)	132
Figure 3.12 Terms for Tension Stiffening Model (Abaqus user Manual, 2014)	134
Figure 3.13 Response of concrete to a uniaxial loading condition in compression (Abaqus Manual, 2014)	135
Figure 3.14 Abaqus input Stress – strain curves for steel (Kwaśniewski et al., 2011)	137
Figure 4.1 Effect of L/D ratios on axial load versus axial deformation curve (Group 1)	142
Figure 4.2 Effect of L/D ratios on axial load versus axial deformation curve (Group 2)	142
Figure 4.3 Effect of L/D ratios on axial load versus axial deformation curve (Group 3)	143
Figure 4.4 Deformed shape and stress contour of concrete at failure (Group 1)	144
Figure 4.5 Deformed shape and stress contour of concrete at failure (Group 2)	144
Figure 4.6 Deformed shape and stress contour of concrete at failure (Group 3)	145
Figure 4.7 Deformed shape and stress contour in structural steel at failure (Group 1)	146
Figure 4.8 Deformed shape and stress contour in structural steel at failure (Group 2)	146
Figure 4.9 Deformed shape and stress contour in structural steel at failure (Group 3)	146
Figure 4.10 Deformed shape and stress contour in reinforcement bar at failure	147
Figure 4.11: Effect of L/D ratios on Lateral Load -Displacement Response of (Group 1)	148
Figure 4.12: Effect of L/D ratios on Lateral Load - Displacement Response of (Group 2)	149
Figure 4.13: Effect of L/D ratios on Lateral Load -Displacement Response of (Group 3)	149
Figure 4.14: Effect of L/D ratios on Lateral Load-Displacement Response of (Group1, 2and 3)	60
Figure 4.15 Effect of s/D ratios on axial load versus axial deformation curve (Group 4)	151
Figure 4.16 Effect of s/D ratios on axial load versus axial deformation curve (Group 5)	151

Figure 4.17 Effect of s/D ratios on axial load versus axial deformation curve (Group 6)	152
Figure 4.18 Stress contour in rebars at failure for (Group4, 5 and 6)	153
Figure 4.19 Stress contour in outer concrete at failure for (Group4)	153
Figure 4.20 Stress contour in structural steel at failure for (Group4)	154
Figure 4.21 Stress contour in outer concrete at failure for (Group5)	154
Figure 4.22 Stress contour in structural steel at failure for (Group5)	154
Figure 4.23 Stress contour in outer concrete at failure for (Group6)	155
Figure 4.24 Stress contour in structural steel at failure for (Group6)	155
Figure 4.25: Effect of L/D ratios on Lateral Load - Displacement Response (Group4)	156
Figure 4.26: Effect of L/D ratios on Lateral Load - Displacement Response (Group5)	156
Figure 4.27 Effect of L/D ratios on Lateral Load - Displacement Response (Group6)	157
Figure 4.28 cross section of experimental sample (Campian et al., 2011)	158
Figure 4.29. Mechanical model and test up procedure for experimentally tested columns (Campian et al., 2011)	158
Figure 4.30: Failure mode of column under experiment (Campian et al., 2011)	159
Figure 4.31: Failure mode and Stress Contour at Failure for finite element	159
Figure 4.32 Hysteresis loops of the specimen subjected to cyclic loading and axial loading.	70
Figure A.1 unconfined concrete input stress-strain curve	168
Figure A.2 Stress-crack opening relation for uniaxial tension	171
Figure B.2 loading protocol adopted under study	174

### ACRONYMS AND ABBREVIATIONS

ASCE	America Society of Civil Engineering
ATC	Applied Technology Council
CDP	Concrete Damage Plasticity
CFST	Concrete Filled Steel Tube
CFT	Concrete Filled Tubes
C3D8R	8-node linear brick, reduced integration, hourglass
ECCS	European cod Convection for Construction of Steel Work
EI	Flexural Rigidity
ECS	Encased Circular Section
EHS	Encased H-Section
ETB	Ethiopian Birr
ETS	Encased Tube Section
FEC	Fully Encased Composite Column
FEM	Finite Element Method
ISO	International Organization for Standardization
JIT	Jimma Institute of Technology
PEC	Partially Encased Composite Column
RC	Reinforced Concrete
RHS	Rectangular Hollow Sections
SAC	Structural Engineers Association of California

SDOF	Single Degree of Freedom
SPRC	Steel Profile-Reinforced Concrete Sections
SRC	Structural Steel Reinforce Concrete
SRCFST	Steel Reinforced Concrete Filled Steel Tube
T3D2	3- dimensional 2-node truss elements
$E_c$	Modulus of Elasticity of concrete (MPa)
$E_{cm}$	Secant modulus of elasticity of concrete (MPa)
$f_{ck}$	Concrete Compressive Strength (MPa )
$f_y$	Steel Yield Strength (MPa)
$\Delta_{yield}$	Yield Deformation
$\Delta_{max}$	Displacement at Ultimate Load
$\varepsilon_{c1}$	Compressive strain of concrete at peak point
$f_{cm}$	Mean value of concrete cylindrical comparative strength (Mpa)
$\psi$	Dilation angle



## CHAPTER ONE

### INTRODUCTION

#### 1.1 Background of the Study

Composite column is a structural member that uses a combination of structural steel shapes, pipes or tubes with or without reinforcing steel bars and concrete to provide adequate load carrying capacity to sustain externally applied loads. In a composite column both the steel and the concrete sections resist the external loading by interacting together by bond and friction. The aim is to achieve a higher level of performance than would have been the case had the two materials functioned separately. The interactive and integral behavior of concrete and the structural steel elements makes the composite column a very cost effective and structural efficient member among the wide range of structural elements in building and bridge constructions.

Composite columns are constructed by providing structural steel inside concrete or concrete inside the structural steel. These columns are being used worldwide for the construction of high rise buildings since it can reduce the size of the columns in the building and increase the usable space of the floor plan (Chang et al., 2012). In addition, composite column enhances the overall rigidity of the building and provides significant shear resistance to strong earthquakes and other lateral loads. Composite columns can be classified as either hollow sections filled with concrete or different steel sections encased in concrete. The latter one is considered in this investigation.

Concrete encased columns are composite columns in a structural member that uses a combination of different structural steel section as encasement, channels, I-beams, pipes or tubes with reinforcing steel bars are presently in used all over the world. Concrete-encased concrete filled steel tube (CFST) is one type of encased steel concrete composite section, which consists of inner concrete filled steel tube (CFST) and outer reinforced concrete (RC). This type of composite column named when steel pipes or rectangular hollow sections (RHS) are used as encasement steel section. This type of composite members has an increasing trend in being used in high-rise building and bridge structures in China (Han et al., 2014).

Under large-magnitude seismic events, concrete shells crack and lower the flexural stiffness of composite columns. Nevertheless, the steel core acts as a back-up system in providing the shear strength and the required ductility to prevent brittle failure modes (Han and An, 2014).

Finite element (FE) model developed in the context of ABAQUS© software is intend to simulate encased composite columns with different steel profile; circular, square and Encased H-section cross-section under axial compression and cyclic loading.

To fully understand the behaviors of CFST columns, much research were carried out from other aspects, such as seismic performance (Dan et al., 2018) and fire behavior (Han and Zhou, 2019) for developments of experimental procedures and finite element methods.

Compared with structural testing, Finite Element Methods are available to carry out huge experiments without any worry about time and money. Many researchers (Zhou and Han, 2018) and (Park et al., 2015) all over the world have done much to the development of the numerical models to simulate performance of CFST columns by ABAQUS©/Standard solver

The purpose of this study was to implement and verify the behavior of encased composite rectangular column with different steel profile under an action of axial load and cyclic loading by using Finite Element method.

The simulation result was used to choose steel profile which have good performance and tie spacing which undergo good performance for the stated loading condition and additionally used as reference for simulation and practice work in the future.

## **1.2 Statement of the Problem**

Several studies have been conducted to investigate the strength of composite column under axial compression, axial compression and bending ,axial tension, pure bending, as well as combined compression and bending, which contribute to tell the performance of those columns separately (Han and An, 2014), (Liu, 2013), (Roeder et al., 2014). Extensive studies have been conducted to analyze the behavior of concrete filled steel tub under cyclic (Lin et al., 2009). Limited studies were found on the performance of FEC columns with various structural steel profile, slenderness ratios, and spacing of transverse reinforcement subjected to axial and cyclic loading conditions. This study aims to perform extensive numerical investigations on FEC columns under concentric axial and cyclic loading.

Therefore, it is necessary to establish a systematic research by finite element program to examine the structural performance/response of encased composite columns with different steel profile subjected to cyclic and axial loading. By considering this loading condition performance of the column was examined and generate information on the effects of controlling parameters through parametric study using a validated numerical model which can adequately predict the performance/response of encased composite columns.

### **1.3 Objective of the Study**

#### **1.3.1 General objective**

It is the purpose of this study to investigate the effect of different steel section profile on the performance of encased rectangular composite column under axial and cyclic loading by comparing the effects of different parameter on the cyclic performance of square tube encased, circular tube encased, and H-section encased columns.

#### **1.3.2 Specific Objectives**

The specific objectives of study will be to:

- ✓ Evaluate the effects of slenderness ratio on performance of encased composite column.
- ✓ Investigate the effect of spacing of tie on the performance of composite column.
- ✓ Determine axial and cyclic load resistance capacity of rectangular composite column for different encased steel profile under specified loading.
- ✓ Identify steel profile which have good performance under axial and cyclic load.

### **1.4 Research Questions**

The research questions that this study will go to explain; are as follows:

1. Does slenderness ratio affect the performance of composite column?
2. Does tie spacing affect the performance of fully encased composite column?
3. Does steel profile affect lateral load carrying capacity of the rectangular composite column?

4. Which steel profile will give good performance under cyclic load resistance for this encased rectangular composite column?

### **1.5 Significance of the Study**

Composite column is among the composite structure widely used now a day. These essentially different materials are completely compatible and complementary to each other; they have an ideal combination of strengths with the concrete efficient in compression and the steel in tension. For encased composite column concrete gives corrosion protection and thermal insulation to the steel at elevated temperatures and additionally can restrain slender steel sections from local or lateral-torsional buckling. Currently different steel profile section are used as encasement in the design of composite column to get column which have good performance under desired loading condition. This investigation can help the structural designer's community to choose easily the appropriate steel profile for good performance. It can contribute significant input for another researchers for further study. Therefore, this research will help any design companies and /or any researchers to have better understand and estimate of the behavior of encased rectangular composite column with different steel profile under axial load and cyclic loading.

### **1.6 Scope of the study**

The study covers the investigation of fully encased rectangular composite columns and extended to demonstrate the influence of shape of steel profile, slenderness ratio and tie spacing on the column performance. The study focuses on modeling different encased steel section in the non-linear finite element program ABAQUS©. Therefore, based on this modeling, the analysis was to show the lateral capacity of encased composite column and deflection in the direction of applied loads on encased composite column for different steel profile. This study is important for providing detailed analytical investigations into structural behavior of encased composite column. ABAQUS© (ABAQUS, 2014) was utilized to model the three prototype of square tube encased, circular tube encased, and H section encased columns subjected to a cyclic loading similar to that suggested by Applied Technology Council (ATC) guidelines (ATC 1992- ATC 24). Each prototype was modeled under concentric axial load level of 50% of their axial load capacity.

## CHAPTER TWO

### RELATED LITERATURE REVIEW

#### 2.1 General

This chapter provides a review of literature of the comparative study on the behavior of encased composite column. The main purpose of a literature review is to establish the academic and research areas that are relevant to the subject under study.

#### 2.2 Theoretical review of composite column

The general term 'composite column' refers to any compression member in which the steel element acts compositely with the concrete. Composite columns are constructed using various combinations of structural steel and concrete in an attempt to utilize the beneficial properties of each material. The interactive and integral behavior of concrete and the structural steel elements makes the composite column a very stiff, more ductile, cost effective and consequently a structurally efficient member in building and bridge constructions so that both elements contribute to the strength. Composite columns have recently undergone increased usage throughout the world, which has been influenced by the development of high strength concrete permitting these columns to be considerably economized. There are two basic types of composite columns mostly used in buildings: those with different steel profile sections encased in concrete (steel-reinforced concrete sections or SPRC) and those with the steel sections filled with concrete (concrete filled tubes or CFST).

Composite column sections used in high-rise construction can be classified into three types, (a) Fully encased composite column (FEC); (b) Partially encased composite column (PEC); and (c) Concrete filled tube (CFST). Typical cross-sections of these three types of composite columns are shown in Figure 2.1 and Figure 2.2. As shown in (Figure 2.1(a)), in FEC columns the structural steel section is fully encased by surrounding concrete whereas in PEC columns (Figure 2. 1(b) and (c)) the steel section is partially encased by concrete. On the other hand in concrete filled tubular composite columns (Figure 2.2(d, e, and f)) the concrete is fully confined by the surrounding steel section. These composite sections have evolved to take the best out of the two materials i.e. concrete and steel. In these composite sections concrete provides compressive strength, stability,

stiffness, improved fire proofing and better corrosion protection whereas steel provides tensile strength, ductility and high speed of construction. Among these three sections FEC column renders better fire proofing and corrosion protection since the steel section is fully encased by concrete. The cost for fire proofing and corrosion resistance is not required for FEC columns as compared to PEC and CFST columns. Hence, for the moist weather condition environment FEC columns can be the best solution for high rise constructions from strength, ductility and economy considerations.

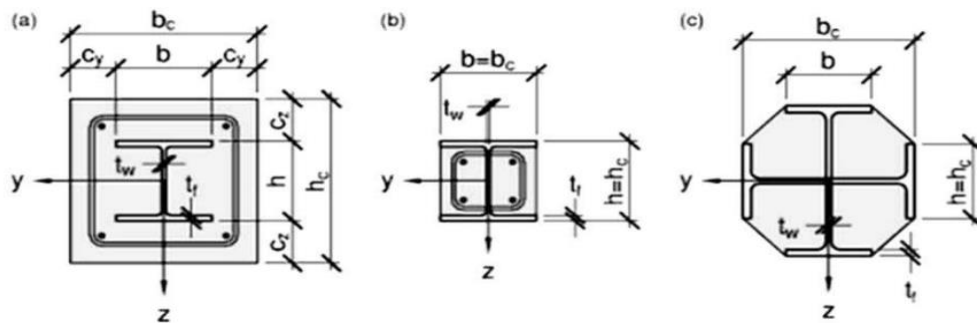


Figure 2.1: Typical Cross-Section of Composite Columns with Fully or Partially Concrete-Encased H-Section (Source: ETHIOPIAN STANDARDS, ES EN 1994-1-1:2015)

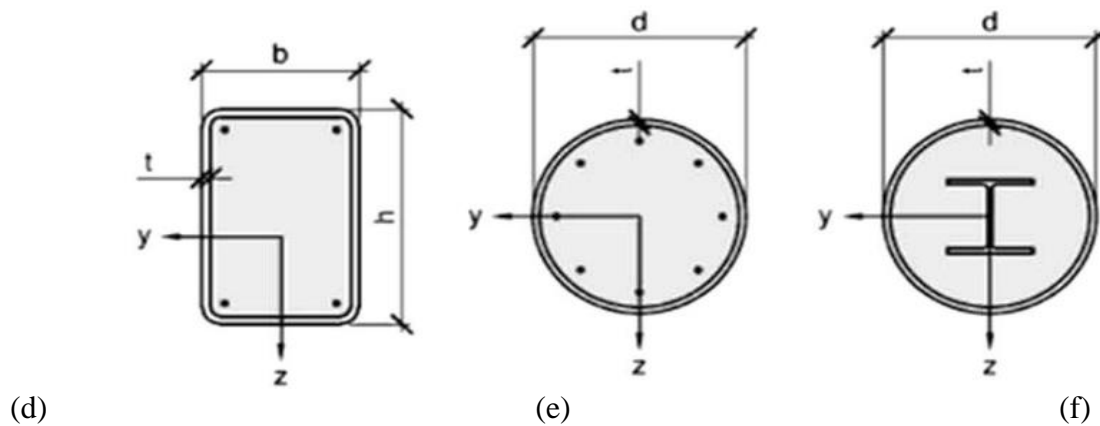


Figure 2.2: Typical Cross-Section of Composite Columns with Concrete-Filled Hollow Section (Source: ETHIOPIAN STANDARDS, ES EN 1994-1-1:2015)

### **2.2.1 Concrete-Filled Composite Column**

In this type of composite columns, a steel pipe, steel tubing, or built up section is filled with concrete (Figure.2.2). The most common steel sections used are the hollow rectangular and circular tubes. Filled composite columns may be the most efficient application of materials for column cross sections. It provides forms for the inexpensive concrete core and increases the strength and stiffness of the column. In concrete-filled tubes, the steel increases the strength of the concrete because of its confining effect, the concrete inhibits local buckling of the steel, and the concrete formwork can be omitted. Concrete filled steel tube structure is a type of new composite structure, the filled concrete that laterally restricted by tube is under the three dimensional pressure, so the concrete would get a higher compressive strength and deformation capacity (Liu, 2013).

### **2.2.2 Concrete Encased Composite Column**

One of the common and popular columns is the encased steel profile (Figure.2.1) where a steel H-section is encased in concrete. Sometimes, structural pipe, tube, or built up section is placed instead of the H-section. In addition to upholding a proportion of the load acting on the column, the concrete encasement enhances the behavior of the structural steel core by and horizontal bar reinforcement, and so making it more effective against both local and overall buckling. The load-bearing concrete encasement performs the additional function of fireproofing the steel core. The cross sections, which normally are square or rectangular, must have one or extra longitudinal bars placed in every single corner and these have to be tied by lateral ties at regular vertical intervals in the manner of a reinforced concrete column. Ties are effective in rising column strength, confinement and ductility. Furthermore, they stop the longitudinal bars from being displaced during construction and they resist the tendency of these same bars to buckle outward under load, which would cause spalling of the outer concrete cover even at low load levels, remarkably in the case of eccentrically loaded columns.

Han and An (2014) compared to the conventional concrete filled steel tube (CFST) columns, concrete-encased CFST columns have higher fire resistance and better durability under corrosive environment due to the protection from the outer by reinforced concrete. This type of composite construction has been applied widely in China (Reoder et al., 2014) in the past. When compared with RC columns, the concrete-encased CFST columns provide higher strength and better

ductility, and allow for the use of high-strength concrete as core concrete in the inner CFST, resulting in a smaller cross-section (Han and An 2014). During construction, the inner CFST is constructed first and then acts as support to carry the construction load before the assemblage of the outer RC component. After the installation of the external formwork and reinforcement, the outer concrete is finally placed (Han and An 2014).

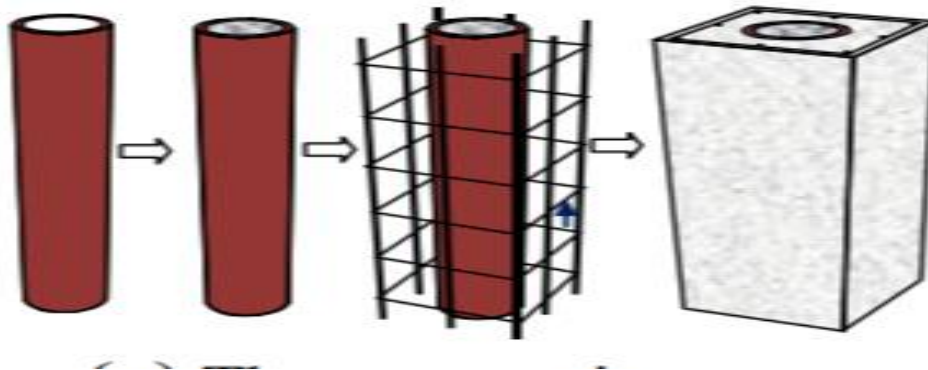


Figure 2.3 construction sequence of concrete filled encased column (source: Han and An 2014)

Know a day, this type of composite column, named as steel profile reinforced concrete (SPRC) column, has been utilized in some high-rise buildings recently. This type of composite column has attracted more and more research interest. Fig 2.4 and fig 2.5 gives a schematic view of different steel profile encased typical cross-sections.

For incased composite columns, the following advantages over conventional concrete filled steel tubular (CFST) columns are expected:

- 1) Higher stiffness.
- 2) The beam-column joints of the SPRC column system can be designed according to the well-established knowledge of conventional reinforced concrete (RC) beam-column joints.
- 3) Higher fire resistance due to the protection of the inner steel tubes provided by the concrete.
- 4) Corrosion of the steel tubes can be prevented due to protection from the outer concrete.
- 5) The possibility of “outward” buckling of the steel tubes is virtually prohibited due to the restraint of the outer concrete (Han et al., 2007).

Compared with conventional RC columns, the following advantages are expected:



- 1) Higher ductility owing to the existence of the inner CFST.
- 2) Faster construction speed is expected. In practice, the inner CFSTs can be built first to bear the construction load alone, and the outer concrete can be poured later (Han et al., 2007).

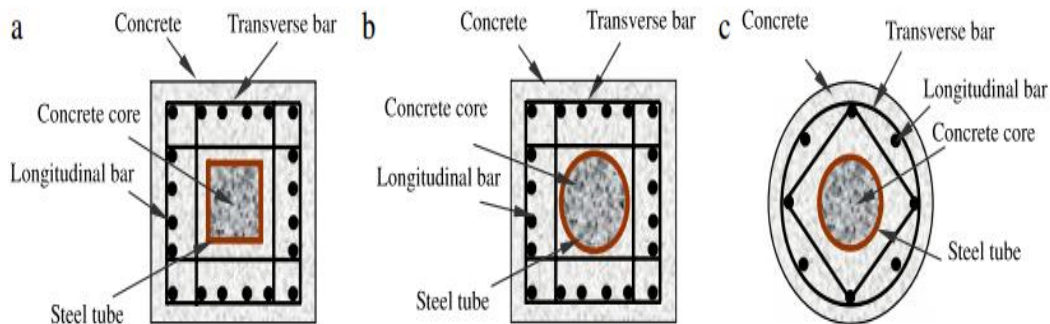


Figure 2.4 Encased composite column with different steel profile. (Source: Han et al., 2007).

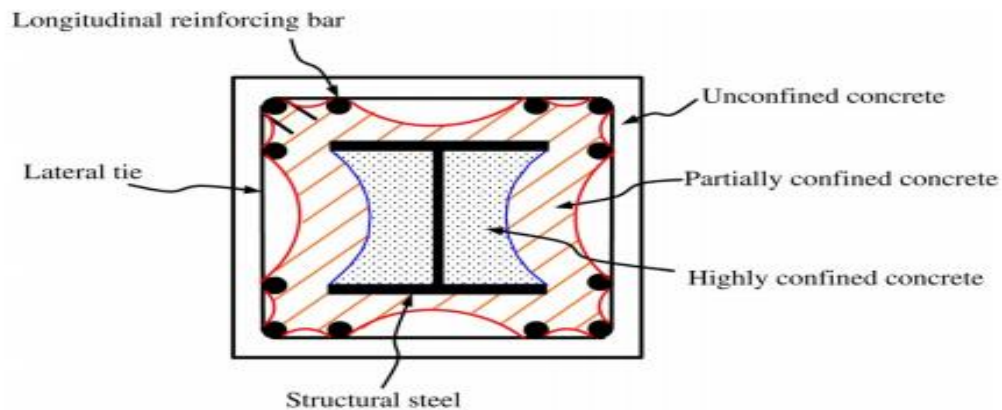


Figure 2.5 Encased composite column with I-profile. (Source: Chen and Lin, 2006)

Some previous research has been carried out on CFST columns (Wang and Chi, 2005) which demonstrates the fact that this type of composite column generally has good performance. However, there is still a lack of information on the composite members under cyclic loading. Also, due to the confinement provided by its outside RC, the outward buckling of the steel tube could be restrained effectively. Concrete-encased CFST columns have higher ductility due to the existence of CFST compared to conventional reinforced concrete (RC) columns (Han et al 2009).

## **2.3 Research on Steel-Encased Concrete Columns**

Extensive experimental and analytical, and a few numerical research works were carried out on FEC columns by previous investigators. Experimental study on composite columns started in the year of 1905 for concentric axial load. Analytical and theoretical studies started from the year of 1976. Recently, the numerical models were developed to determine the behavior and strength of FEC columns. Successive sections will focus on the experimental, analytical and numerical investigations on FEC columns under various conditions of loading.

### **2.3.1 Experimental investigations**

Extensive experimental researches were carried out on FEC columns, by several research groups to investigate the behavior of columns under various loading conditions. A large number of tests were performed on short FEC columns constructed with normal strength concrete subjected to concentric, eccentric and biaxial load. A few long column tests were carried out using normal strength under static loading conditions. Findings of these experimental investigations are presented below:

Dundar et al., (2008) conducted an experimental study on the behavior of reinforced and concrete-encased composite columns subjected to biaxial bending and axial load. The primary objective of this investigation was to examine the ultimate strength capacity and load-deflection behavior of short and slender reinforced concrete columns. The experimental results were compared with the ultimate capacities obtained theoretically. Theoretical results were calculated using various stress-strain models for the materials done by previous authors. The experimental program included fifteen (15) reinforced concrete columns. Five specimens were short square (100 mm × 100 mm) tied columns with 870 mm length. Seven specimens were slender square tied columns with two different sizes. Other three specimens were L-shaped section slender tied columns. Ultimate capacity of these reinforced concrete columns were determined experimentally for eccentric axial load and compared with calculated theoretical results. A computer program was developed based on these theoretical calculations. The ultimate capacity was determined using this computer program for the tested FEC columns. The authors reported that the theoretical results could predict the experimental results for different cross section of reinforced and composite column members with good accuracy.

Dundar and Tokgoz (2008) carried out experimental tests on biaxially loaded concrete encased composite columns. The main objective of this study was to observe the load deflection behavior and load carrying capacities of short and slender FEC columns. The researchers also, compared these experimental results with theoretical results. The theoretical results were calculated considering the flexural rigidity ( $EI$ ) and slenderness ratio of these composite columns. The slenderness effect due to the additional eccentricity of the applied axial load was considered by the moment magnification method. The main variables in the tests were eccentricity of applied axial load, concrete compressive strength, cross section, and slenderness effect. This experimental study consisted of ten composite column specimens. The complete experimental load-deflection behavior of the composite column specimens were determined. An interactive theoretical method including slenderness effect was suggested to perform the ultimate strength analysis and to determine the complete load-deflection behavior of composite columns. Good agreement was achieved between the complete experimental and the theoretical load-deflection diagrams in the study. In addition, the flexural rigidity was significant effect on the slenderness of composite columns.

Kim et al. (2012) carried out experimental study for eccentric axial load of concrete-encased steel column using high strength steel and concrete. Seven concrete-encased steel columns using high-strength structural steel (nominal yield strength  $f_{ys} = 913$  and  $806$  MPa) and high strength concrete (cylinder compressive strength  $f_{cu} = 94$  MPa) were tested to investigate the seven eccentric axial load-carrying capacity and the deformation capacity. Out of seven, four were fully encased square composite columns and designated as C1 to C4 with cross section  $260 \text{ mm} \times 260 \text{ mm}$ . The test parameters of the fully encased composite columns were the eccentricity of the axial load. These columns were tested experimentally for two different eccentricity ( $120 \text{ mm}$  and  $60 \text{ mm}$ ). The test results showed that in the case of inadequate lateral confinement, the load-carrying capacity was limited by the early crushing of concrete. However, because of the high-strength steel section, all test specimens showed ductile flexural behavior after the delamination of the concrete. The test results were compared with the predictions by nonlinear numerical analysis and current design codes.

Shih et al. (2013) carried out study on axial strength and ductility of square composite columns with two interlocking spirals. The axial compressive capacity and load– displacement behavior of

composite columns confined by two interlocking spirals were experimentally and analytically investigated. The innovative spiral cage used for a square column was fabricated by interlocking a circular spiral and a star-shaped spiral to enhance the confinement effect for the core concrete. Eight full-scale square composite columns were tested under monotonically increased axial compression. Experimental results demonstrated that, with significant savings of the transverse reinforcement, the composite columns confined by two interlocking spirals achieved excellent axial compressive strength and ductility. It revealed that the spirally reinforced concrete column achieved better load carrying capacity and behavior than the rectilinearly tied reinforced concrete column, although the amount of the spirals was less than that of the rectilinear hoops. Moreover, an analytical model was developed to take into account the concrete confinement due to the structural steel in addition to the transverse reinforcement and distributions of the longitudinal bars. The analytical results accurately predicted the axial compressive capacity and load–displacement behavior of the specimens.

### **2.3.2 Numerical and analytical investigations**

Analytical methods were developed parallel to experimental study in early 1900 to determine the strength and behavior of FEC columns. Successively, computer analysis method was developed to determine the nonlinear behavior of FEC columns under different loading conditions. Numerical analyses for FEC columns using FE model started very recently as compared to other methods. It has numbers of advantages over experimental research. However, it was found that very limited research on numerical simulation of FEC column has been conducted.

Kim et al., (2012 and 2013) carried out numerical studies on FEC columns with high strength steel and concrete with varying eccentricity and structural steel shapes. Total eight (8) FEC columns were numerically investigated using fiber section analysis in these studies. The analysis results were compared with the test results, in terms of the axial load-strain relationship and the moment-curvature relationship. In material models for the high-strength concrete the tensile stress of the concrete was ignored. The concrete area in the composite 18 section was divided into three regions according to confinement level: unconfined (concrete cover), partially confined (confined by lateral rebar's), and highly confined (confined by lateral rebar's and steel section) concrete zones. Authors reported that the nonlinear numerical analysis showed good agreement with the test

results. But, it is observed from the study that the difference between experimental and numerical results of mentioned columns were 5% to 12%.

(Mote and Vijay, 2013) investigated the behavior of pin-ended axially loaded concrete encased steel composite columns. A non-linear 3-D finite model was developed to analyses the inelastic behavior of steel, concrete, longitudinal and transverse reinforcing bars as well as the effect of concrete confinement of the concrete encased steel composite columns. The experimental investigation on concrete encased steel composite columns was conducted with different slenderness ratio, different steel sections and different concrete and steel strength.

Ellobody et al., (2010) studied the responses of concrete encased steel composite columns to eccentrically load acting along the major axis. Many variables that influence this response such as the concrete strength, the steel section yield stress, eccentricities, column dimensions, and structural steel sizes were investigated. A three-dimensional finite element analysis using ABAQUS© has been developed and it has been validated against experimental result. Eccentric Load–concrete strength curves, axial load-moment curves, and ultimate capacity were obtained. The results showed that the increase in steel section yield stress has significant effect on the strength of eccentrically load composite column with small eccentricity with concrete lower than 70 MPa compressive strength.

Ellobody and Young (2011) investigated the behavior of pin-ended axially loaded concrete encased steel composite columns. The main objective of the study was to understand the structural response and modes of failure of the columns and to assess the composite column strengths against current design codes. A nonlinear 3-D finite element model was developed to analyses the inelastic behavior of steel, concrete, longitudinal and transverse reinforcing bars as well as the effect of concrete confinement on concrete encased steel composite columns. The finite element model was validated against published experimental results. Furthermore, the variables that influence the composite column behavior and strength comprising different slenderness ratios, concrete strength and steel yield stress were investigated in a parametric study. The authors reported that the increase in structural steel strength had a small effect on the composite column strength for the columns having higher relative slenderness ratios due to the flexural buckling failure mode.

The dominant point that was noticed during the review in literature was the cyclic behavior of the composite beam-columns has not received the same level of attention as monotonic behavior, especially for concrete-encased steel composite columns. A limited number of studies have been made on this behavior because it is expensive regarding the cost of research; preparing a full-scale testing is expensive and time consuming. However, a remarkable number of researchers tried to capture and monitor the composite columns seismic behavior by means of strength, stiffness, ductility, and energy dissipation. For instance, Varma, et al., (2004) investigated the seismic behavior of square concrete-filled steel tube beam-columns. Cyclic load tests conducted on eight beam-column specimens having different width-to-thickness ratio, different yield stress of the steel tube, and different level of axial load. The results indicate that in the plastic hinge zone, where the stress concentrations highly increase, most of the flexural energy was dissipated. Moreover, it was shown that the increase in axial load level has inverse effect on the cyclic curvature ductility. Also at lower axial load levels, the ductility is reduced for beam-columns having higher width-to-thickness ratio or yield stress of the steel tube.

Qian, et al., (2016) studied an investigation on the analytical behavior of concrete-encased CFST columns under cyclic lateral loading. The main objectives of this research are firstly, to develop a nonlinear 3-D finite element analysis (FEA) model on composite columns under cyclic loading with consideration of the cumulative damage of concrete as well as the interaction between concrete and steel. Secondly, to present analytical results of concrete-encased CFST columns under cyclic lateral loading, including the load–displacement relationships, the contact stress between steel tube and concrete and the axial load distribution among inner CFST and outer RC components. Meanwhile, comparisons on the behavior of concrete-encased CFST, conventional CFST and RC columns are also conducted. Thirdly, to provide a moment versus curvature hysteretic model using the verified FEA model, which can reasonably predict the behavior of composite columns under cyclic lateral loading. The analytical results show that components of the composite column work together well under cyclic loading. The axial load level effects on the axial load distribution among components. The proportion of the axial load resisted by the outer reinforced concrete increases at first, and then decreases with the increase of the displacement level when under a low axial load level.

In order to give a further understanding of steel-reinforced concrete-filled steel tubular (SRCFST) columns under cyclic loading conducted (Chang, et al., 2012). In this contribution, the ABAQUS®/standard solver is employed to investigate and predict the resistances of SRCFST columns under cyclic loading. Validation of this numerical method is carried out by comparing the computed results with the experimental observation of five tested specimens. A parametric study, including the thickness of steel tube, steel ratio of section steel, yield strength of section steel and strength of concrete, is also carried out. The presence of the section steel can carry the lateral load and reduce the tensile zone of the concrete section. As a result, the SRCFST columns have higher stiffness and peak lateral load than the common CFST columns even with the same geometrical and material parameters. The section steel can also enhance the deformation ability of a SRCFST column.

#### **2.4 Review of Effect of Confinement and stirrup**

The strain in the materials during the early loading is different there is often little initial confinement of the concrete in a CFST. However, as the concrete begins to crack, it expands faster than the steel tube and becomes well confined at higher load value. This confinement results in a higher load carrying capacity. ES EN 1994-1-1:2015 allows an increase of concrete compressive capacity factor from  $0.85f_{ck}$  to  $f_{ck}$  for all CFSTs due to effect of confinement. Confinement has a significant effect of increasing load capacity for circular sections.

For the purpose of further increase of bearing capacity and survivability of encased composite column, it is offered to supply their concrete with additional tie reinforcement. Such reinforcement also has a positive effect on the fire resistance of the columns, as tie reinforcement, mounted with some distance from the inner surface of the steel pipe, is able to provide significantly longer resistance of the volumetrically compressed reinforced concrete core in fire conditions. The main variation was the spacing of the stirrup shear reinforcement. Due to the confinement effect of the stirrup shear reinforcement, the concrete core in the SRCFT specimens showed different behavior in shear failure compared to the CFST specimens (Hamidian, et al., 2016) and (Krishan, et al., 2017).

## 2.5 Review of Design code

For satisfaction of the main aim of this study; investigate the cumulative damage of composite columns subjected to axial and cyclic loading by comparing the effects of different parameter on the cyclic capacity of encased composite columns, it is first necessary to review the design procedures that will be used for composite, steel, and reinforce concrete columns to be able to used them in this investigation. In fact, Eurocode presents the most recent rules and comprehensive review among other design codes and specifications. As a result, Eurocode 2, 3, and 4 were chosen for design of reinforce concrete, steel, and composite columns, respectively. For the composite columns design, Eurocode has mentioned some limitations which shall satisfy; the longitudinal reinforcement which can be used should be no more than 6% and not less than 0.3% of the concrete area, concrete grade used was normal concrete from C20/25 to C60/75, the steel contribution ratio must between 0.2 and 0.9 and 0.2 and 5 are given as limits for the depth to width ratio of the composite cross-section.

In order to calculate the plastic resistance of composite columns, the plastic resistance of its components; the structural steel, the concrete and the reinforcement, should be adding. The plastic resistance equation for encased-composite column is:

$$N_{pl\ rd} = A_a f_{yd} + 0.85 A_c f_{cd} + A_s f_{sd} \quad (2.1)$$

Where

$A_a$  the cross-sectional area of the structural steel

$A_c$  the cross-sectional area of the concrete

$A_s$  the cross-sectional area of the reinforcement

$f_{cd}$  Design value of the cylinder compressive strength of concrete

$f_{sd}$  Design value of the yield strength of reinforcing steel

$f_{yd}$  Design value of the yield strength of structural steel



## 2.6 Review of cyclic testing

All structural elements have limited strength and deformation capacities; and collapse safety as well as damage control depend on our ability to assess these capacities with some confidence. To characterize or to model structural element or a structural detail for which the expected load condition is characterized by cyclic loading history with known or unknown amplitude as, for instance, for structure in seismic area, a cyclic test is necessary. There is no unique and “best” loading history, because no two earthquakes are alike and because the specimen may be part of many different structural configurations. The overriding issue is to account for cumulative damage effects through cyclic loading. If there is no cumulative damage, there is no need for cyclic loading. The number and amplitudes of cycles applied to the specimen may be derived from analytical studies in which models of representative structural systems are subjected to representative earthquake ground motions and the response is evaluated statistically. There are three main type of experimental testing that can be realized in the laboratory.

- a) Dynamic Tests with shaking machines or shaking tables simulate effectively dynamic loads or seismic events, but they are generally very expensive.
- b) Pseudo-Dynamic Tests, characterized by the application of variable step-by-step static forces in order to simulate the dynamic behavior, provide a realistic seismic simulation using an equipment considerably less expensive than the shaking table, but are suitable only for structures that can be easily modelled with a few degrees of freedom (cantilevers, one or two story frames, etc.)
- c) A Quasi-Static Cyclic Test, whose apparatus is the most common in research laboratories, is less suitable than dynamic and pseudo-dynamic tests to simulate seismic load conditions, but it is simple and less expensive.

(Castiglioni and Drei, 2016) stated to achieve an adequate knowledge of the cyclic structural behavior of a steel structure by means of quasi static testing, the first step is to define the “minimum sub assemblage” that should be tested. For a framed steel structure, the minimum sub-assemblage is a two story spatial frame, made with three rows of two bays plane frames, with concrete slabs at each floor level. This specimen contains beams, columns, two, three and four ways beam-to-column joints and can be loaded vertically, to simulate gravity loads and horizontally, to simulate earthquake loading. A first simplification can be the testing of part of the sub-assemblage that is

only one plane frame (two bays, two storeys). The specimen becomes less complete, because the interaction among the frames due to the transversal effect of the slabs cannot be taken into account, but both the gravity and the seismic loads can still be considered.

As the most critical details, whose cyclic behavior should be investigated, are usually the beam-column joints, the next step toward a simplification of the specimens is to consider a single node of the plane frame, made with part of a column and part of a beam. This test setup is simple, it is the less expensive, but it is the less complete. The test configuration can be a horizontal T, with vertical column and horizontal beam, or an inverted T, with horizontal column and vertical beam. This set up is shown in the Fig 2.6 below.

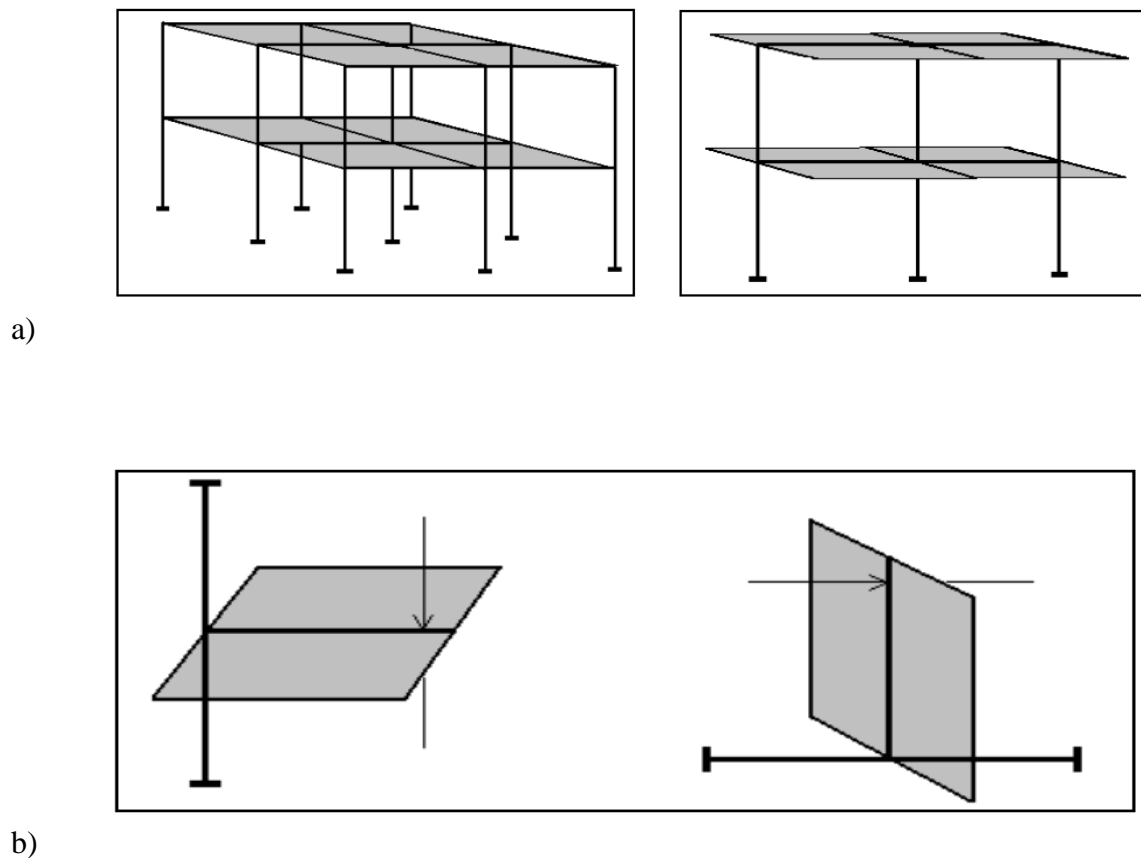


Figure 2.6 a) Spatial frame and Plane frame sub-assembly of the structure b) Testing setup outline for Horizontal T and inverted T specimens (Castiglioni and Drei, 2016).

(Filiatrault et al., 2018) studied scientifically based quasi-static cyclic loading protocols have been proposed over the years for the cyclic testing of structural and non-structural elements and systems. In the context of his study “scientifically based” relates to the development of a loading protocol based on the statistical analyses of inelastic excursions obtained from time-history dynamic response analyses of singled-degree-of-freedom (SDOF) systems subjected to ground motions. Two other cyclic loading protocols that have been developed from a scientific basis and widely used to test light-frame wood components and sub-assemblies are also reviewed. Finally, two recent cyclic loading protocols developed specifically for the testing of structural and non-structural elements are reviewed and compared to the structural cyclic loading protocols. Note that before the development of these recent non-structural cyclic loading protocols, cyclic loading protocols developed for testing steel and wood structures were also used to test non-structural elements.

### **2.6.1 Quasi-static cyclic loading protocols**

Any loading protocol will always be a compromise that will provide deformation histories whose realism will depend on many parameters. For one, actual histories, as experienced in earthquakes, will depend on the intensity and frequency content (magnitude, distance, and soil type dependence) of the ground motion the specific component (or assembly) will be subjected to as part of the structural system. Equally important, the number and amplitudes of cycles the component will experience depend on the configuration, strength, stiffness, and modal properties (periods and participation factors) of the structure and on the deterioration characteristics of the structural systems and its components. Many loading protocols have been proposed in the literature, and several have been used in multi-institutional testing programs (e.g., ATC 1992, Clark et al., 1997), or are contained in standards or are proposed for standards.

#### **i, ATC-24 Protocol (ATC-24, 1992)**

This protocol, which was specifically developed for components of steel structures, was one of the first formal protocols developed in the U.S. for seismic performance evaluation of components using a cyclic loading history. It uses the yield deformation,  $\Delta_{yield}$ , as the reference for increasing the amplitude of cycles. The history contains at least 6 elastic cycles (amplitude  $< \Delta_{yield}$ ), followed by three cycles each of amplitude  $\Delta_{yield}$ ,  $2\Delta_{yield}$ , and  $3\Delta_{yield}$ , followed by pairs of cycles whose

amplitude increases in increments of  $\Delta_{yield}$  until severe cyclic deterioration occurs. The relative and absolute amplitudes of the cycles were derived from statistical studies of time history responses of SDOF systems, and therefore represent global (roof or story) drift histories and not local deformation histories such as those experienced, for instance, by links in eccentrically braced frames.

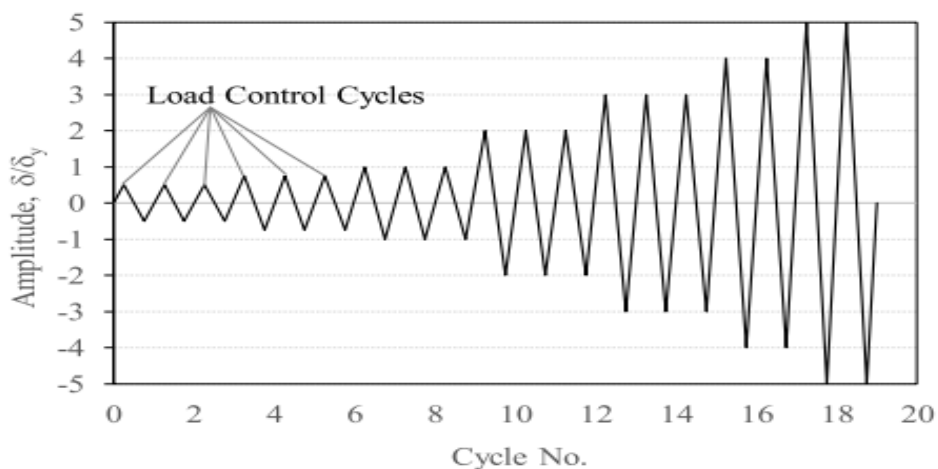


Figure 2.7 loading protocol of ATC-24 (ATC-24, 1992)

Table 2.1 Sequence of loading of ATC-24 cyclic loading protocol

Cycle group	No of cycle	Amplitude
1	3	$0.5\delta_y$
2	3	$0.75\delta_y$
3	3	$1\delta_y$
4	3	$2\delta_y$
5	3	$3\delta_y$
6	2	$4\delta_y$
7	2	$5\delta_y$
8 and greater	2	Increment of $\delta_y$ until failure

**ii, The ISO cyclic loading protocol**

The International Organization for Standardization (ISO) Technical Committee on Timber Structures developed the ISO loading protocol. Originally developed for wood connection testing, the procedure is also considered appropriate for testing light-frame wood shear wall assemblies. The load history is based on the displacement at ultimate load ( $\Delta_{max}$ ) obtained from the mean values of prior monotonic tests. The amplitude of each cycle is a percentage of  $\Delta_{max}$ , as shown in table 2.1 presents the sequence of loading of the ISO cyclic loading protocol.

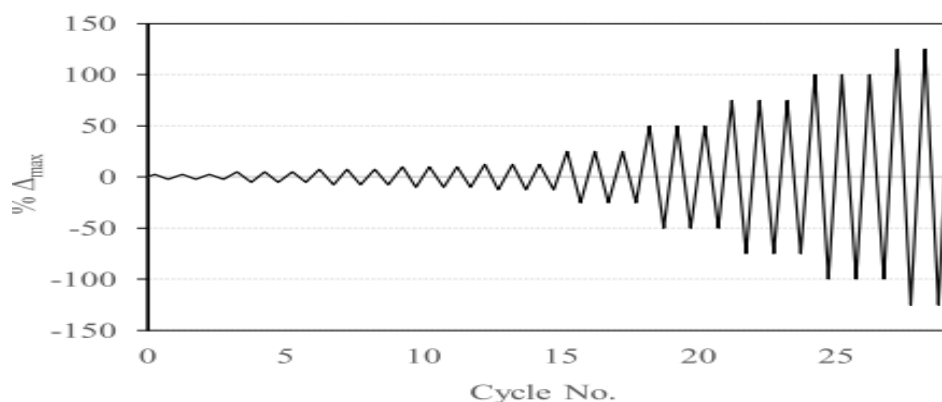


Figure 2.8 ISO cyclic loading protocol (Filiatrault et al., 2018).

Table 2.2 Sequence of loading of ISO cyclic loading protocol (Filiatrault et al., 2018)

Cycle group	No of cycle	Amplitude (% $\Delta_{max}$ )
1	3	2.5
2	3	5
3	3	7.5
4	3	10
5	3	12.5
6	3	25
7	3	50
8	3	75
9	3	100
>9	3	Increment of 25% up to failure

$\Delta_{max}$  = Ultimate load displacement obtained from mean value of prior monotonic tests

### iii, SAC Protocol (Clark ,et al., 1997)

Because of the  $\Delta_{yield}$  ambiguity, and because of the opportunity the SAC program offered to develop a specific loading protocol for steel moment frames, a statistical study was performed on the number and amplitudes of story drift cycles of the SAC Los Angeles and Seattle 3 and 9 story frame structures (Krawinkler et al., 2000). The outcome of this study is the SAC loading protocol shown in Figure 2.8, which uses story drift rather than yield deformation as the amplitude control parameter. For steel frame structures the story yield drift is confined to a rather narrow range around 0.01 radians, which permits an approximate correlation between the ATC-24 and SAC protocols. The SAC protocol contains more small (elastic) cycles (which were added because of the observed Northridge weld fractures that occurred before yielding took place), two cycles of an intermediate amplitude of 0.015 radians, but slightly fewer cycles of larger amplitude. In general the two protocols are very similar in cumulative damage potential, but because of the commitment to story drift as the control parameter, the SAC protocol should not be applied to configurations other than steel beam-to-column assemblies that are representative of typical stories.

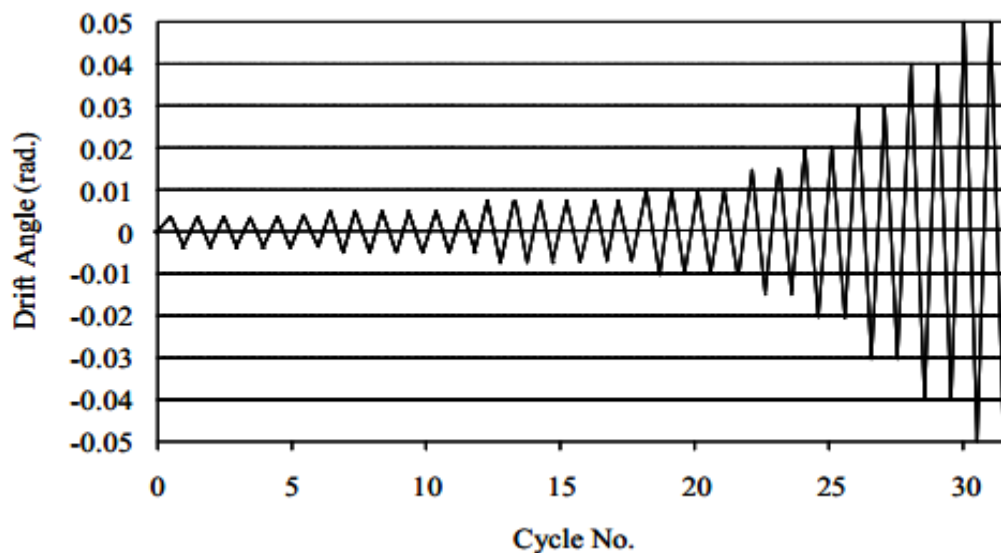


Fig. 2.9 SAC (Clark et al., 1997) loading protocol

Table 2.3 Sequence of loading of SAC standard protocol

Cycle group	No of cycle	Drift angle amplitude(rad)
1	6	0.00375
2	6	0.0075
3	6	0.015
4	4	0.02
5	2	0.03
6	2	0.04
7	2	0.05
8 and greater	2	Increment of 0.01 up to failure

**iv. Load protocol proposed by ECCS:**

Loading protocol provided by the European Convention for Constructional steel work (ECCS) for carry out test in order to characterize the structural behavior of structural components under cyclic load as implemented this paper. ECCS loading protocol apply different approach from EN 15129 protocol, the amplitude of load cycles is depending on the yield displacement ( $e_y$  identical to  $\delta_y$ ) in this case as shown below. The third testing procedure provided by ECCS is cyclic test with increase of displacement. The characteristics are defined as follow:

- One cycle in the  $\frac{e_y^+}{4}, \frac{e_y^-}{4}$  interval;
- One cycle in the  $\frac{2e_y^+}{4}, \frac{2e_y^-}{4}$  interval;
- One interval in the  $\frac{3e_y^+}{4}, \frac{3e_y^-}{4}$  interval;
- One interval in the  $\frac{e_y^+}{4}, \frac{e_y^-}{4}$  interval;
- Three cycle in the  $\frac{2e_y^+}{4}, \frac{2e_y^-}{4}$  interval;

Three cycle in the  $(2+2n) \frac{2e_y^+}{4}, (2+2n) \frac{2e_y^-}{4}$  interval ( $n=1,2,\dots$ ) More cycle or more intervals may be used if necessary.

## CHAPTER THREE

### RESEARCH METHODOLOGY

#### 3.1 General

This chapter presents and describes the approaches and techniques the researcher will use to collect data and investigate the research problem. This include the research design, study population, sample size and selection, sampling techniques and procedure, data collection methods, data quality control (validity and reliability), procedure of data collection, data analysis, Ethical consideration.

#### 3.2 Research Methodology

The research design is theoretical research which are essential for the comparative study of encased composite column with different steel section on combined action of axial load and cyclic loading using finite element analysis of ABAQUS©. This research is a systematic investigation to fill the gap of knowledge on the performance of encased composite column. On the other hand, it is a process for collecting, analyzing and interpreting information to provide a recommendation to the research findings.

After comprehensively, organizing literature review of different previous published researches, designate the comparative study of encased Composite column with different steel profile. Validation for the finite element modeling is conducted on pre-qualified and practical tested for encased composite column under axial and cyclic loading. After that specific study parameters will be introduced in this study for encased composite column to investigate the influence of this parameters on performance of composite column in cooperative technique.

#### 3.3 Study Variables

##### 3.3.1 Dependent Variables

The dependent variables, which are to be observed and measured to determine the effect of the independent variables, are listed below

- Lateral load capacity and Axil deformation of composite column



- Hysteretic behavior of composite column
- Failure mode

### **3.3.2 Independent Variables**

The independent variables, which are to be measured and manipulated to determine its relationship to observed phenomena, are selected and listed below.

- Steel profile section type
- Spacing of tie (s/D)
- slenderness ratio (L/D)

### **3.4 Population and Data Collection Process**

The main purpose of this study was to investigate the cumulative damage of encased composite column subjected to cyclic loading and constant concentric axial loading by comparing the effect of profile of encasement and effect of length to width ratio of the column to evaluate the stiffness, strength and ductility of the column. To achieve this, a finite element analysis was conducted with all appropriate parameters considered. The finite element method is a numerical analysis technique for obtaining approximate solutions to a wide variety of engineering problems. For this study there was a total of nineteen (19) columns which was selected as a sample with different independent variable. Of nineteen, eighteen (18) are for parametric study and one (1) column is from experimental literature for validation of the model. For the entire assembly the cyclic loading protocol suggested by Applied Technology Council (ATC) guidelines (ATC 1992- ATC 24) was applied. Axial loads of 50% (3627KN) of column capacity were applied concentrically on top of the columns and cyclic load is laterally applied at the top of the column. The failure modes, peak load, load-deflection behavior of the specimens were examined for these two types of loads in this study.

The data collection for this research used the related topic literatures from high rated journals, ongoing researches, books, and seismic resistance structural design journals, construction engineering journals and construction management journals, relevant practices related to comparative study of encased composite column with previous experimental results using finite elements analysis ABAQUS© software and which will related to cyclic performance of encased composite column will be accessed. An approach is going to conduct number of Finite Element

Analysis to observe the behavior of encased composite column with different steel section profile under axial and cyclic loading.

### **3.4.1 Model samples and cross sections used in this study**

#### **Study Program**

The study program consisted of eighteen (18) fully encased composite column (FEC) columns of three different encasement with square tube, circular tube and H section composite column. These FEC columns were square in size and constructed with normal strength concrete. The columns were tested for concentric and cyclic loads, to observe the failure behavior and the lateral load carrying capacity of FEC columns. The load versus deflection behavior of these FEC are analyzed by finite element method.

#### **Description of model specimens**

In total, 18 FEC columns were analyzed for the parametric study. Details of these columns are given in Tables 3.6 and 3.7. The first letter in the column designation refers to encasement (E=encased), second letter to refer incased steel structure profile (T= tube profile, C = circular profile and H=H profile) and the third later is to say section (S= section). The number used in the column designation is simply the serial number as they appeared in the table. Depending on the parametric study of this model the whole columns are categorized into six groups. Group 1, 2 and 3 are for investigation of effect of slenderness ratio. All columns of these groups have modeled with identical material properties except length of column and encasement type of steel structure.

Next groups are group 4, 5 and 6 which are for investigation of effect of spacing of tie on column performance. All columns of these groups have modeled with identical material properties except spacing of spiral tie and encasement type of steel structure. The cross section used under this investigation was shown in the figure 3.1 and 3.2 below.

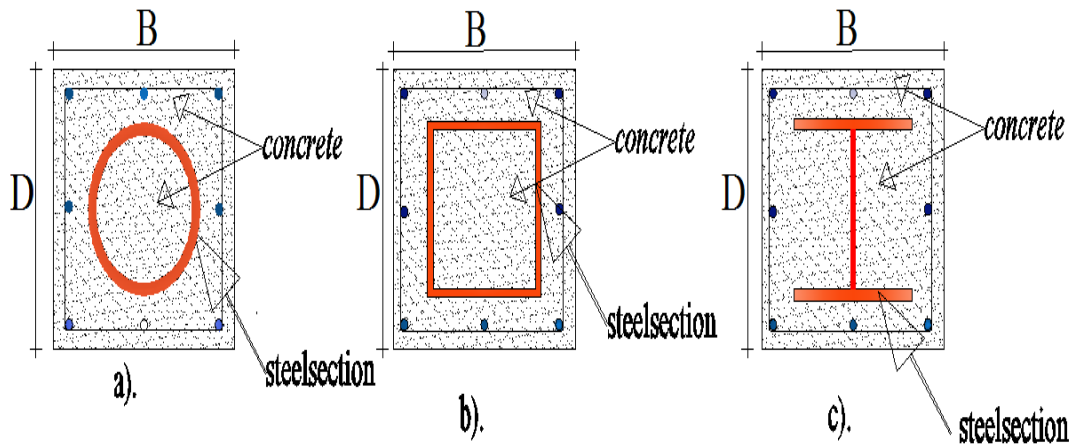


Figure 3.1 Cross-section taken for the analysis (a ,b ,c)

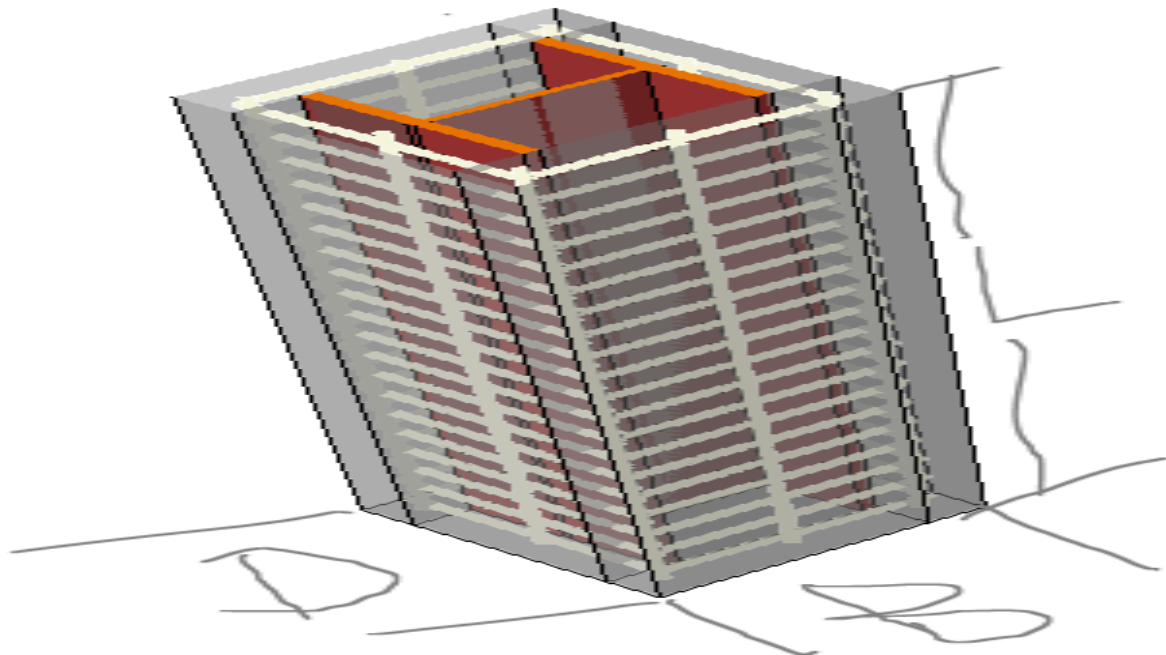


Figure 3.2 3D-view taken for the analysis

Table 3.1 Geometric properties of t specimens under the study

Si. No	Specimen designation	Dimension (mm)			Ratio (L/D)	Longitudinal bar	Tie bar (mm)	Structural steel size Encasement type
		B	D	L				
1	ETS1	400	400	3000	7.5	8 $\phi$ 16mm	$\phi$ 8@150mm	Square tube of $d \times w \times t$ (mm) 250 $\times$ 250 $\times$ 12.5
2	ETS2	400	400	4500	11.25	8 $\phi$ 16mm	$\phi$ 8@150mm	
3	ETS3	400	400	6000	15	8 $\phi$ 16mm	$\phi$ 8@150mm	
4	ECS1	400	400	3000	7.5	8 $\phi$ 16mm	$\phi$ 8@150mm	Circular tube of $D \times t$ (mm) 245 $\times$ 16.5
5	ECS2	400	400	4500	11.25	8 $\phi$ 16mm	$\phi$ 8@150mm	
6	ECS3	400	400	6000	15	8 $\phi$ 16mm	$\phi$ 8@150mm	
7	EHS1	400	400	3000	7.5	8 $\phi$ 16mm	$\phi$ 8@150mm	H section of $bf \times d \times tf \times tw$ (mm) 260 $\times$ 260 $\times$ 17.5 $\times$ 10
8	EHS2	400	400	4500	11.25	8 $\phi$ 16mm	$\phi$ 8@150mm	
9	EHS3	400	400	6000	15	8 $\phi$ 16mm	$\phi$ 8@150mm	

### 3.5 Finite element method

Finite element analysis is a powerful computer method of analysis that can be used to obtain solutions to a wide range of structural problems involving the use of ordinary or partial differential equations. FE solvers can either use linear or non-linear analysis. Initially, the use of FE required the designer to define the location of every node for each element by hand and then the data were entered as code that could be understood by a computer program written to solve the stiffness matrix. Nowadays this is often known as the 'solver'. The output was produced as text data only. The use of FEA has been the preferred method to study the behavior of encased composite column (for economic reasons). Now a day FEA is applied almost in all engineering areas of study such as flexural performance of concrete-encased column (An et al., 2014). Nonlinear analysis of concrete-filled steel (Ellobody & Young, 2014), cyclic performance of concrete-filled composite columns under flexural loading (Han and Yang, 2005) behavior of concrete-encased concrete-filled steel tube (CFST) members under axial tension (Han et al., 2016).

### 3.6 Data Processing and Analysis

An analysis of encased composite column will be using finite elements analysis. Finite Element Analysis (FEA) of encased composite column specimens is performed in a nonlinear static analysis format and the analysis procedure considers both material and geometric nonlinearities. In a nonlinear analysis, the total specified loads acting on a finite element body will be divided into a number of load increments. At the end of each increment the structure is in approximate equilibrium and the stiffness matrix of structure will be modified in order to reflect nonlinear changes in structure's stiffness.

The general-purpose finite element program ABAQUS© will be used in this study is to investigate the effect of using different steel profile, different length of column and varying spacing of tie reinforcement under axial load and cyclic loading. A three-dimensional 3D finite element model will be developed to account for geometric and material nonlinear behavior of encased composite column. Every complete finite-element analysis consists of three separate stages:

- **Pre-processing or modeling:** This stage involves creating an input file, which contains an engineer's design for a finite-element analyzer. Pre-processing involves creating a geometric representation of the structure, then assigning properties, then outputting the information as a formatted data file (.dat) suitable for processing by ABAQUS©
- **Processing or finite element analysis (solver):** This is sets of linear or nonlinear algebra equations are solved simultaneously to obtain nodal results, such as displacement values at different nodes or temperature values at different nodes in heat transfer problems.
- **Post-processing or generating:** In this process, the results can be processed to show the contour of displacements, stresses, strains, reactions and other important information. Graphs as well as the deformed shapes of a model can be plotted and report, image, animation are also prepared from this output.

ABAQUS/Standard uses the Newton-Raphson method to obtain solutions for nonlinear problems. Newton-Raphson equilibrium iterations provide convergence at the end of each load increment within tolerance limits for all degrees of freedom in the model. In addition to this commercial

computer software package ABAQUS© program, the following programs will be applying: Microsoft Word and Microsoft excel will be used for preparation of the report.

### **3.7 An overview of ABAQUS©**

ABAQUS is one of the well-known leading structural analysis systems. The ABAQUS© system uses finite element analysis techniques to provide accurate solutions for all types of linear and nonlinear stress, dynamic, and thermal problems. It is an associative feature-based modeler. The model geometry is entered in terms of features which are sub-divided (discretized) into finite element in order to perform the analysis. Increasing the discretization of the features will usually result in an increase in accuracy of the solution, but with a corresponding increase in solution time and disk space required.

Compared with structural testing, Finite Element Methods are available to carry out huge experiments without any worry about time and money. Many researchers (Han et al., 2016), (Ma et al., 2018) and (Portolés et al, 2013) all over the world have done many research toward the development of the numerical models to simulate performance of composite columns. By ABAQUS©/Standard solver, (Zhang et al., 2011) investigated the axial compressive behavior of short concrete-filled elliptical steel columns, such as the ultimate load capacity, load versus end-shortening relationship and failure modes. Meanwhile, the simulation results are consistent to experimental results, so they stated the simulation results could be used to predict compressive characteristics of short concrete-filled elliptical steel columns.

#### **3.7.1 Linear analysis**

In a linear finite element analysis, all materials are assumed to have linear elastic behavior and deformations are small enough not to significantly affect the overall behavior of the structure. This is currently the most widely used method of FE analysis, but it is less sophisticated than non-linear analysis.

#### **3.7.2 None linear analysis**

Many FE packages are capable of carrying out non-linear (iterative) analysis, but this is useful only for reinforced concrete design where it can be used to model the cracked behavior of concrete. Non-linear analysis is used for RC design because as the slab is loaded it will crack and this affects

its stiffness. The program carries out an analysis with un-cracked section properties; it can then calculate where the slab has cracked, adjust the material properties and run the analysis again. This process continues until the variation in section properties between runs reaches a predetermined tolerance.

### 3.8 Finite Element Modelling of encased composite column

This section provides a description of the finite element model developed in this study. It begins with an overview of the process that led to development of the model followed by a more in-depth look at individual aspects of the model; examining first the simplification of the physical specimens geometry, followed by a description of the mesh elements used to discretize the geometry, an overview of boundary conditions imposed on the mesh, and a description of the various material models that define the behavior of the model.

A complete 3D finite element model was developed in this study to investigate the behavior and strength of FEC columns encompassing a wide variety of geometry and material properties. Both material and geometric nonlinearities were incorporated in the FE model. ABAQUS®/Standard (ABAQUS element Analysis User's Manual) finite code was used to develop the nonlinear FE model for FEC columns in this study. Descriptions of the mesh and elements used in the finite element models of the test specimens, along with the boundary conditions including steel-concrete interaction are presented in the subsequent sections.

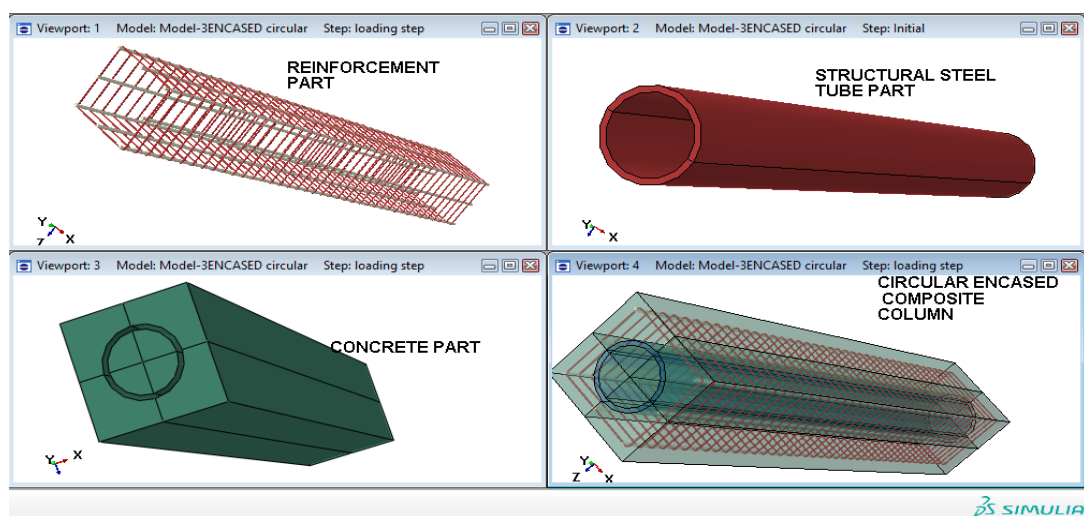


Figure 3.3 Modeling of circular tube incased composite Components in ABAQUS®CAE

A total of 5 parts were used to represent circular tube incased composite column in finite element model. The FEM of the concrete-encased steel composite columns was carried out by modeling the reinforcement bars, stirrups, circular structural steel tub, unconfined concrete which consists the concrete cover were and confined concrete and their properties.

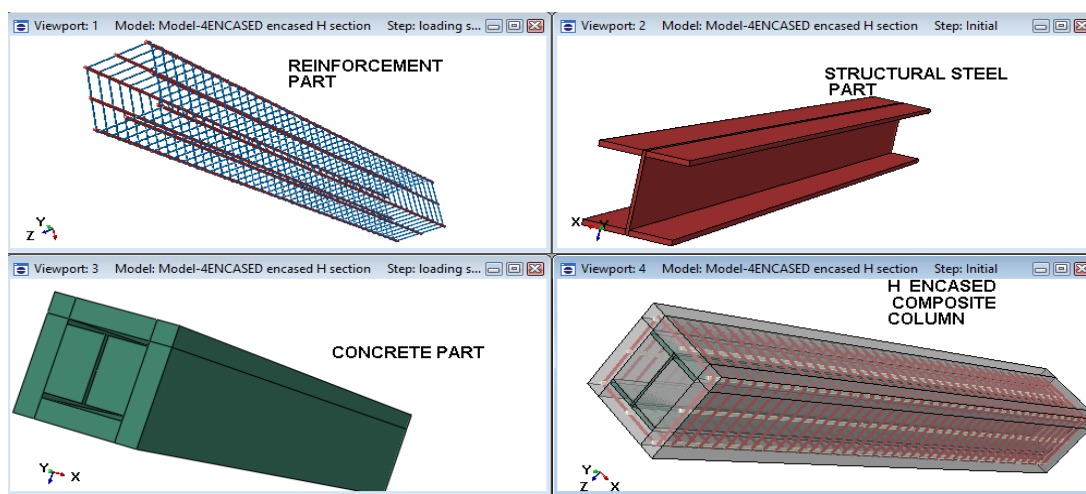


Figure 3.4 Modeling of H profile incased composite Components in ABAQUS©CAE

A total of 4 parts were used to represent the column in finite element model. The FEM of the concrete-encased steel composite columns was carried out by modeling the reinforcement bars, stirrups, H profile structural steel, concrete part and their properties.

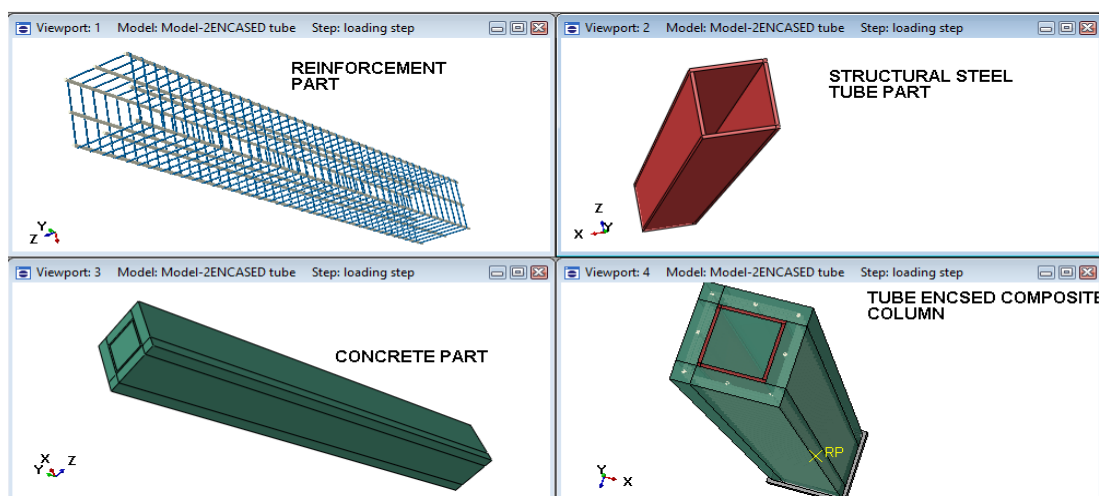


Figure 3.5 Modeling of square tube incased composite Components in ABAQUS©CAE



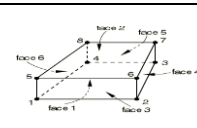
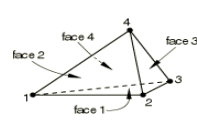
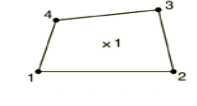
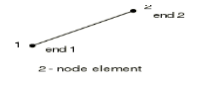
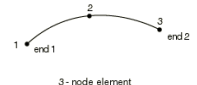
A total of 5 parts were used to represent square tube incased composite column in finite element model. The FEM of the concrete-encased steel composite columns was carried out by modeling the reinforcement bars, stirrups, square structural steel tub, unconfined concrete which consists the concrete cover were and confined concrete and their properties.

### **3.8.1 Element type and selection**

The FEC columns investigated in this study comprised of four components, such as structural steel section, longitudinal reinforcement, transverse reinforcement and concrete. The key in finite element analysis is the appropriate selection of element type. The ABAQUS© standard modules consist of a comprehensive element library that provides different types of elements catering to different situations. When carrying out FE analysis, the selection of a particular type of element is no longer necessary, as most commercially available software packages for composite column design do not offer an option. For reference, it is usual to use a 'beam' element; this will provide results for flexure, shear and displacement directly. Beam and truss elements are generally triangular or quadrilateral with a node at each corner. However, elements have been developed that include an additional node on each side, this gives triangle elements with six nodes and quadrilateral elements with eight nodes. Since the only places where the forces are accurately calculated are at the nodes (they are interpolated at other positions), the accuracy of the model is directly related to the number of nodes. By introducing more nodes into an element, the accuracy of the results is increased; alternatively, the number of elements can be reduced for the same number of nodes, so reducing computational time. For this reason 3D 8-noded hexahedral (brick) elements having 3 degrees of freedom in each node (translations in X, Y and Z directions) are utilized for modeling concrete elements and structural steel with reduced integration (C3D8R) to prevent the shear locking effect. In order to model reinforcements, 2-noded truss elements (T3D2) having 3 degrees of freedom in each node (translations in X, Y and Z directions of global coordinates system) are used. The embedded method with perfect bond between reinforcement and surrounding concrete is adopted to properly simulate the reinforcement-concrete bonding interaction. It is notable that the effects usually associated with reinforcement-concrete interface, such as bond slip and dowel action are modeled indirectly by defining "tension stiffening" into the reinforced concrete model to approximately simulate load transfer across cracks through the rebar (ABAQUS© user's manual (2014)). ABAQUS© has an extensive library of elements that can be

used to model concrete, including both continuum and structural elements. Elements are classified first by the “family” to which they belong.

Table 3.2: Various Elements Used in ABAQUS© (ABAQUS, 2014)

Element	Description	D.O.F	Element shape
C3D8	Hexagonal Element	24	
C3D4	Tetrahedral Element	12	
S4R	shell elements	8	
T3D2	3-dimensional 2-node truss elements	6	
T2D3	2-dimensional 3-node truss elements	6	

### 3.8.2 Meshing

There was two of bodies needed to be discretized through meshing in this study. These are line bodies and solid bodies. Line bodies can be represented by beam and/or truss elements, solid bodies can be meshed with a variety of solid elements ranging from four node tetrahedral elements to polyhedral shapes, shell bodies can be meshed using a variety of shell elements. In ABAQUS© meshing can be done individually on parts and then assembled or vice-versa. In this analysis parts will individually meshed and then assembled for further process. Meshes are composed by tri-dimensional continuum solid elements with 8 node called C3D8R, 8 node linear brick elements with reduced integration and hourglass control are used for both materials, concrete and steel. The

engineer has to assess how fine the mesh should be; a coarse mesh may not give an accurate representation of the forces, especially in locations where the stresses change quickly in a short space e.g. at supports, near openings or under point loads. This is because there are insufficient nodes and the results are based on interpolations between the nodes. However, a very fine mesh will take an excessive time to compute.

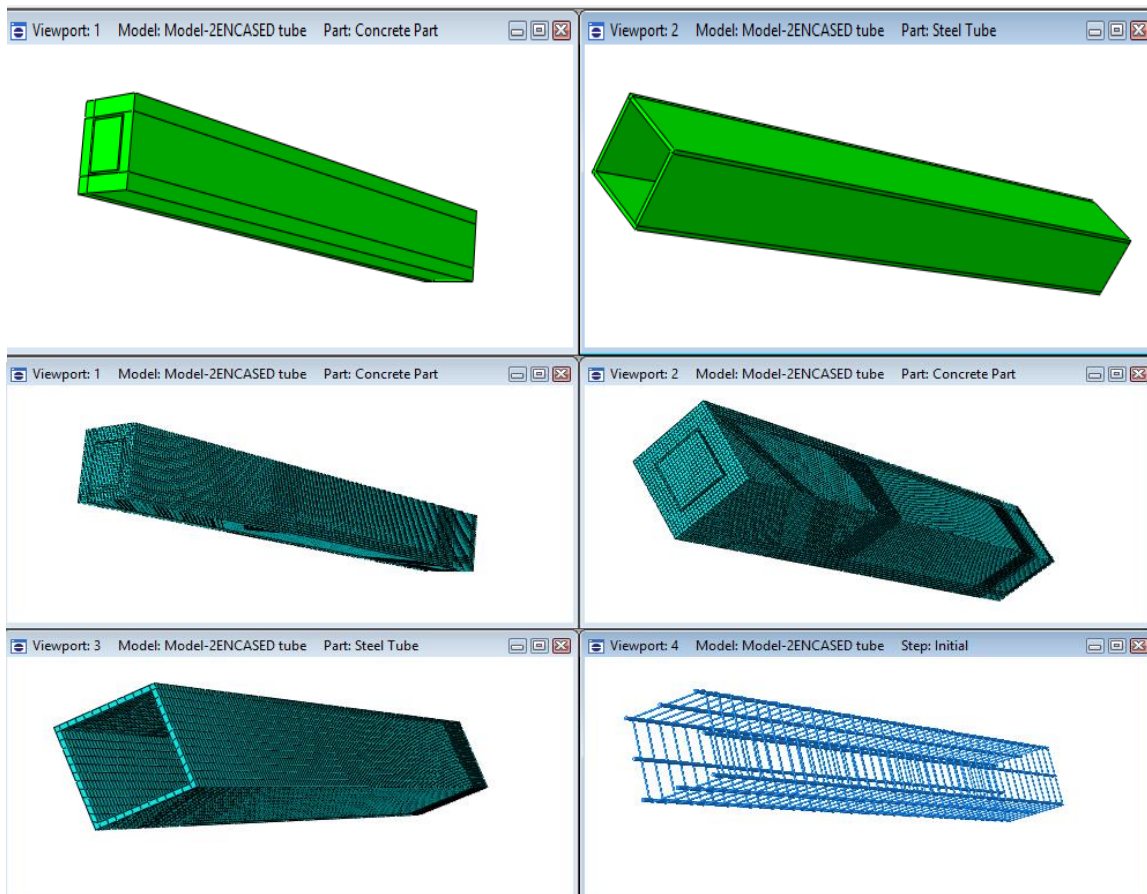


Figure 3.6 Finite element mesh for FEC columns

### 3.8.3 Interactions and Kinematic Constraints between Components.

Kinematic relationship between the various components are required to be defined within the finite element model in order to ensure strain compatibility between the various components. In other words, interactions had to defined such that the equal and opposite loading applied between the bodies results in the one or more bodies deforming together. The interactions that was utilized in the construction of this model was embedded constraints that were used to define the interaction

between the concrete and the steel reinforcement. The second one is surface to surface interaction between structural steel and concrete.

### **EMBEDDED CONSTRAINT**

The elements used for rebars and the structural steel shape of the FEC columns were defined using embedded element option in ABAQUS®/Standard (ABAQUS® user's manual (2014)). This option ensures bonding between concrete and steel part of the column. The embedded element technique is used to specify an element or groups of elements embedded in host elements. In FEC columns, the concrete was defined as the host element whereas the structural steel section and reinforcement were defined as the embedded elements.

### **SURFACE TO SURFACE CONTACT**

The second interactions defined in this model take the form of a surface-based constraint in which a constraint is formed between two surfaces on the geometry, a master and a slave surface. First the surfaces of different components that will be in contact must be created. After that pairs of surfaces which are going to be in contact must be identified. There are two components which define the interaction of contacting surfaces, one normal to the surfaces and one tangential. In ABAQUS® the default normal interaction between the surfaces is called the 'hard contact', meaning that the surfaces can contact each other when the clearance between them becomes zero and they can transmit between each other the unlimited magnitude of pressure but cannot penetrate each other. For interaction, surface to surface contact was created between structural steel profile and concrete with tangential behavior. Penalty method (also known as stiffness method) is used for imposing frictional constraints. This stiffness method allows the relative motion between the surfaces of two materials even when they are sticking.

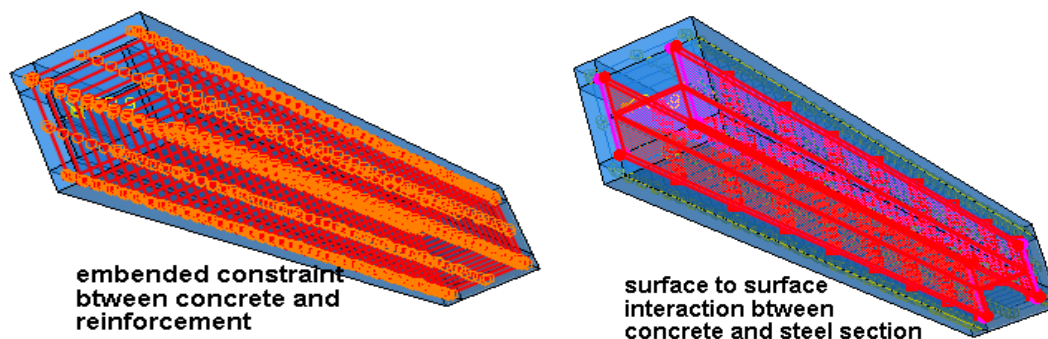


Figure 3.7 Kinematic Constraints between Components

### 3.8.4 Boundary Conditions and Loading

The way in which the bodies within the finite element model interact with each other and with the imposed boundary conditions can impact both the results and stability of the analysis. The first were reactionary boundary conditions that are constant conditions externally imposed on the model. Another type of external boundary condition is those intended to load the structure and change during the course of an analysis.

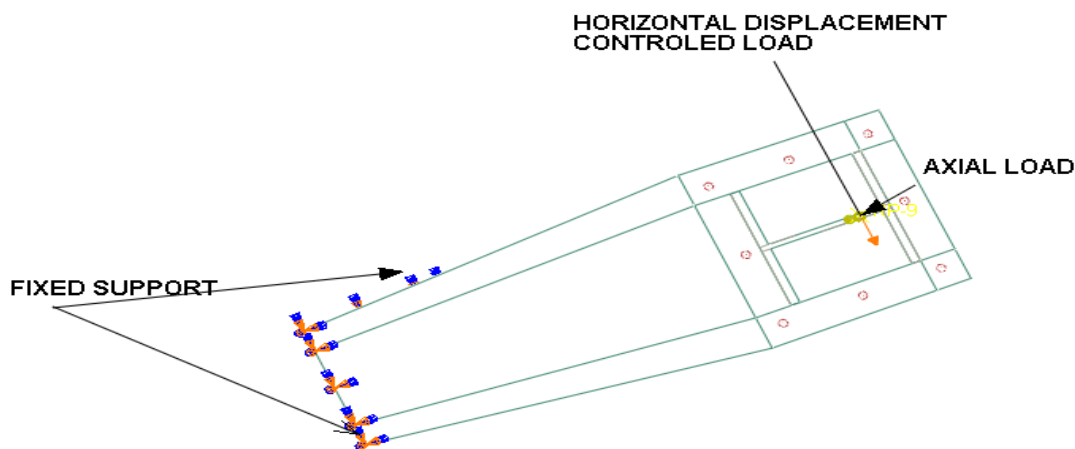


Figure 3.8 End boundary conditions in FE model for concentric load

The boundary conditions applied in the FE model to simulate the conditions for concentrically loaded specimens are shown in Figure 3.6. In concentrically loaded column tests, the bottom end of the column was fixed and the axial load was applied through rigid body reference node at the center of the top end of the column. The rotations and horizontal translations at the top surface

were fixed. Since the load is applied at the top the vertical restraint was released. The axial load was applied using a displacement control technique. In the finite element model for concentrically loaded test specimens, cantilever conditions were applied at the end eccentric points located on the end rigid planes. A rigid body reference node is defined on the top of the column to apply displacement.

### **3.9 Material Modeling**

The material definition is an important part of finite element analysis, and each component should be defined carefully and all parts should be defined with appropriate material parameters. Steel, concrete and rebars are the main materials used in construction of FEC columns for this study. The nonlinear behavior of these three materials were incorporated in the FE model using the appropriate material models for steel, concrete and rebars that available in the ABAQUS® (HKS 2013) finite element code. The description of the material models for steel and concrete along with their mechanical properties (stress versus strain relationship) used in the FE model is described in the following sections.

#### **3.9.1 Compression properties of concrete**

Concrete is one of our most common building materials and is used both for buildings, bridges and other heavy structures. Typically, concrete structures are very durable, but sometimes they need to be strengthened. Concrete is a material that can withstand compressive loads very well but is sensitive to tensile forces. Therefore, concrete structures are typically reinforced by casting in steel bars in areas where tension can arise. This study involve two major variation in concrete application in encased composite column, concrete is in state of confinement and in concrete cover only it is in state of un confined. Concrete experiences different characteristics in both condition. But for this study, since the concrete in the concrete section is very small it is modeled as confined concrete as whole in the column.

##### **3.9.1.1 Unconfined properties of concrete in concrete cover section**

(EBCS EN1992, 2015) will be used in this study for the unconfined concrete, the relation between  $\sigma_c$  and  $\varepsilon_c$  under uniaxial loading was described in (EBCS EN1992, 2015), and it proposed single equation to describe unconfined concrete stress strain behavior as follow by expression (3.1). On the basis of uniaxial compression test results one can accurately determine the way in

which the material behaved. However, a problem arises when the person running such a numerical simulation has no such test results or when the analysis is performed for a new structure. Then often the only available quantity is the average compressive strength ( $f_{cm}$ ) of the concrete. Another quantity which must be known in order to begin an analysis of the stress-strain curve is the longitudinal modulus of elasticity ( $E_{cm}$ ) of the concrete. Its value can be calculated using the relations available in the literature (EBCS EN1992, 2015).

$$\frac{\sigma_c}{f_{cm}} = \frac{k\eta - \eta^2}{1 + (k - 2)\eta} \quad (3.1)$$

Where; 
$$\eta = \frac{\epsilon_c}{\epsilon_{c1}}, \quad (3.2)$$

$$k = 1.05E_{cm} \times \frac{|\epsilon_{c1}|}{f_{cm}} \quad (3.3)$$

$$E_{cm} = 22(0.1f_{cm})^{0.3} \quad (3.4)$$

$$\epsilon_{c1} = 0.7(f_{cm})^{0.31} \quad (3.5)$$

$$\epsilon_{cu} = 3.5\% \quad (3.6)$$

$$f_{cm} = f_{ck} + 8 \quad (3.7)$$

$\epsilon_{c1}$  is strain at average compressive strength,

$f_{cm}$  is mean value of concrete cylindrical comparative strength (Mpa)

$E_{cm}$  is the longitudinal modulus of elasticity (Mpa)

$f_{ck}$  is characteristic cylindrical strength of concrete(Mpa) all of the equation are from EBCS EN 1992-1-1:2013

The above equation is valid for  $0 < \epsilon_c < \epsilon_{c_{ul}}$  where  $\epsilon_{c_{ul}}$  nominal ultimate strain.

Figure 3.9 describe the developed stress strain relationship as provided in (EBCS EN1992, 2015), the specific development for this study was provided in appendix A.

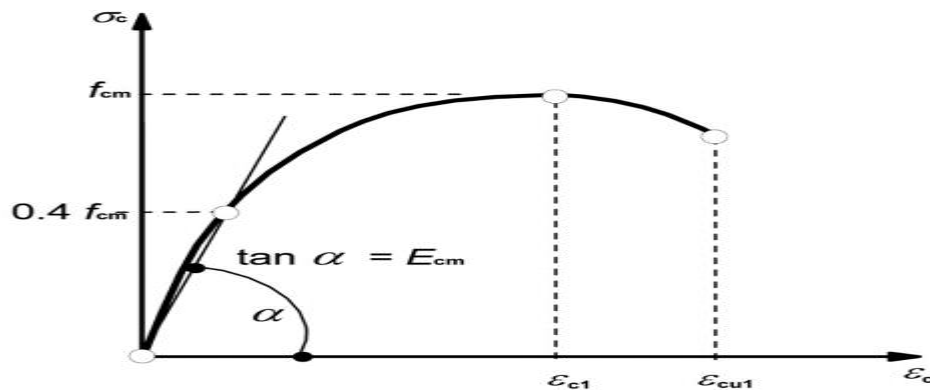


Figure 3.9 Stress-strain relation for non-linear structural analysis (EBCS EN1992, 2015).

### 3.9.1.2 Confined properties of concrete in column

The confinement of the concrete by stirrups has been recognized in early research. This confinement can provide a confining pressure which leads in an enhancement in the strength and ductility of concrete (Chen & Lin, 2006). Confinement of concrete results in a modification of the effective stress relationship: higher strength and higher critical strains are achieved. The other basic material characteristics may be considered as unaffected for design. For encased composite columns, the amount of the confining pressure depends on the steel section shape and its yield strength in addition to the factors that mentioned earlier. As a result, a highly confined zone occurs resulting from arching action formed by steel section. In the absence of more precise data, the stress-strain relation shown in Fig. 3.2 (compressive strain shown positive) may be used, with increased characteristic strength and strains according to:

$$f_{ck,c} = f_{ck} \left( 1.00 + 5.0 \frac{\sigma_2}{f_{ck}} \right) \quad \text{for } \sigma_2 \leq 0.05 f_{ck} \quad (3.8)$$

$$f_{ck,c} = f_{ck} \left( 1.25 + 2.5 \frac{\sigma_2}{f_{ck}} \right) \quad \text{for } \sigma_2 \geq 0.05 f_{ck} \quad (3.9)$$

$$\epsilon_{c2,c} = \epsilon_{c2} \left( \frac{f_{ck,c}}{f_{ck}} \right)^2 \quad (3.10)$$

$$\epsilon_{cu2,c} = \epsilon_{cu2} \frac{\sigma_2}{f_{ck}} \quad (3.11)$$



Where:  $\sigma_2 = \sigma_3$  is the effective lateral compressive stress at the ULS due to confinement and  $\varepsilon_{c2,c}$  and  $\varepsilon_{cu2,c}$  follow from code provision.

$$\varepsilon_{c2} = 2\% \tag{3.12}$$

$$\varepsilon_{cu2} = 3.5\% \tag{3.13}$$

Confinement can be generated by adequately closed links or cross-ties, which can reach the plastic condition due to lateral extension of the concrete

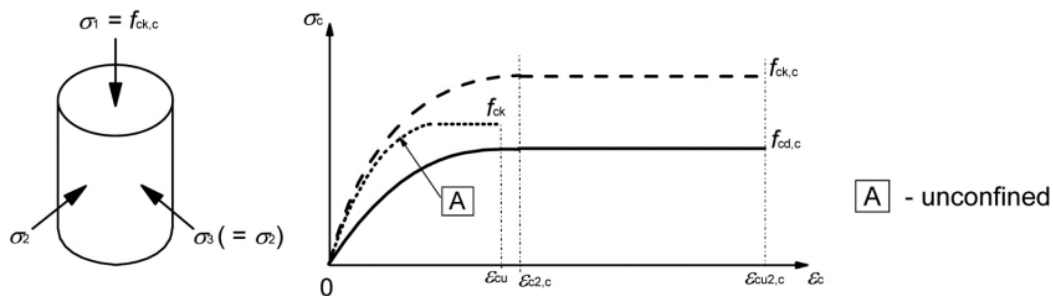


Figure 3.10 Stress-strain relationship for Confined Concrete (EBCS EN1992, 2015).

### 3.9.2 Tension properties of concrete

ABAQUS© provides a number of option for defining tensile behavior of concrete. The stress can be related to the strain in the direction of the cracking or displacement which refers to crack width, and fracture energy,  $G_f$ . Alternatively, the fracture energy,  $G_f$  can be specified directly as a material property; in this case, define the failure stress, as a tabular function of the associated fracture energy. This model assumes a linear loss of strength after cracking (ABAQUS© software (SIMULIA, 2014)). The cracking displacement at which complete loss of strength takes place is, therefore,  $\varepsilon_{to} = 2 \frac{G_f}{\sigma_{to}}$  Typical values of  $G_f$  range from 40 N/m for a typical construction concrete

(with a compressive strength of approximately 20 MPa, to 120 N/m for a high-strength concrete (with a compressive strength of approximately 40 MPa. If tensile damage,  $d_t$  is specified, ABAQUS© automatically converts the cracking displacement values to “plastic” displacement values using the relationship:

$$\epsilon_t^{pl} = \epsilon_t^{ck} - \frac{d_t}{(1-d_t)} * \left( \frac{\sigma_t}{E_o} \right) \tag{3.14}$$

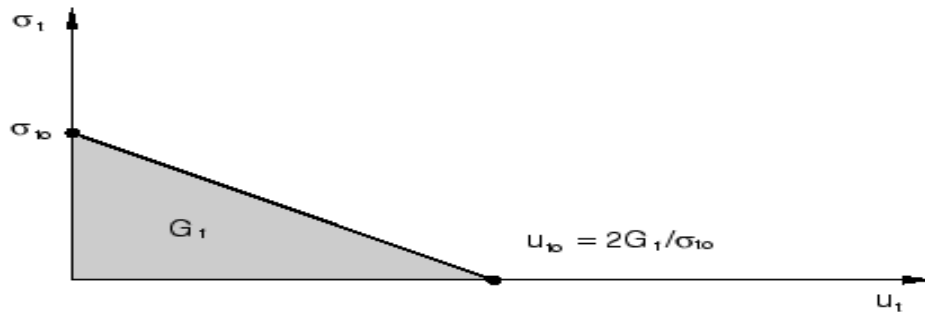


Figure 3.11 Post failure stress-fracture energy curve. (Abaqus user Manual, 2014)

### 3.9.3 Damage plasticity modeling of concrete

Damage is defined both for uniaxial tension and compression on during softening procedure in concrete damage plasticity model. Damage in compression occurs just after reaching to the maximum uniaxial compressive strength corresponding to strain level  $\epsilon_o$ . The degradation of elastic stiffness in softening regime is characterized by two damage variables,  $dt$  and  $dc$  corresponding to tensile and compressive damage, respectively, which are assumed to be functions of the plastic strains. Tensile and compressive damage in concrete damage plasticity model in the presented numerical model is assumed to be according to equations above and diagrams of Figure 3.10 and Figure 3.11.

ABAQUS© software (SIMULIA, 2014) provides the capability of simulating the damage using either of the three crack models for concrete elements: (1) Smearred crack concrete model, (2) Brittle crack concrete model, and (3) Concrete damaged plasticity model. Out of the three concrete crack models, the concrete damaged plasticity model is selected in the present study as this technique has the potential to represent complete inelastic behavior of concrete both in tension and compression including damage characteristics (Najafgholipour et al., 2017). Further, this is the only model which can be used both in ABAQUS©/Standard and ABAQUS©/Explicit and thus enable the transfer of results between the two. Therefore, development of a proper damage simulation model using the concrete damaged plasticity model will be useful for the analysis of reinforced concrete structures under any loading combinations including both static and dynamic

loading (“ABAQUS© Analysis User Manual – ABAQUS© Version 6.14” [ABAQUS© Manual], 2014).

The concrete damaged plasticity model assumes that the two main failure mechanisms in concrete are the tensile cracking and the compressive crushing. In this model, the uniaxial tensile and compressive behavior is characterized by damaged plasticity (Wahalathantri et al., 2012). Concrete damaged plasticity model “takes into consideration the degradation of the elastic stiffness induced by plastic straining both in tension and compression. It also accounts for stiffness recovery effects under cyclic loading.” The compressive behavior is elastic until initial yield and then is characterized by stress hardening followed by strain softening after the ultimate point. ABAQUS© manual proposes an exponential function which can calculate the tensile damage variable ( $d_c$ ) and the compressive damage variable ( $d_t$ ).

### 3.9.3.1 Tension Stiffening Relationship

In order to simulate the complete tensile behavior of reinforced concrete in ABAQUS©, a post failure stress-strain relationship for concrete subjected to tension (similar to Figure 3.12) is used which accounts for tension stiffening, strain-softening, and steel concrete interaction with concrete. To develop this model, user should input young’s modulus ( $E_0$ ), stress ( $\sigma_t$ ), cracking strain ( $\epsilon_t^{ck}$ ) values and the damage parameter values ( $d_t$ ) for the relevant grade of concrete. The cracking strain ( $\epsilon_t^{ck}$ ) should be calculated from the total strain using (equation 3.15) below:

$$\epsilon_t^{ck} = \epsilon_t - \epsilon_{ot}^{el} \quad (3.15)$$

Where:

$$\epsilon_{ot}^{el} = \frac{\sigma_t}{E_0}, \text{ the Elastic strain corresponding to the undamaged material,}$$

$$\epsilon_t = \text{total strain}$$

Having defined the yield stress-inelastic strain pair of variables, one needs to define now degradation variable  $d_c$ . It ranges from zero for an undamaged material to one for the total loss of load-bearing capacity (Kmieciak and Kamiski, 2011). These values can also be obtained from uniaxial compression tests, by calculating the ratio of the stress for the declining part of the curve

to the compressive strength of the concrete. Thanks to the above definition the CDP model allows one to calculate plastic strain from the formula:

$$\varepsilon_t^{pl} = \varepsilon_t^{ck} - \frac{d_c}{(1-d_c)} \frac{\sigma_t}{E_o} \tag{3.16}$$

Where;  $E_o$  stands for the initial modulus of elasticity for the undamaged material. Knowing the plastic strain and having determined the flow and failure surface area one can calculate stress  $\sigma_t$  for uniaxial compression and its effective stress  $\overline{\sigma}_t$ .

$$\sigma_t = (1-d_c) E_o (\varepsilon_t - \varepsilon_t^{pl}) \tag{3.17}$$

The damage plasticity constitutive model was based on the following stress–strain relationship:

$$\overline{\sigma}_t = \frac{\sigma_t}{(1-d_c)} = E_o (\varepsilon_t - \varepsilon_t^{pl}) \tag{3.18}$$

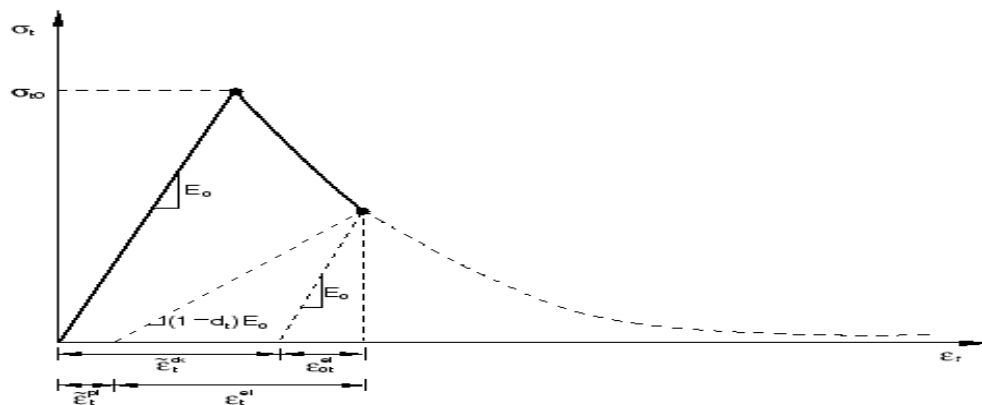


Figure 3.12 Terms for Tension Stiffening Model (Abaqus user Manual, 2014)

Where  $d_t$  and  $d_c$  were two scalar damage variables, ranging from 0 (undamaged) to 1 (fully damaged) (Hafezolghorani et al., 2017). The damage model used for concrete was based on plasticity and considered the failure process of tensile cracking and compressive crushing. The uniaxial compressive and tensile responses of concrete with respect to the concrete damage plasticity model subjected to compression and tension load were given by:

$$\varepsilon_c^{pl} = \varepsilon_c^{ck} - \frac{d_c}{(1-d_c)} \frac{\sigma_c}{E_o} \tag{3.19}$$

$$\sigma_c = (1-d_c) E_o (\varepsilon_c - \varepsilon_c^{pl}) \tag{3.20}$$

$$\bar{\sigma}_c = \frac{\sigma_c}{(1-d_c)} = E_o(\epsilon_c - \epsilon_c^{pl}) \tag{3.21}$$

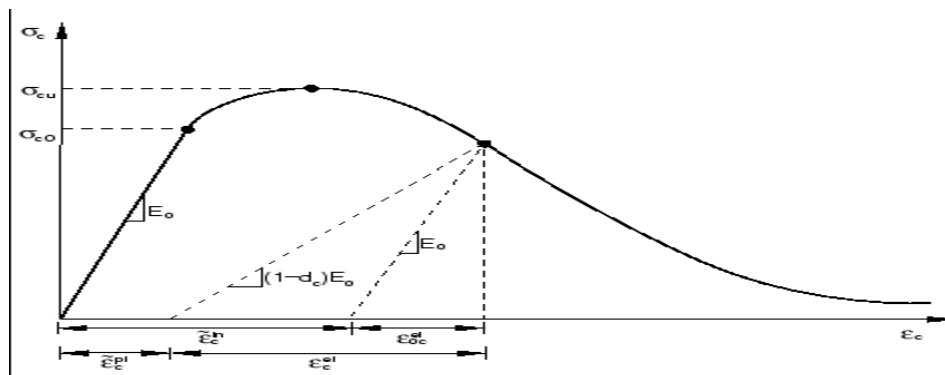


Figure 3.13 Response of concrete to a uniaxial loading condition in compression (Abaqus Manual, 2014)

Another parameter describing the state of the material is the point in which the concrete undergoes failure under biaxial compression.  $(f_{b0} / f_{c0})$  is a ratio of the strength in the biaxial state to the strength in the uniaxial state. The ABAQUS user’s manual specifies default  $(f_{b0} / f_{c0}) = 1.16$ . The last parameter characterizing the performance of concrete under compound stress is *dilatation angle*, i.e. the angle of inclination of the failure surface towards the hydrostatic axis, measured in the failure plane. Physically, dilatation angle  $\psi$  is interpreted as a concrete internal friction angle. In simulations usually  $\psi = 36^\circ$  or  $\psi = 40^\circ$  is assumed.

Table 3.3 Default parameters of CDP model under compound stress

Parameter name	Value
Dilatation angle	36
Eccentricity	0.1
$f_{b0} / f_{c0}$	1.16
k	0.667
Viscosity parameter	0

### 3.9.4 Structural Steel and Reinforcement material modeling

The structural steel section and the reinforcement bars are modeled as an elastic– plastic material in both tension and compression as given in (Euro code 3, 2005), (Abaqus Manual, 2014)

and (Euro code 2, 2005). Steel is a ductile material which experiences large inelastic strain beyond the yield point. So the true stress and logarithmic strain graph which is also called hardening curve, as shown in Figure 3.14, is considered for modeling the material behavior of steel. The stress–strain responses in compression and tension are assumed to be the same. This response exhibits a linear elastic portion followed strain hardening stage until reach the ultimate stress. The metal plasticity model in ABAQUS© was used to define the non-linear behavior of materials. The “ELASTIC” option was used to assign the value of  $2.0 \times 10^5$  N/mm<sup>2</sup> for the Young’s modulus and 0.3 for the Poisson’s ratio. The “PLASTIC” option also used to define the plastic part of the stress–strain curve. According to ABAQUS© manual (ABAQUS, 2014), true stress and true strain should be used to define the non-linear behavior of material properties. So, the true stresses were assigned in ABAQUS© as a function of the true plastic strain. To investigate numerically the post buckling behavior of the columns it is necessary to represent correctly the inelastic material properties in the FE models. The Mises yield surface is defined by giving the value of the uniaxial yield stress as a function of uniaxial equivalent plastic strain. The curve in Figure 3.14 named “ABAQUS input” depicts the relation between true stress  $\sigma_{true}$  and true plastic strain  $\epsilon_{true}$ : The stress and strain data obtained from the uniaxial tension tests are converted to true stress,  $\sigma_{true}$  and logarithmic plastic strain,  $\epsilon_{true}$ , for FE analysis using the following relationships:

$$\sigma_{true} = \sigma_{nom} (1 + \epsilon_{nom}) \quad (3.22)$$

$$\epsilon_{true} = \ln(1 + \epsilon_{nom}) \quad (3.23)$$

Where;

$\epsilon_{nom}$  is the nominal or engineering strain

$\sigma_{nom}$  is the nominal or engineering stress

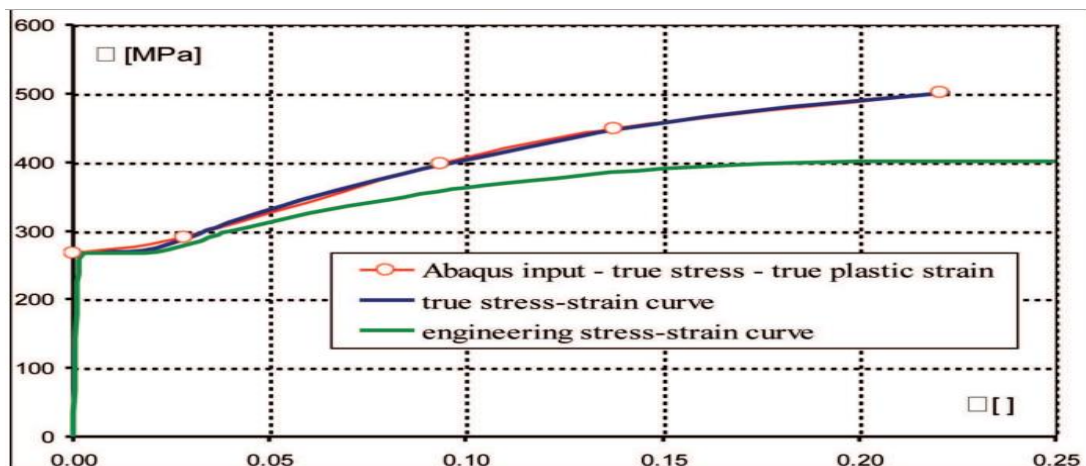


Figure 3.14 Abaqus input Stress – strain curves for steel (Kwaśniewski et al., 2011)

Mechanical properties for the steel section and reinforcement bars that are used in these simulations are given in Table 3.4

Table 3.4: Mechanical Properties of the Steel Section and Reinforcement Bars and concrete used for this study

Part	Yield stress (N/mm <sup>2</sup> )	Ultimate stress (N/mm <sup>2</sup> )	Density (Kg/m <sup>3</sup> )	Young's modulus (KN/mm <sup>2</sup> )	Poisson ratio
Steel section	355	510	7850	210	0.3
Reinforcement bars	400	560	7850	200	0.3
Concrete			2400	36.283	0.2

### 3.9.4.1 Mechanical properties of structural steel

The material coefficients to be adopted in calculations for the structural steels covered by this Eurocode Part should be taken as follows:

Modulus of elasticity  $E = 210\,000\text{ N/mm}^2$

Shear modulus  $G = E/2(1+\nu) = 81000\text{ N/mm}^2$

Poisson's ratio  $\nu = 0.3$

Hot rolled or cold rolled steel was used for composite structure construction. But hot rolled was recommended for their rough surface finish which was used in bondage of concrete to steel.

### 3.10 PARAMATRIC STUDY

#### Design of Parametric Study

For this parametric study a square column with outer dimensions of 400 mm × 400 mm was selected. Typical cross section and elevation of FEC column used in the parametric study are shown in Figure 3.1 and 3.2. This column was designed and analyzed during the parametric study to incorporate the effects of several geometric parameters that can significantly affect the FEC column behavior. The geometric variables are shape of structural steel, over all column slenderness and spacing of ties. .

#### Column slenderness ratio (L/D)

The column slenderness ratio used in this study is defined as the ratio of the length (L), to the depth of the column cross-section (D). The global stability of the column is controlled by the slenderness (L/D) ratio. Three different slenderness ratios 7.5, 11.25 and 15 were employed in the parametric study (as shown in Table 3.5) to cover the range of short, intermediate and long columns. These parametric studies were carried out on different type of structural steel profile H shaped, circular tube and square tube of the same cross sectional area.

Table 3.5 Columns for investigating the effect of slenderness ratio (L/D)

Group	Specimen	Section(mm)	Length(mm)	L/D	s/D	Encased steel type
Group1	ETS1	400x400	3000	7.5	0.375	Square tube of d x b x t (mm) 250 x 250 x 12.5
	ETS2	400x400	4500	11.25	0.375	
	ETS3	400x400	6000	15	0.375	
Group2	ECS4	400x400	3000	7.5	0.375	Circular tube of D x t (mm) 245 x 16.5
	ECS5	400x400	4500	11.25	0.375	
	ECS6	400x400	6000	15	0.375	
Group3	EHS7	400x400	3000	7.5	0.375	H section of b <sub>f</sub> x d x t <sub>f</sub> x t <sub>w</sub> (mm) 260 x 260 x 17.5 x 10
	EHS8	400x400	4500	11.25	0.375	
	EHS9	400x400	6000	15	0.375	



### Transverse reinforcement spacing ratio ( $s/D$ )

The primary purpose of transverse reinforcement in concrete-encased composite columns is to provide concrete confinement to prevent spalling around the structural steel core and to properly support longitudinal reinforcement to prevent buckling of the bars. Transverse reinforcement can also provide additional shear capacity. Therefore, transverse reinforcement spacing is an important parameter affecting the ultimate strength and behaviour of columns. The effect of the transverse reinforcement spacing was studied by varying the ratio of transverse tie spacing, ( $s$ ), to the depth of the column cross-section, ( $D$ ). Three values of the  $s/D$  ratio 0.1875 (75mm/400mm), 0.375(150mm/400mm) and 0.5(200mm/400mm) (Table 3.6) were used in the parametric study to determine the effect.

Table 3.6 Columns for investigating the effect of transverse reinforcement spacing, ( $s/D$ )

Group	Specimen	Section(mm)	Length(mm)	L/D	$s/D$	Encased steel type
Group4	ETS10	400x400	6000	15	0.1875	Square tube of $d \times b \times t$ (mm) 250 x 250 x 12.5
	ETS11	400x400	6000	15	0.375	
	ETS12	400x400	6000	15	0.5	
Group5	ECS13	400x400	6000	15	0.1875	Circular tube of $D \times t$ (mm) 245 x 16.5
	ECS14	400x400	6000	15	0.375	
	ECS15	400x400	6000	15	0.5	
Group6	EHS16	400x400	6000	15	0.1875	H section of $b_f \times d \times t_f \times t_w$ (mm) 260 x 260 x 17.5 x 10
	EHS17	400x400	6000	15	0.375	
	EHS18	400x400	6000	15	0.5	

## CHAPTER FOUR

### RESULTS AND DISCUSSION

#### 4.1 General

The main purpose of this study was to determine the effects of different encased structural profile on the cyclic capacity of square tube encased, circular tube encased, and H profile encased composite columns. To achieve this, a finite element analysis was conducted with all appropriate parameters considered and data was collected. This data was then analyzed to provide understandings into encased composite columns behavior under horizontal cyclic and axial loading. Factors explored included lateral load capacity and axial deformation, Lateral Load versus lateral displacement response (Hysteretic behavior) and failure mode. Observations are made through the aid of plots of output data and photographs in developing relationships between parameters and behavior. Next sections provide a summary of key specimen results.

#### 4.2 Effect of overall column slenderness ratio

The global stability of the column is controlled by the overall slenderness ratio. The column slenderness ratio is defined as the ratio of the length (L), to the depth of the column cross-section (D). Figure 4.1 through 4.3, shows the effect of overall column slenderness (L/D) ratio on the load displacement response of the column. Nine columns (Tables 3.6) divided into three groups (Group 1, 2 and 3) were analyzed to observe the effects of overall slenderness ratio. Columns in Group 1 (ETS1, ETS2 and ETS3) was modeled with normal strength concrete (30 MPa) and had a square tube structural steel as encasement. On the other hand, Group 2(ECS4, ECS5 and ECS6) columns were modeled using (30 MPa) concrete and had circular tube structural steel as encasement. The column in Group 3(EHS7, EHS8 and EHE9) column were modeled with normal strength concrete (30 MPa) and had H profile structural steel as encasement. The axial load was applied concentrically on the upper part of column at loading point. The slenderness ratios (L/D) of these columns were varied as 7.5, 11.25 and 15. All the columns were constructed with constant transverse reinforcement spacing of ( $s/D = 0.375$ ) 150 mm.

**4.2.1 Axial Load versus axial deformation response**

Figures 4.1, 4.2 and 4.3 show the effects of slenderness (L/D) ratios on the axial load versus axial deformation responses for Group 1, Group 2, and Group 3 respectively. The axial capacity and stiffness of FEC columns were observed to decrease with the increase in slenderness ratio. The ascending part of axial load versus axial deformation curve (Figure 4.1) of column ETS (L/D = 7.5) was comparatively stiffer than other columns of this Group 1. Similar behavior was also observed for columns in Group 2 and 3. As the column gets slender the axial deformation increases accompanied by a decrease in the axial load. Encased composite column of ETS shows a good performance than other two types of column (ECS and EHS) for all length of the column. This is generally due to greater stiffness of ETS column than the rest of column. For this particular study ETS is 44% stiffer than ECS type of column. Columns length 3000mm (ETS1, ECS4 and EHS7) are used as a reference to determine the effects of selected parameter (L/D).

Table 4.1 Effect of slenderness ratio (L/D) on peak axial load and axial deformation

Group	Specimen	Length(mm)	L/D	s/D	Peak axial load(KN)	Percent Difference (%)	Axial Deformation(mm)	Percent Difference (%)
Group 1	ETS1	3000	7.5	0.375	3500.07	ref column	7.708	ref column
	ETS2	4500	11.25	0.375	3381.52	3.4	8	3.7
	ETS3	6000	15	0.375	3155.88	9.83	9	16.76
Group 2	ECS4	3000	7.5	0.375	3525.474	ref column	7	ref column
	ECS5	4500	11.25	0.375	3207.491	3.363	7.5	7.1
	ECS6	6000	15	0.375	2953.505	13.18	8	14.28
Group 3	EHS7	3000	7.5	0.375	3383.779	ref column	8	ref column
	EHS8	4500	11.25	0.375	3156.274	6.74	8.5	10
	EHS9	6000	15	0.375	2915.804	13.83	10	25

Figures 4.1 show the effects of slenderness (L/D) ratios on the axial load versus axial deformation responses for Group 1. The axial capacity and stiffness of FEC columns were observed to decrease with the increase in slenderness ratio. It was observed from these Figures that the axial load and stiffness of the FEC column is greatly affected by the slenderness ratio (L/D). When overall slenderness ratio increases, the axial load capacity is reduced by 3.4% to 9.83%,

respectively for L/D of 11.25 and 15 for ETS group. But the axial deformation increased by 3.7% and 16.76%.

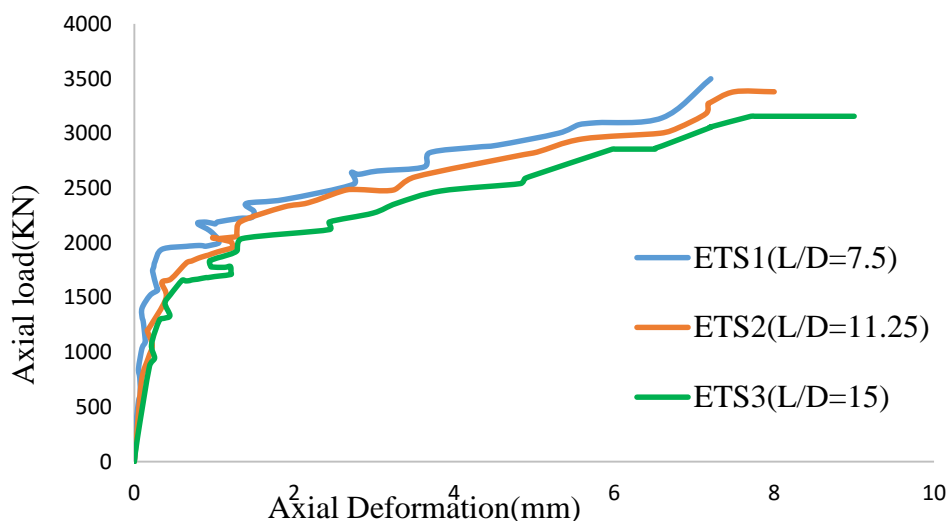


Figure 4.1 Effect of L/D ratios on axial load versus axial deformation curve (Group 1)

Figures 4.2 show the effects of slenderness (L/D) ratios on the axial load versus axial deformation responses for Group 2. The axial capacity and stiffness of FEC columns were observed to decrease with the increase in slenderness ratio. It was observed from these Figures that the axial load and stiffness of the FEC column is greatly affected by the slenderness ratio (L/D). When overall slenderness ratio increases, the axial load capacity is reduced by 6.363% to 13.18%, respectively for L/D of 11.25 and 15 for ECS group. For this group axial deformation was increased by 7.1% and 14.28% respectively.

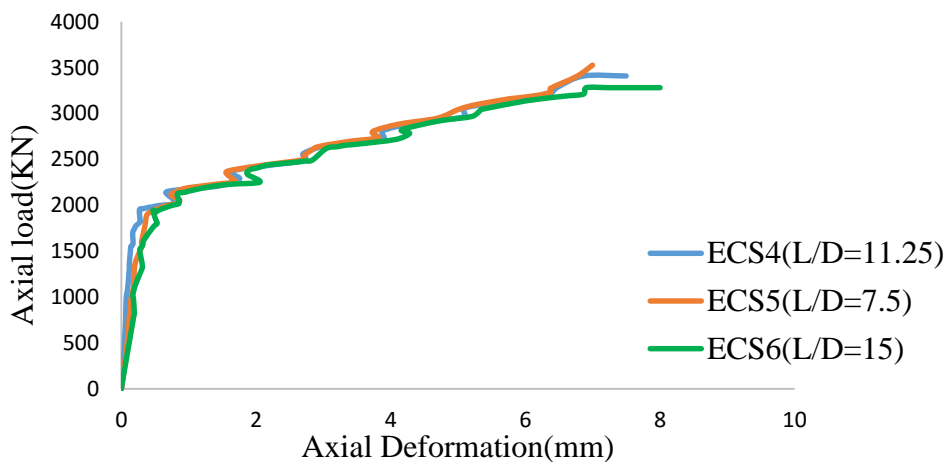


Figure 4.2 Effect of L/D ratios on axial load versus axial deformation curve (Group 2)

Axial load versus axial displacement curve for the columns of Group 3 was shown in the Figures 4.3. The nonlinear behaviour occurred due to the increased second order displacement in the slender columns. The axial capacity and stiffness of FEC columns were observed to decrease with the increase in slenderness ratio. It was observed from these Figures that the axial load and stiffness of the FEC column is greatly affected by the slenderness ratio ( $L/D$ ). When overall slenderness ratio increases, the axial load capacity is reduced by 6.74% to 13.83%, respectively for  $L/D$  of 11.25 and 15 for EHS group. As the column gets slender the axial deformation increases accompanied by a decrease in the axial load.

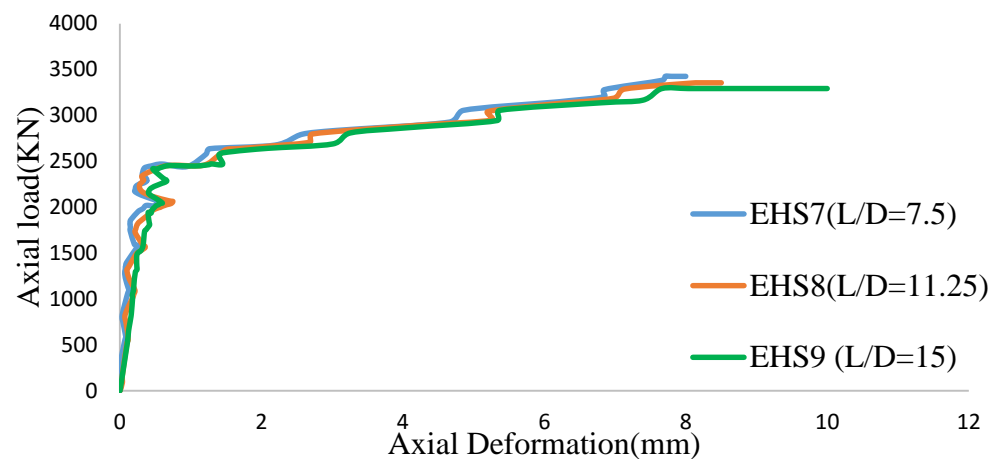


Figure 4.3 Effect of  $L/D$  ratios on axial load versus axial deformation curve (Group 3)

#### 4.2.2 Modes of failure

The influence of slenderness ratio ( $L/D$ ) on the failure mode of FEC is showed in the figure 4.4 through 4.10. The failure in the columns in Group 1, 2 and 3 was attained by crushing of concrete followed by yielding of structural steel and reinforcement bar respectively. The failure mechanisms of all the columns ETS, ECS and EHS were almost the same for each of which have the same slenderness ratio.

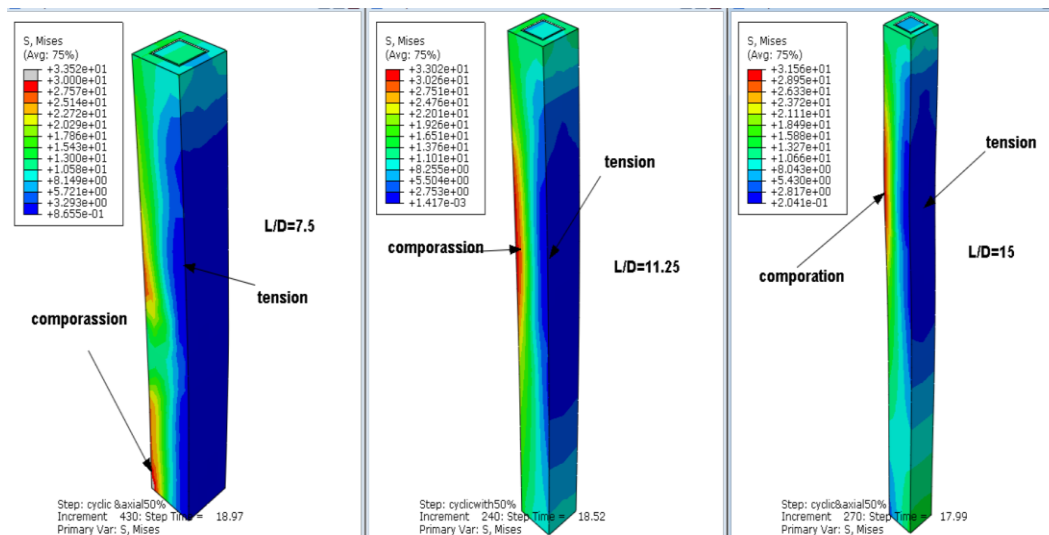


Figure 4.4 Deformed shape and stress contour of concrete at failure (Group 1)

Figure 4.4 shows that the sequence of failure mode for columns ETS was as follows: crushing/ failure of concrete occurred at the lower part of the column for columns type of  $L/D=7.5$  and with increasing over all slender ratio the crushing/ failures concrete starts at mid height and above mid height of columns for column type of  $L/D=11.25$  and columns type of  $L/D=15$  respectively. Next to crushing/ or failure of concrete followed by yielding of structural steel encasement. Finally the yielding of reinforcement bar was occurred.

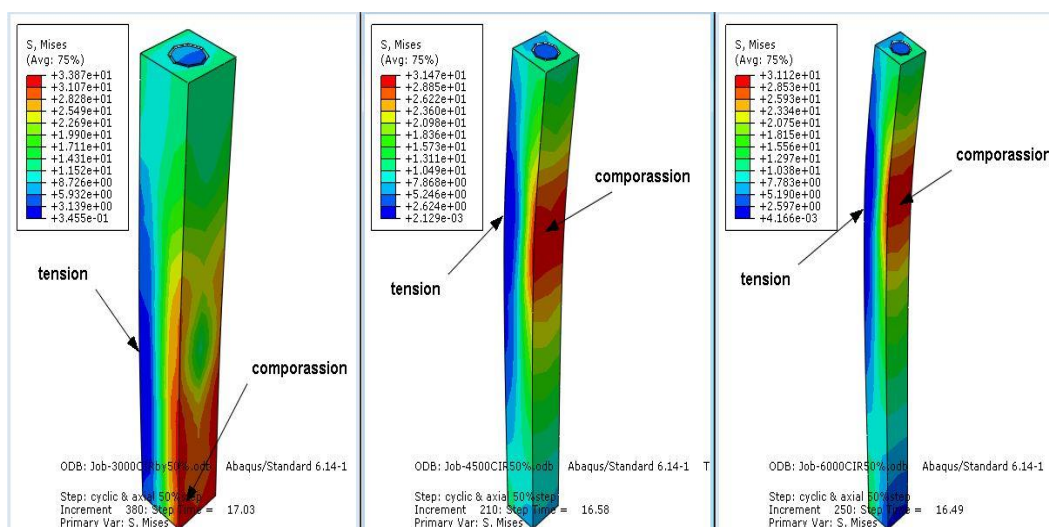


Figure 4.5 Deformed shape and stress contour of concrete at failure (Group 2)

Figure 4.5 depicts the failure condition of each specimens and the deformed shape along with stress contour at failure for ECS ( $L/D = 7.5, 11.25, 15$ ) from output of FEM analysis

respectively. Crushing/ failure of concrete occurred at the lower part of the column for columns type of  $L/D=7.5$  and with increasing over all slender ratio the crushing/ failures concrete starts at mid height and above mid height of columns for column type of  $L/D=11.25$  and columns type of  $L/D=15$  respectively.

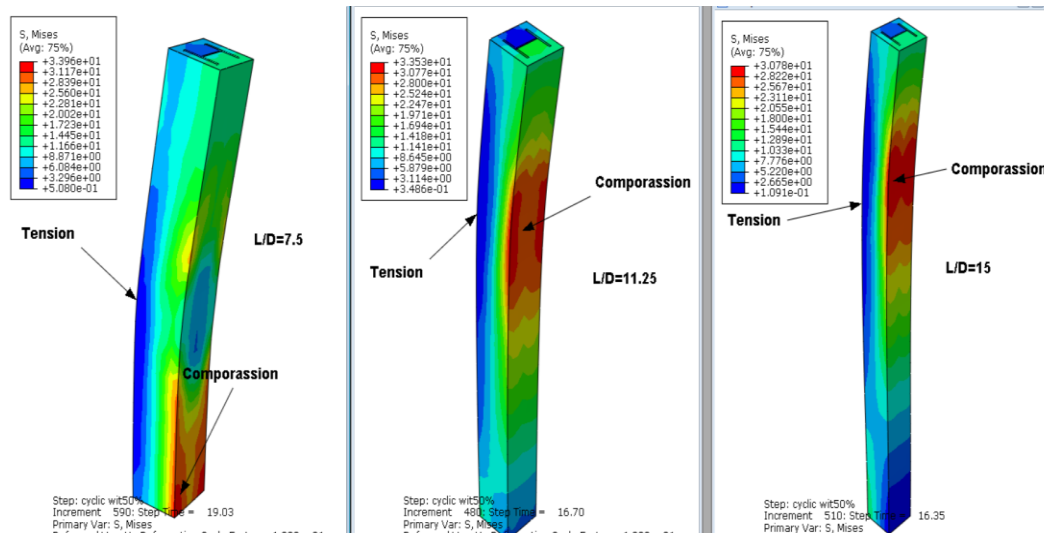


Figure 4.6 Deformed shape and stress contour of concrete at failure (Group 3)

Figure 4.6 shows the failures of the columns EHS were attained mainly due to crushing of concrete at the compression side of the column. It was found that the compressive stress of concrete was comparatively higher at failure of the column with lower slenderness ratio ( $L/D=7.5$ ) than that with higher slenderness ratios. The tensile stress of concrete decreased with the increase of slenderness ratio. It was observed from the Figures that the tensile stress of concrete in column ( $L/D = 15$ ) is comparatively greater than other columns.

The data obtained from FE analysis showed that the structural steel reached its yield stress and the flexural buckling failure mode was governed by the concrete elements at the maximum stressed fibers. Figure 4.7, 4.8, 4.9 shows the deformed shape of structural steel at failure for specimen ETS ( $L/D = 7.5, 11.25, 15$ ), ECS ( $L/D = 7.5, 11.25, 15$ ) and EHS ( $L/D = 7.5, 11.25, 15$ ) respectively.

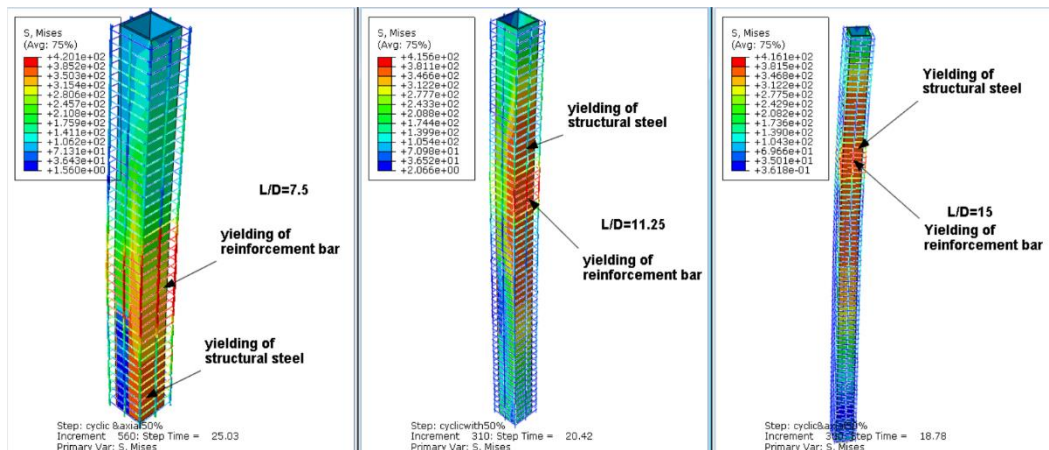


Figure 4.7 Deformed shape and stress contour in structural steel at failure (Group 1)

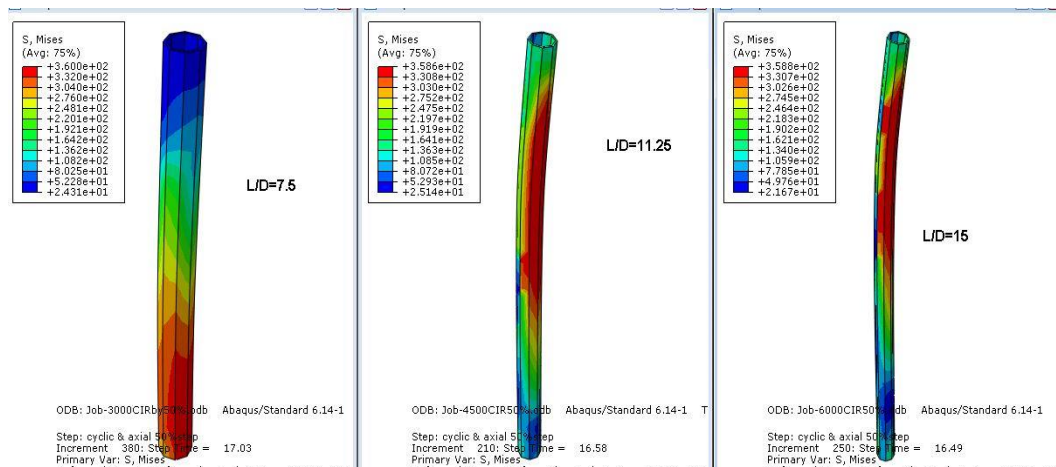


Figure 4.8 Deformed shape and stress contour in structural steel at failure (Group 2)

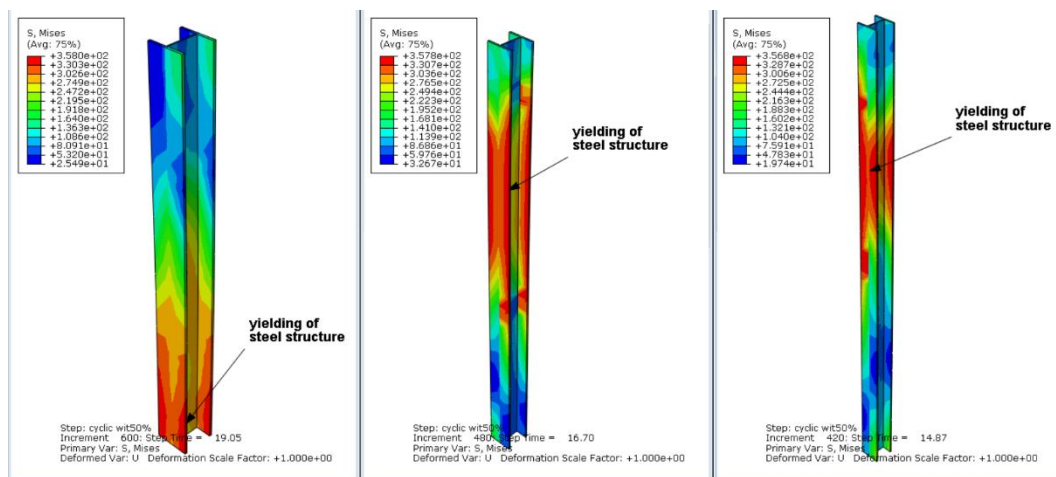


Figure 4.9 Deformed shape and stress contour in structural steel at failure (Group 3)



Figure 4.10 shows the failure mode of reinforcement bar as the slenderness ratio of column increased from 7.5 to 11.25 and then to 15

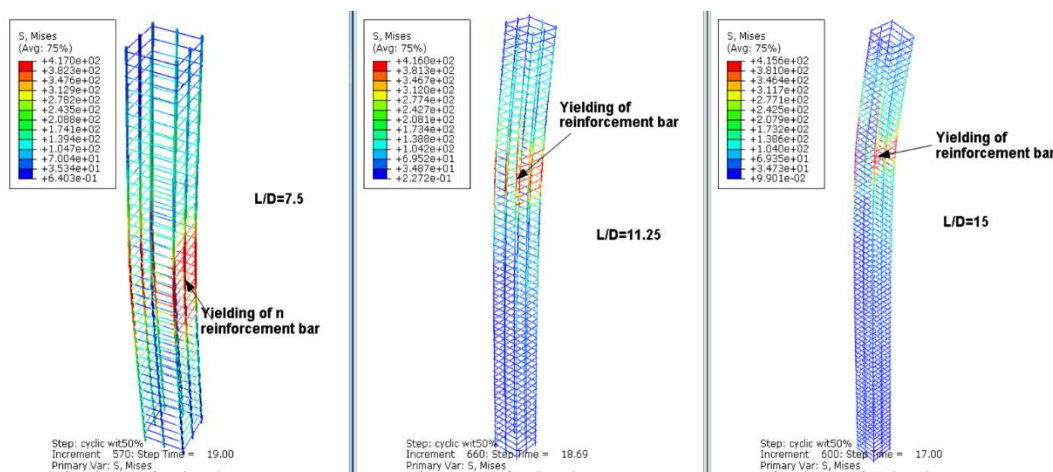


Figure 4.10 Deformed shape and stress contour in reinforcement bar at failure

#### 4.2.3 Lateral Load versus lateral displacement response (Hysteretic behavior)

Lateral load versus lateral displacement curve for the columns of Group 1, 2 and Group 3 are showed in the Figures 4.11 to 4.13. Those three figures depicts, that lateral load versus lateral displacement curves for the short columns (ETS1, ECS3 and EHS6) showed they displaced laterally less and resist high lateral load. It also expresses that the longer columns ( $L/D=11.25$  and  $L/D=15$ ) displaced laterally high and resists less lateral load. On the other hand, as the slenderness ratio ( $L/D$ ) increases, the lateral displacement increases. This increment behavior occurred due to the increased second order displacement in the slender columns. The effect of the encased steel shape can be discussed by comparing the behavior of columns Group1, 2 and Group3 which are identical in all terms except for the shape of the encased steel section.

Based on all the previous measurements, it is obvious that the ultimate lateral load and corresponding lateral deformation of the tested columns varied depending on both the configuration of the lateral steel reinforcement and the encased steel shape which are not considered in the available design codes. It is believed that the existence of inside concrete filled steel tube plays an important role in improving the performance of the encased composite columns under cyclic lateral load. The resulting hysteretic loops of these specimens indicated a stable response with considerable amount of energy dissipation of ETS than ECS and EHS profile encasement.

Table 4.2 Effect of slenderness ratio (L/D) on peak lateral load and lateral deformation

Group	Specimen	Length(mm)	L/D	s/D	Peak lateral load(KN)	Percent Difference (%)	Axial Deformation(mm)	Percent Difference (%)
Group1	ETS1	3000	7.5	0.375	3500.07	ref column	7.708	ref column
	ETS2	4500	11.25	0.375	3381.52	3.4	8	3.7
	ETS3	6000	15	0.375	3155.88	9.83	9	16.76
Group2	ECS4	3000	7.5	0.375	3525.474	ref column	7	ref column
	ECS5	4500	11.25	0.375	3207.491	3.363	7.5	7.1
	ECS6	6000	15	0.375	2953.505	14.18	8	14.28
Group3	EHS7	3000	7.5	0.375	3383.779	ref column	8	ref column
	EHS8	4500	11.25	0.375	3156.274	6.74	8.5	10
	EHS9	6000	15	0.375	2915.804	15.83	10	25

Figure 4.11 depicts Effect of L/D ratios on lateral load displacement response of (Group 1). For group1 as slenderness ratio increased from L/D =7.5 to L/D = 11.25 and L/D = 15, the ultimate lateral load resistance of column was decreased by 3.4% and 9.83% respectively when compared with column of L/D= 7.5 and lateral displacement increased by 3.7% and 16.76% respectively.

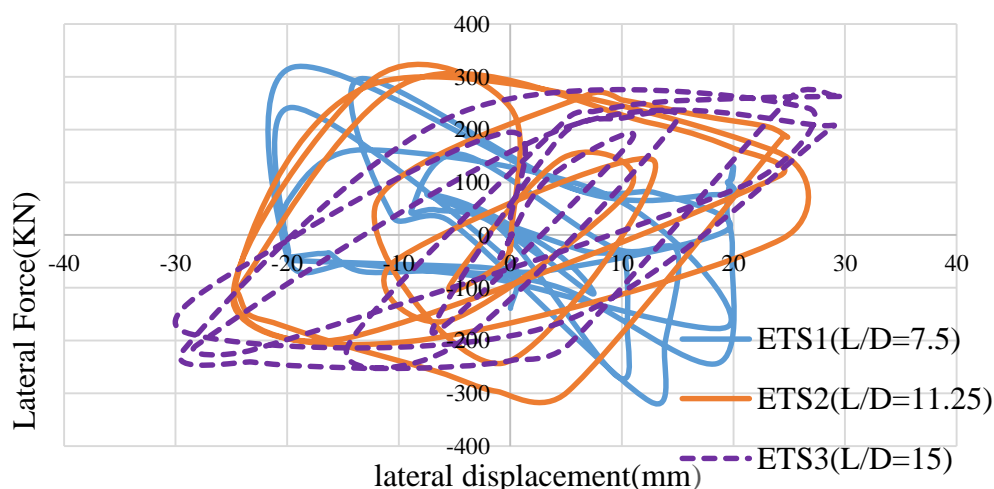


Figure 4.11: Effect of L/D ratios on Lateral Load- Displacement Response of (Group 1)

Figure 4.12 depicts Effect of L/D ratios on lateral load displacement response of (Group 2). For group2 as slenderness ratio increased from L/D =7.5 to L/D = 11.25 and L/D = 15, the ultimate lateral load resistance of column was decreased by 3.363% and 14.18% respectively when compared with column of L/D= 7.5 slenderness ratio.

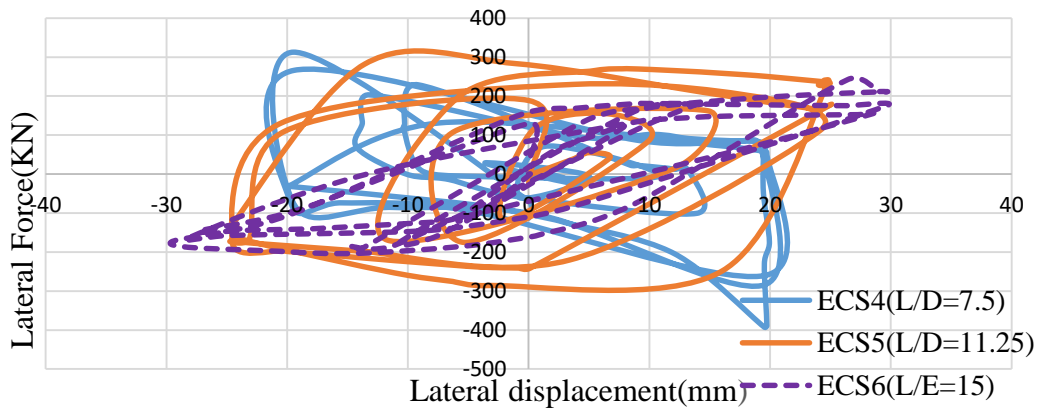


Figure 4.12: Effect of L/D ratios on Lateral Load- Displacement Response of (Group 2)

Figure 4.13 depicts Effect of L/D ratios on lateral load displacement response of (Group 3). For group3 as slenderness ratio increased from L/D =7.5 to L/D = 11.25 and L/D = 15, the ultimate lateral load resistance of column was decreased by 6.74% and 15.83% respectively when compared with column of L/D= 7.5 slenderness ratio.

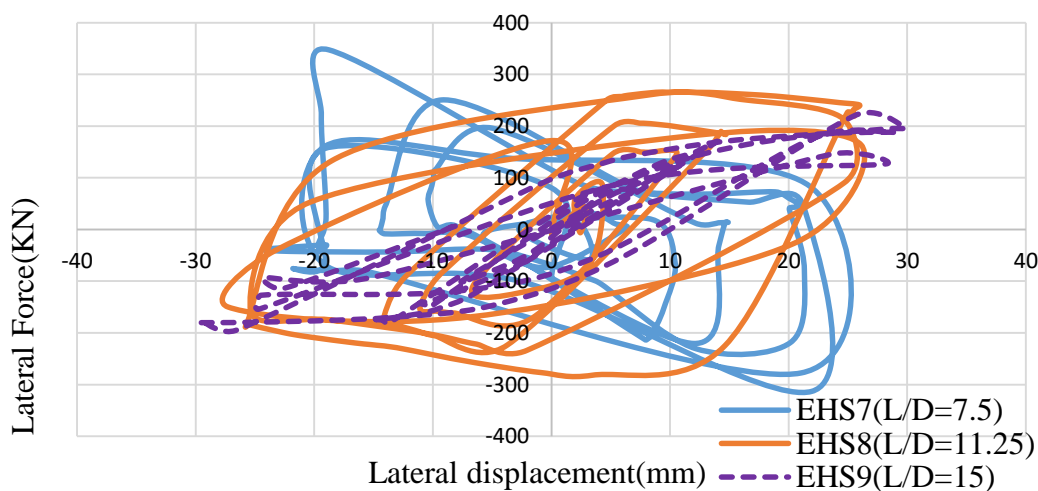


Figure 4.13: Effect of L/D ratios on Lateral Load- Displacement Response of (Group 3)

Figure 4.14 shows that, when ETS, ECS and EHS are compared to each other, EST column performs high lateral load and less lateral displacement. ETS resists 9.2% then ECS and ECS resists 5.2% then EHS. From the result the performance of ETS was greater than that of ECS and EHS column. So the performance of ETS column was good relative to other column under consideration ECS and EHS.

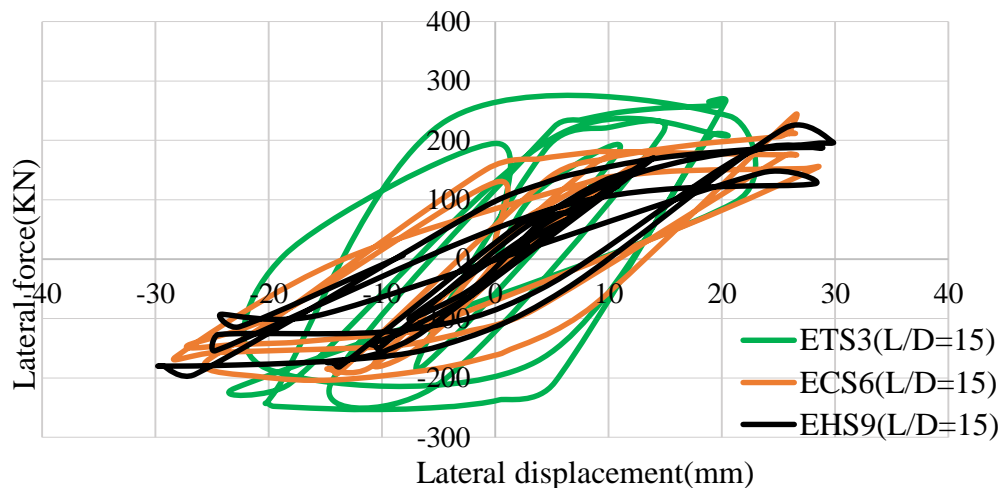


Figure 4.14: Effect of L/D ratios on Lateral Load -Displacement Response of (Group1, 2and 3)

### 4.3 Effect of transverse reinforcement spacing

The effect of transverse reinforcement spacing was studied on FEC columns modeled with normal concrete strength. It plays vital role on the ductility, confinement and early crushing of concrete. Nine FEC columns were analyzed to observe the effect of transverse reinforcement. Nine of FEC columns (Table 3.7) included in three Groups (Group 4, 5 and Group 6) were modeled with normal strength of concrete and square structural steel tube, circular structural tube and H profile structural steel as encasement. All the columns the same length were analyzed for concentric axial load of 50% axial load capacity and cyclic loading. The effect of the transverse reinforcement spacing was studied by varying the ratio of transverse tie spacing, ( $s$ ), to the depth of the column cross-section, ( $D$ ). Only transverse reinforcement spacing ( $s$ ) was varied to understand the effect of this parameter. The transverse ratio ( $s/D$ ) used were 0.1875 (75mm), 0.375 (150mm) and 0.5 (200mm).

### 4.3.1 Axial Load versus axial deformation response

Figures 4.15 shows the effect of the spacing of tie on the axial load versus average axial deformation curve for the Group4 of columns. From the Figures it was observed that increase in the spacing of tie (s/D) resulted in significant decrease in axial capacity and initial stiffness of the FEC column. As the spacing of tie reinforcements increases from 75 mm to and 150mm and then to 200mm, the axial resistance capacity of composite column was decreased by 2.44% and 2.94% respectively when compared to column of spacing 75mm as a reference column for this ETS group4.

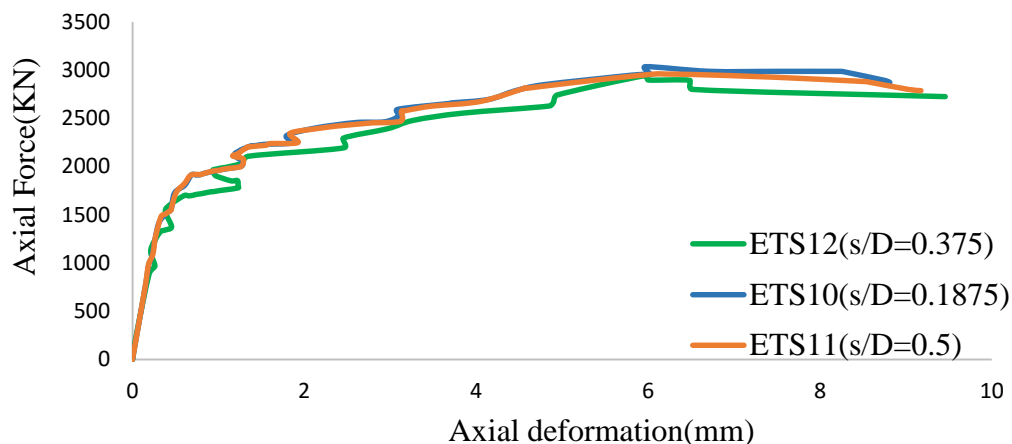


Figure 4.15 Effect of s/D ratios on axial load versus axial deformation curve (Group 4)

Figures 4.16 shows the effect of the spacing of tie on the axial load versus average axial deformation curve for the Group5 of columns. From the Figures it was observed that increase in the spacing of tie (s/D) resulted in significant decrease in axial capacity and initial stiffness of the FEC column. As the spacing of tie reinforcements increases from 75 mm to and 150mm and then to 200mm, the axial resistance capacity of composite column was decreased by 1.4% and 2.54% respectively when compared to column of spacing 75mm as a reference column for this ECS group5.

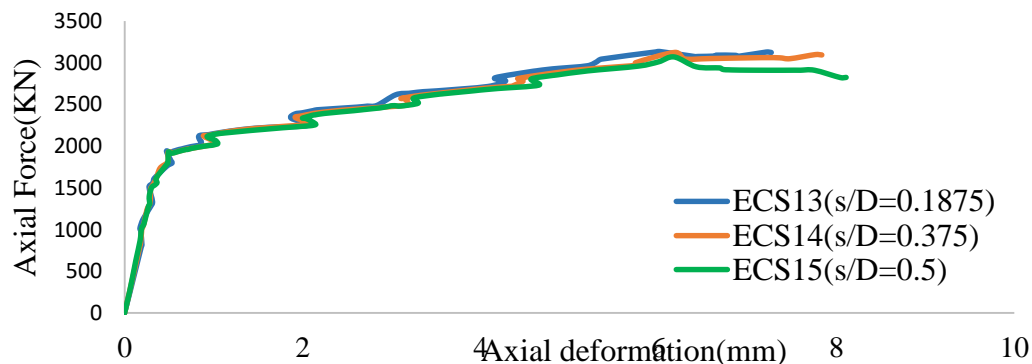


Figure 4.16 Effect of s/D ratios on axial load versus axial deformation curve (Group 5)

Figures 4.17 shows the effect of the spacing of tie on the axial load versus average axial deformation curve for the Group5 of columns. From the Figures it was observed that increase in the spacing of tie (s/D) resulted in significant decrease in axial capacity and initial stiffness of the FEC column. As the spacing of tie reinforcements increases from 75 mm to and 150mm and then to 200mm, the axial resistance capacity of composite column was decreased by 2.28% and 3.204% respectively when compared to column of spacing 75mm as a reference column for this EHS group6.

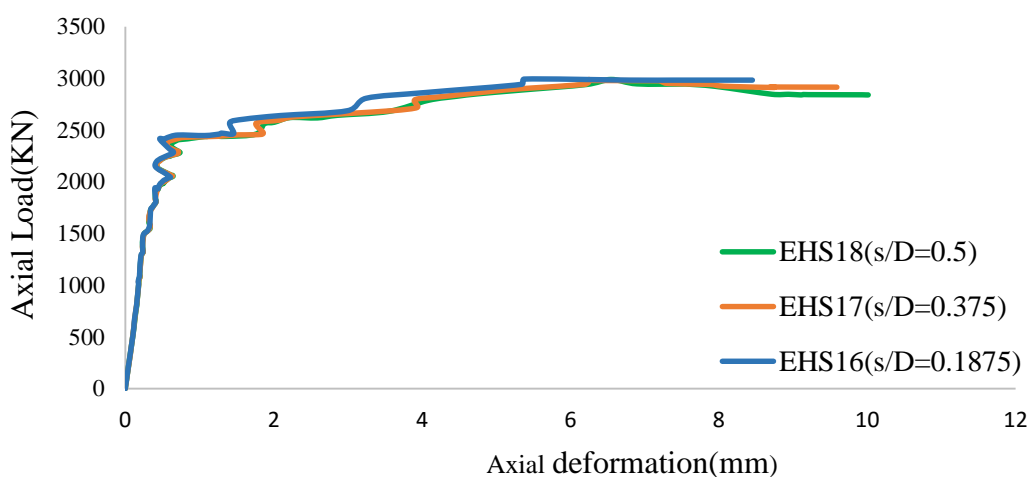


Figure 4.17 Effect of s/D ratios on axial load versus axial deformation curve (Group 6)

Table 4.3 Effect of transverse reinforcement spacing on peak axial load and axial deformation

Group	Specimen	Length(mm)	L/D	s/D	Peak axial load(KN)	Percent Difference (%)	Axial Deformation(mm)	Percent Difference (%)
Group4	ETS10	6000	15	0.1875	2869.931	ref column	8.01475	ref column
	ETS11	6000	15	0.375	2785.686	2.94	9.175	14.47
	ETS12	6000	15	0.5	2799.994	2.44	9.457	17.99
Group5	ECS13	6000	15	0.1875	3136.507	ref column	7.26	ref column
	ECS14	6000	15	0.375	3092.784	1.4	7.835	7.9
	ECS15	6000	15	0.5	3069.784	2.15	8.1112	11.72
Group6	EHS16	6000	15	0.1875	2984.951	ref column	8.483	ref column
	EHS17	6000	15	0.375	2916.617	2.28	9.59	13.45
	EHS18	6000	15	0.5	2991.053	3.204	10.01266	18.45

### 4.3.2 Modes of failure

The failure modes were concrete crushing (CC), structural yielding (SY), and flexural buckling (F). The three modes were identified by examining the output stress of the concrete and structural steel elements at failure state. In this analysis failure was initiated by crushing of concrete followed by yielding of structural steel and buckling of longitudinal rebars. Figure 4.18 shows that how buckling of longitudinal bar increase with increasing of spacing of tie. At the end of the analysis, the column failed because of concrete crushing in the compression side. However, the exact location of the critical section differed in each specimen. After analysis, buckling of the longitudinal rebars and crushing of the confined concrete was observed in the fully encased specimens. In column, with relatively large tie spacing, the ties did not yield.

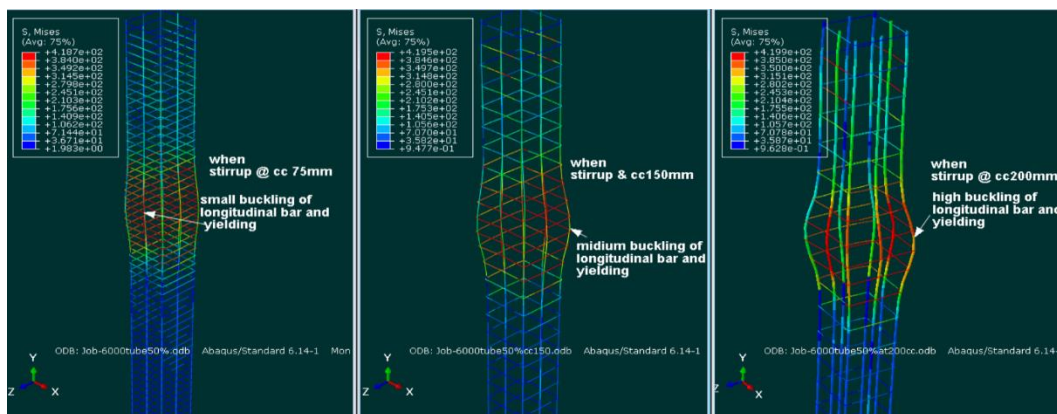


Figure 4.18 Stress contour in rebars at failure for (Group4, 5 and 6)

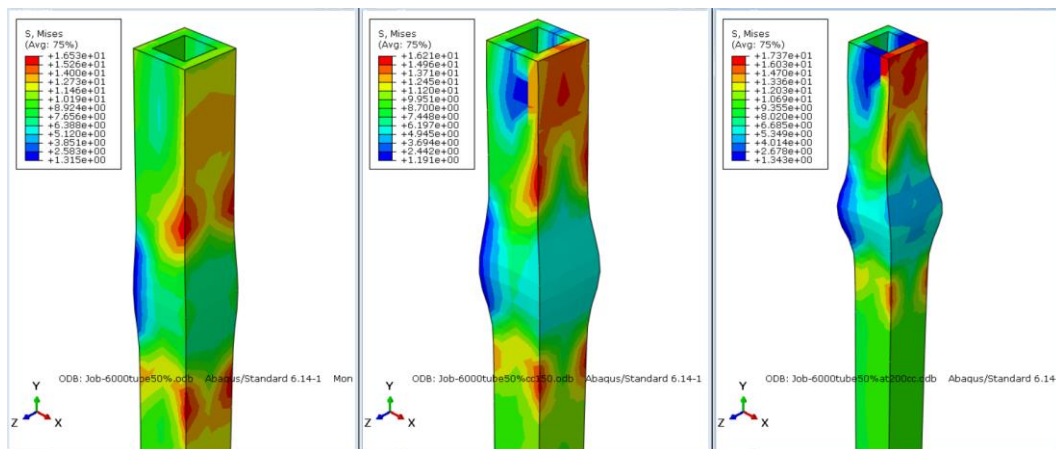


Figure 4.19 Stress contour in outer concrete at failure for (Group4)

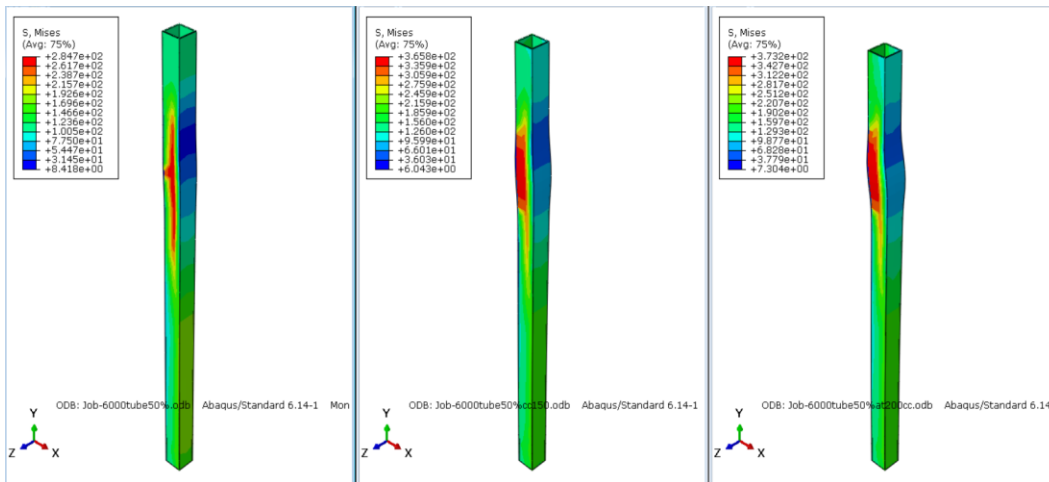


Figure 4.20 Stress contour in structural steel at failure for (Group4)

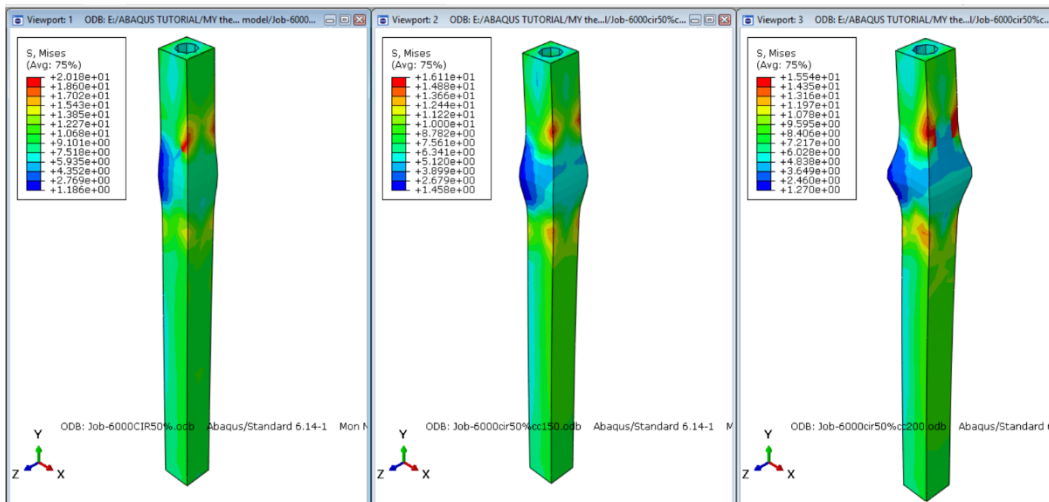


Figure 4.21 Stress contour in outer concrete at failure for (Group5)

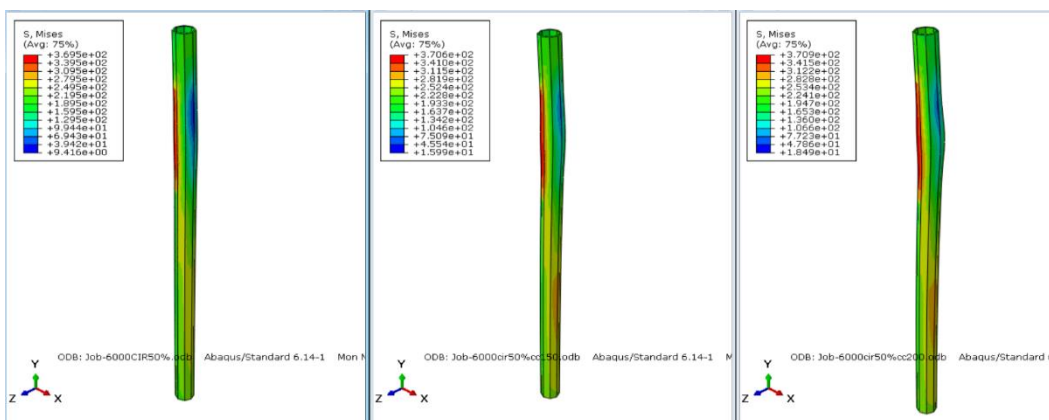


Figure 4.22 Stress contour in structural steel at failure for (Group5)



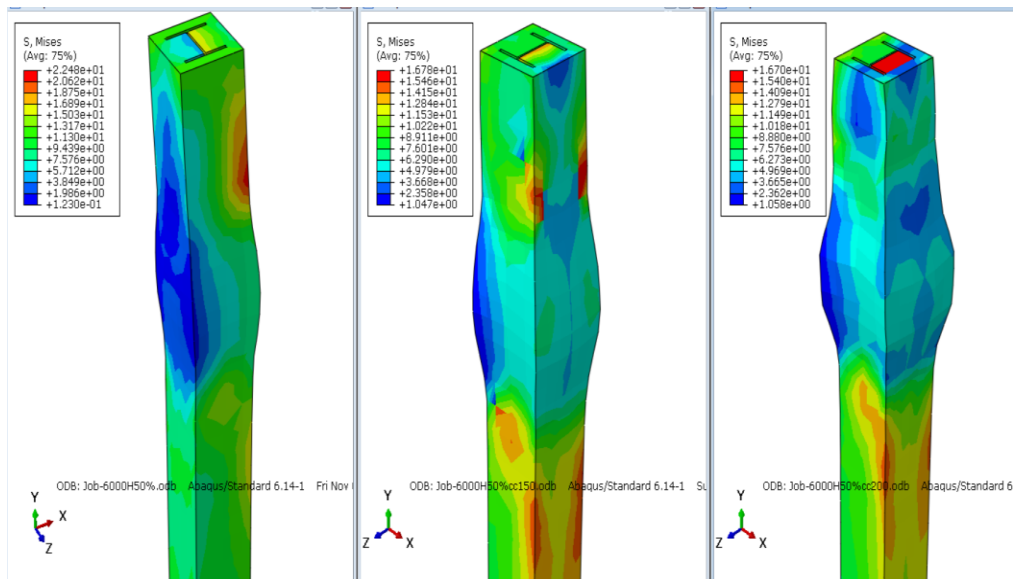


Figure 4.23 Stress contour in outer concrete at failure for (Group6)

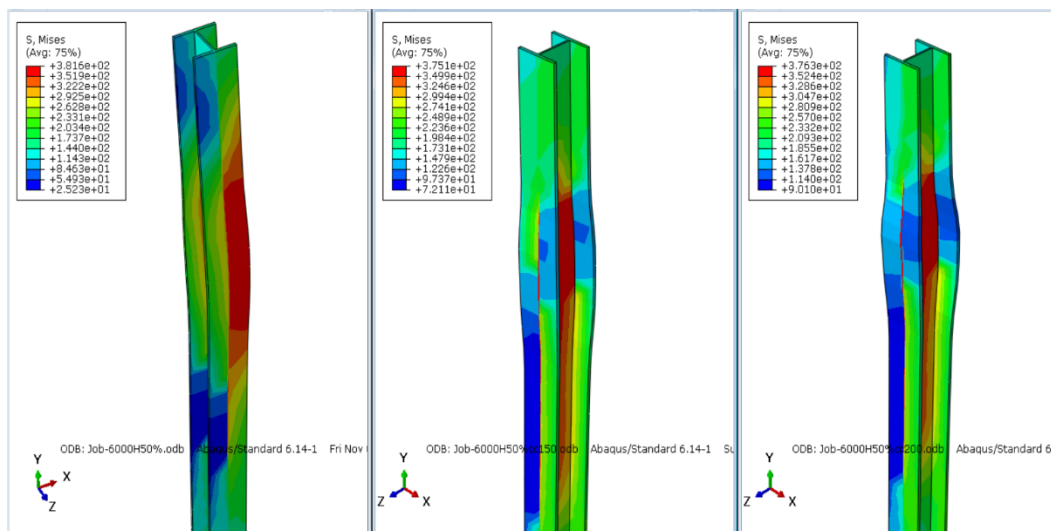


Figure 4.24 Stress contour in structural steel at failure for (Group6)

### 4.3.3 Lateral Load versus lateral displacement responses

Reinforcing bars that undergo repeated loading into the inelastic range can be subjected to inelastic buckling. This phenomenon is generally assumed dependent on tie spacing. As a matter of fact, collapse composite column subjected to axial load is strongly dependent if not coincident with the instability of the reinforcing bars. However theoretically it is noticed that longitudinal

bars could also buckle over a length greater than one stirrup interval. This type of buckling of longitudinal bars increases strength and ductility decay in structural element due to the strong reduction of concrete confinement.

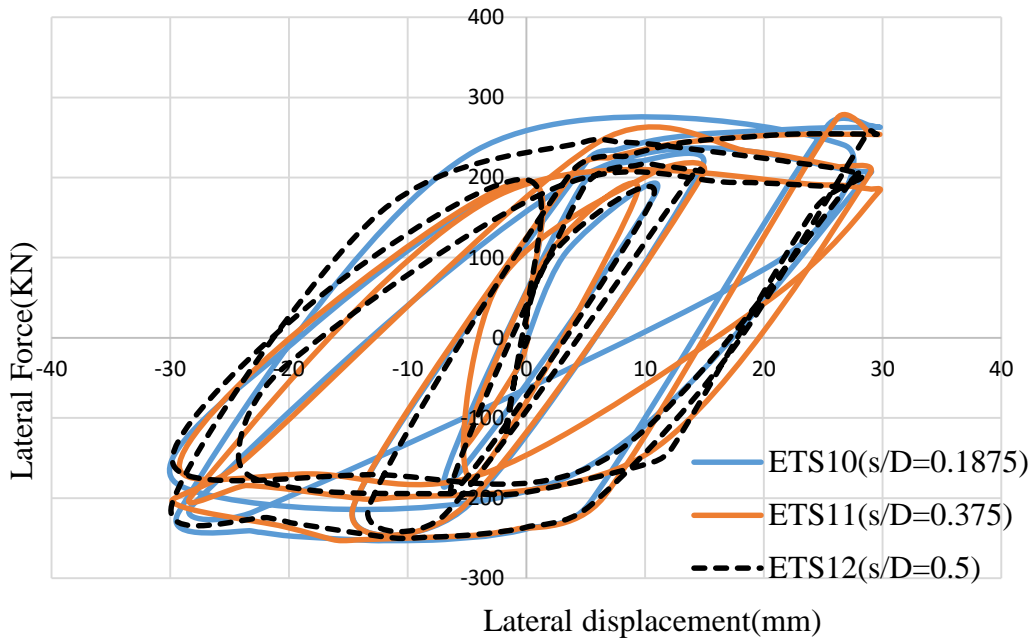


Figure 4.25: Effect of L/D ratios on Lateral Load -Displacement Response of (Group4)

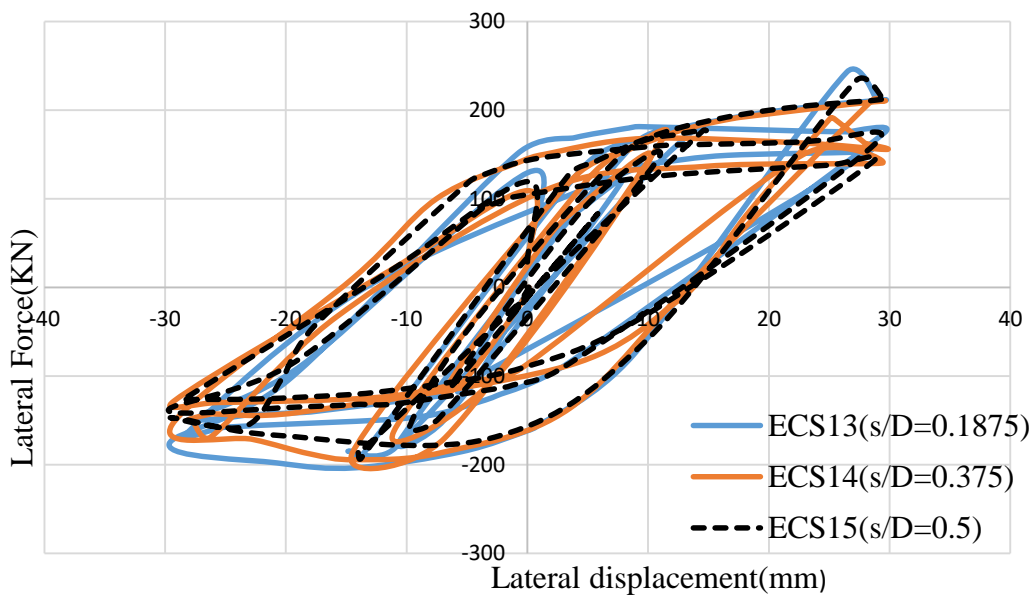


Figure 4.26: Effect of L/D ratios on Lateral Load -Displacement Response of (Group5)

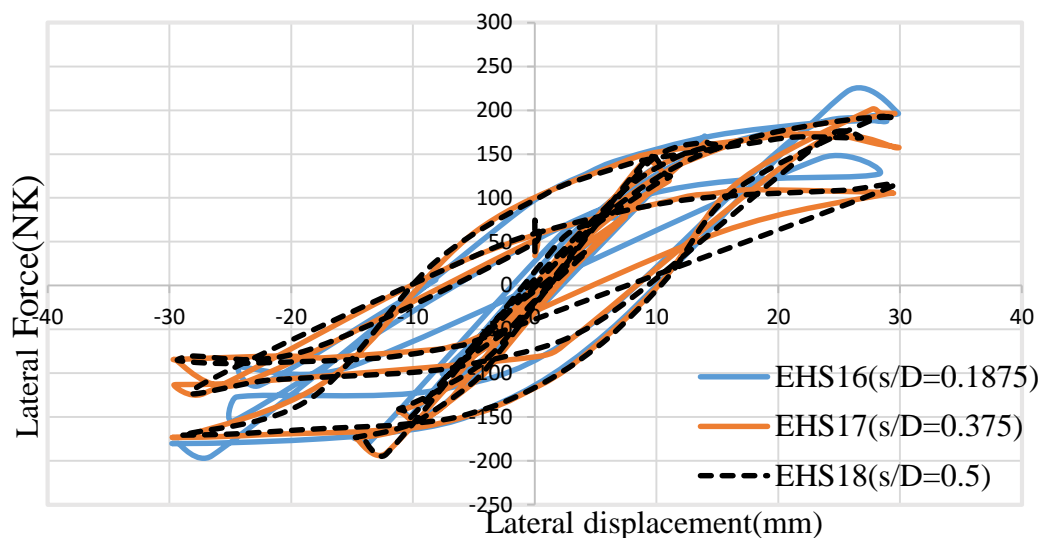


Figure 4.27 Effect of L/D ratios on Lateral Load -Displacement Response of (Group6)

Table 4.4 Effect of transverse reinforcement spacing on peak lateral load and lateral deformation

Group	Specimen	Length(mm)	L/D	s/D	Peak axial load(KN)	Percent Difference (%)	Axial Deformation(mm)	Percent Difference (%)
Group4	ETS10	6000	15	0.1875	273.6118	ref column	29.7978	ref column
	ETS11	6000	15	0.375	264.998	3.14	29.813	0.05
	ETS12	6000	15	0.5	257.158	6.01	29.575	0.75
Group5	ECS13	6000	15	0.1875	242.6579	ref column	29.7514	ref column
	ECS14	6000	15	0.375	233.347	3.84	29.703	0.16
	ECS15	6000	15	0.5	211.481	12.85	29.702	0.17
Group6	EHS16	6000	15	0.1875	220.542	ref column	29.770	ref column
	EHS17	6000	15	0.375	201.361	2.288.7	29.704	0.235
	EHS18	6000	15	0.5	192.392	12.76	129.656	0.4

#### 4.4 MODEL VERIFICATION

##### 4.4.1 Verification of FEM of the Encased Composite Columns

The aim is to prove that the model developed in this study using the finite element program ABAQUS© is valid for the analysis of the fully encased composite columns. The finite element models of encased composite columns developed in this study were verified against tests detailed in (Campian et al., 2011). To validate the model and ensure that the model can be considered

accurate and is a credible representation of the system’s behavior, the results predicted by the finite element model were compared against the experimental results. The details of the specimens, geometry and materials properties of encased composite columns are shown in Table 4.5 and Figure 4.27 shows cross section of experimental sample.

Table 4.5: Specimen dimension and materials properties (Campian et al., 2011)

TEST	Dimension(mm)			Steel section	Reinforcement		Material properties		
	B	D	L		Longitudina l	Trasverse	Concrete(Mpa )	$f_{ys}$ (Mpa)	$f_{yr}$ (Mpa)
1	170	220	2000	IPN 120 H 120 x 64 x 6.3 x4.4	4 $\phi$ 12	$\phi$ 8@100mm	C20/25	275	559
2	170	220	2500		4 $\phi$ 12	$\phi$ 8@100mm	C20/25	275	559

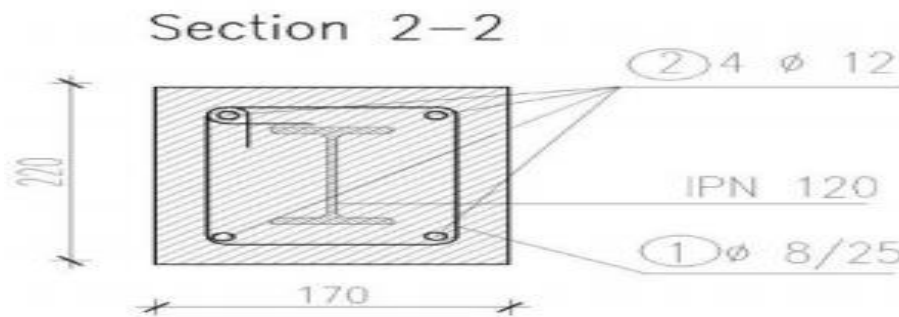


Figure 4.28 cross section of experimental sample (Campian et al., 2011)

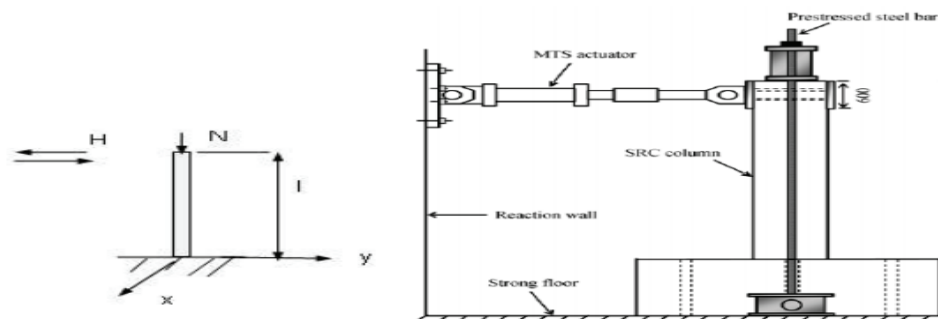


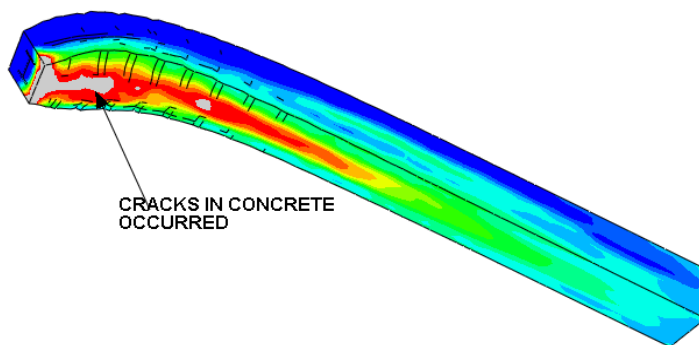
Figure 4.29. Mechanical model and test up procedure for experimentally tested columns (Campian et al., 2011)

The analytical model was validated in comparison to an experimental research on Failure mode, highest level of lateral force and Hysteresis loops of the specimen of fully encased composite columns done by (Campian et al., 2011). A difference of 10%-12% was noted in the validation results which occurred mainly due to the difference in mix standards practiced in different countries.

Table 4.6 Values for axial force N and lateral force H

Specimen	Loading type	Axial force N [kN]	Max.lateral force H [kN]	From FE	Percentage difference(%)
1	cyclic	200	20.4	18	11.76
2	cyclic	400	21.7	24	10.6

Figure 4.30: Failure mode of column under experiment (Campian et al., 2011)



ODB: Job-5cyclicand200KN.odb Abaqus/Standard 6.14-1 Sun Oct 13 04:18:05 Russia TZ 3 Standard Time 2019

Figure 4.31: Failure mode and Stress Contour at Failure for finite element

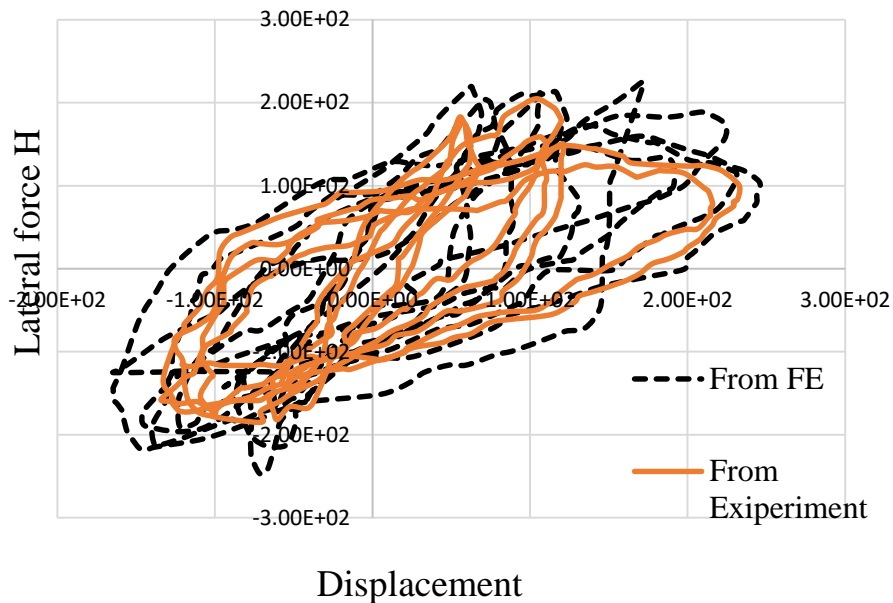


Figure 4.32 Hysteresis loops of the specimen subjected to cyclic loading and axial loading.

This validated numerical model provides the necessary tool to expand the investigation into the cyclic behavior of encased composite column of different profile of steel structure without the need to conduct repetitive, expensive and time-consuming lab tests.

## CHAPTER FIVE

### CONCLUSIONS AND RECOMMENDATIONS

#### 5.1 CONCLUSIONS

The aim of this study was to investigate the effect steel profile section of fully encased composite columns under axial and lateral cyclic loading. The result shows that circular tube encasement composite concrete column is better to be used for areas where earth quake may happen. A nonlinear 3-D finite element models were developed to model different composite column and Based on the Findings of this study, and Within the present scope of work and investigation carryout, the following conclusions may be drawn.

- The confining effect is obviously influenced by the shape of the encased steel section. The circular tub shaped steel section led to better confinement than the square tube steel and H section steel which resulted in a noticeable increase in both ductility and ultimate axial capacity of the columns.
- The lateral load capacity and stiffness of FEC columns were decreased with the increase in the slenderness ratio. As the slenderness ratio is increased from 7.5 to 15 the lateral load capacity of FEC columns were reduced by 15.83%
- The axial capacity of the FEC column was less affected by the spacing of the transverse reinforcement. However, the load versus axial deformation and failure modes are more affected by spacing of tie.

#### 5.2 RECOMMENDATIONS

The following recommendations are made for future investigations.

- ✓ The effects of percentage of steel section, material properties of the concrete, the confinement effect of the concrete, and concrete and steel strength on the behavior of encased composite columns under axial and cyclic loading should be investigated.
- ✓ The effects of thickness of structural steel on the behavior of encased composite columns under cyclic loading should be investigated.
- ✓ This research is made based on theoretical basis, but it has to be checked by laboratory works before implementation.
- ✓ Finite element models should be developed to predict the behavior of fully encased composite column under various loading.



## REFERENCES

- Anon., 1982. *ASCE Task Committee on Concrete and Masonry Structure*. New York: State of the art report on finite element analysis of reinforced concrete.
- An, Y. F., Han, L. H. & Roeder, C., (2014). Flexural performance of concrete-encased concrete filled steel tubes. *Magazine of Concrete Research*, 66(5), p. 249–267.
- An, Y. F., Han, L. H. & Zhao, X. L., (2013). Experimental behavior of box concrete-encased CFST eccentrically loaded column. *Magazine of Concrete Research*, 65(20), p. 1219–1255.
- Chang, X., Wei, Y. Y. & Yun, Y. C., (2012). Analysis of steel-reinforced concrete-filled steel tubular (SRCFST) columns under cyclic loading. *Construction and Build Material*, Volume 28, p. 88–95.
- Chen , C. C., Weng, C. C., Lin, I. M. & Li, J. M., (1999). *Seismic behavior and strength of concrete encased steel stub columns and beam–columns*, in Chinese: Report no. MOIS 881012-1 Architecture and Building.
- Dai , X. & Lam , D., (2010). Numerical modelling of the axial compressive behavior of short concrete-filled elliptical steel columns. *Journal of Construction Steel Research*, 66(7), pp. 931-942.
- Ellobody, E. & Young, B., (2006). Nonlinear analysis of concrete-filled steel SHS and RHS columns. *Thin-Walled Structures*, p. 919–930.
- Ellobody, E. & Young, B., (2011). Numerical simulation of concrete encased steel composite columns. *Journal of Constructional Steel Research*, Volume 67, p. 211–222..
- Espinos , A., Romero, M. L. & Hospitaler, A., (2010). Advanced model for predicting the fire

response of Concrete filled tubular columns. *Journal of Construction Steel Research*, 66(8), pp. 1030-1046.

Hafezolghorani, M., Hejazi, F., Vaghei, R. & Jaafar, M. S., (2017). Simplified Damage Plasticity Model for Concrete. *Article in Structural Engineering International* .

Hafezolghorani, M. et al., (2017). Simplified Damage Plasticity Model for Concrete. *Structural Engineering International*, pp. 68-78.

Hamidian, M. R. et al., (2016). Pitch spacing effect on the axial compressive behavior of spirally reinforced concrete-filled steel tube. *Thin Walled Structure* , p. 213–223.

Han , L. H. & Yang, Y. F., (2005). Cyclic performance of concrete-filled steel CHS columns under flexural loading. *Journal of Construction Steel Research*, 61(4), pp. 423-452.

Han, L. H. & An , Y. F., (2014). Performance of concrete-encased CFST stub columns under axial compression. *Journal of Constructional Steel Research* , Volume 93, p. 62–76.

Han, L. H. & An, Y. F., (2014). Behavior of concrete-encased CFST columns under combined compression and bending. *Journal of Constructional Steel Research* , Volume 101, pp. 314-330.

Han, L. H., An, Y. F., Roeder, C. & Ren, Q. X., (2015). Performance of concrete-encased CFST box members under bending. *Journal of Constructional Steel Research*, Volume 106, pp. 138-153.

Han, L. H., Liao, F. Y., Tao, Z. & Hong, Z., (2009). Performance of concrete filled steel tube reinforced concrete columns subjected to cyclic bending. *Journal of Constructional Steel Research*, 65(8), p. 1607–1616.

Han, L. H., Li, W. & Bjorhovde, R., (2014). Developments and advanced applications of

- Concrete-filled steel tubular (CFST) structures. *Journal of Construction Steel Research*, Volume 100, p. 211–228.
- Han, L. H., Wang, Z. B., Xu, W. & Tao, Z., (2016). Behavior of concrete-encased CFST members under axial tension. *Journal of Structural Engineering*, 142(2).
- Ji, X. D., Kang, H. Z., Chen, X. C. & Qian, J. R., (2014). Seismic behavior and strength capacity of steel tube-reinforced concrete composite columns. *Earthquake Engineering and Structural Dynamics*, 43(4), p. 487–505.
- KMIECIK, P. & KAMISKI, M., (2011). Modelling of reinforced concrete structures and composite structures with concrete strength degradation taken into consideration. *ARCHIVES OF CIVIL AND MECHANICAL ENGINEERING*, 11(3), pp. 623-636.
- Krishan, A. L., Troshkina, E. A. & Astafyeva, M. A., (2017). *Materials Science and Engineering*. s.l., IOP Conference Series.
- Kwaśniewski, L., Szmigiera, S. & Siennicki, M., (2011). Finite Element Modeling Of Composite Concrete-Steel Columns. *Archives Of Civil Engineering*.
- Liao, F. Y., Han, L. H. & Tao, Z. H., (2014). Behavior of composite joints with concrete encased CFST columns under cyclic loading, Experiments. *Journal of Engineering Structures*, Volume 59, pp. 745-764.
- Li, Y. J., Han, L. H., Xu, W. & Tao, Z., (2016). Circular concrete-encased concrete-filled steel tube (CFST) stub columns subjected to axial compression. *Magazine of Concrete Research*, 66(19), p. 995–1010.
- Ma, D. Y., Han, L. H., Li, W. & Zhao, X. L., (2018). Seismic Performance of Concrete-Encased CFST Piers Analysis. *Journal of Bridge Engineering*, 23(1).

- Najafgholipour, M. A., Dehghan, S. M., Dooshabi, A. & Niroomandi, A., (2017). Finite Element Analysis of Reinforced Concrete Beam-Column Connections with Governing Joint Shear Failure Mode. *Latin American journal of solid and structures*.
- Park, H. G. et al., (2015). Concrete filled steel tube columns encased with thin precast concrete. *Journal of Structural Engineering ASCE 2015; 141 (12)*, 141(12).
- Portolés, J. M., Romero , M. L. & Filippou, F. C., (2013). Simulation and design recommendations of eccentrically loaded slender concrete-filled tubular columns. *Engineering Structures*, 33(5), pp. 1576-1593.
- Roeder, C., An, Y. F. & Han , L. H., (2014). Flexural performance of concrete-encased concrete filled steel tubes. *Magazine of Concrete Research* , 66(5), pp. 249-267.
- Wahalathantri, B. L., Thambiratnam, D. P., Chan, T. H. & Fawzia, S., (2011). A Material Model For Flexural Crack Simulation In Reinforced Concrete Elements Using Abaqus. pp. 260-264.
- Wang, L. J. & Wang, W. H., (2005). Experimental research on the bearing capacity of axially loaded composite columns with concrete core encased by steel tube. *Proceedings of the fourth international conference on advances in steel structures*, pp. 593-624.
- Wang, Z., Han, L., Li, W. & Tao, Z., (2016). Seismic performance of concrete-encased CFST piers: Experimental study. *Journal of Bridge Engineering*.
- Won , D. H. et al., (2014). Optimum confining effect in steel composite hollow RC column with inner tube under compressive load. *Magazine of Concrete Research* , 66(9), p. 433-446.
- Yao, G. H., Han, L. H. & Tao, Z., (2007). Performance of concrete-filled thin-walled steel tubes

underpure torsion. *Thin-Walled Structure* , p. 24–36.

Yonas, T. Y., Temesgen, W. & Senshaw, F. W., (2018). Finite Element Analysis of Slender Composite Column Subjected to Eccentric Loading. *International Journal of Applied Engineering Research* , 13(15), pp. 11730-11737.

Zhang , J. G., Liu , Y. J. & Yang, J., (2011). Experimental Research and Finite Element Analysis of Concrete-Filled Steel Box Columns with Longitudinal Stiffeners. *Advanced Materials Research* , Volume 287, pp. 1037-1042.

Zhou, K. & Han, L. H., (2018); . Experimental performance of concrete-encased CFST columns subjected to full-range of fire including heating and cooling. *Journal of Engineering Structures*, Volume 165, pp. 331-348.

**APINDEX**

**A . MATERIAL INPUT DATA SHEET FOR ANALYSIS**

i. Unconfined concret input for CDP Model in Abaqus CAE

Dailation angle	eccentricity	$f_{bo}/f_{co}$	k	viscosity
36	0.1	1.16	0.667	0

$f_{cm}$ (Mpa)	38
$E_{cm}$ (Gpa)	32.83657
$\epsilon_{c1}$	2.161877
$\epsilon_{cu}$	3.5
$\eta$	$\epsilon_c/\epsilon_{c1}$
k	1.961528
k-2	-0.03847

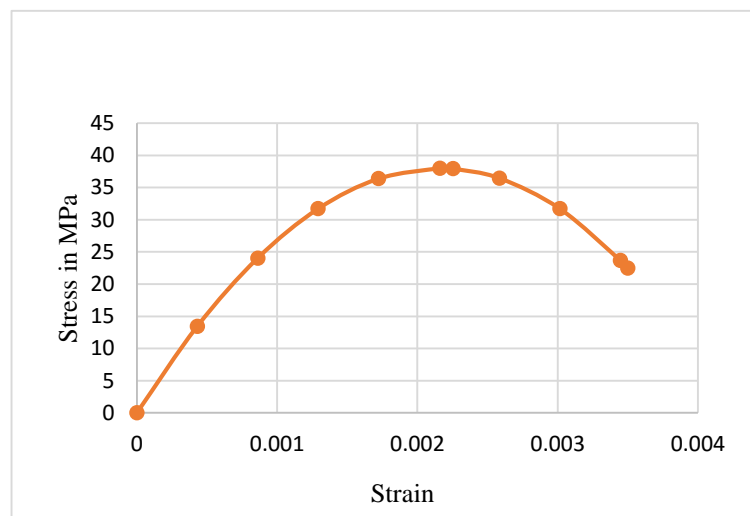


Figure A.1 unconfined concert input stress-strain curve

Table.A.1 compressive behavior

$\epsilon_c$	$\eta$	$\sigma_c$	$\epsilon_{el}$	$\epsilon_{in}$	dc	yield stress(YS)	inelastic strain
0		0	0	0	0	0	0
0.000431	0.19936381	13.45302849	0.000409	2.13035E-05	0	13.453028	2.13E-05
0.000862	0.39872761	24.04789195	0.000732	0.000129649	0	24.047891	0.0001296
0.001293	0.59809142	31.71727497	0.000965	0.000327087	0	31.717274	0.0003270
0.001724	0.79745522	36.39173156	0.001108	0.000615732	0	36.391731	0.0006157
0.002162	1	38	0.001157	0.00100463	0.58333	38	0.001004
0.002255	1.04307513	37.92654451	0.001155	0.001099991	0.58027	37.926544	0.001091
0.002586	1.19618283	36.46691456	0.001110	0.001475442	0.51945	36.466914	0.001475
0.003017	1.39554664	31.71731052	0.000965	0.002051086	0.32155	31.717310	0.002051
0.003448	1.59491044	23.67192777	0.000720	0.002727099	0.01366	23.671927	0.002727
0.0035	1.61896362	22.47458591	0.000684	0.002815562	0.06355	22.474585	0.002815

Table A.2 Tensile behavior

yield stress	displacement	Damage parameter(dt)	Crack strain
2.896468154	0	0	0
2.446548478	0.01	0.155333894	0.022047509
1.996628802	0.02	0.310667787	0.044088402
1.546709126	0.03	0.466001681	0.066116905
0.55	0.04	0.810113569	0.102567416
0.6	0.045	0.798541842	0.111692982
0.58351714	0.05	0.80825021	0.122426806
0.55539716	0.06	0.792851166	0.106261968

fck (Mpa)	30
fctm (Mpa)	2.896468
GF (N/m)	149.1738
w1 (mm)	0.051502
wc (mm)	0.25751
0.2fctm	0.579294



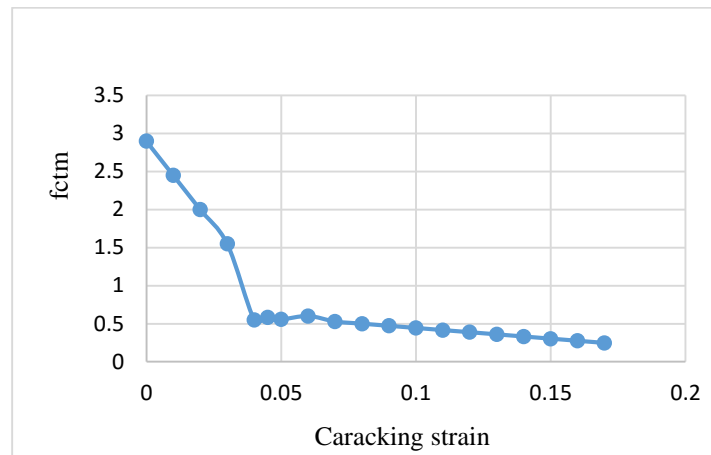


Figure A.2 Stress-crack opening relation for uniaxial tension

ii. Confined concrete CDP model

Dailation angle	eccentricity	$f_{bo}/f_{co}$	k	viscosity
36	0.1	1.16	0.667	0

Table.A.3 Abaqus compression input

$\sigma_c$ (MPa)	$\epsilon_{in}$	dc
0	0	0
13.45302849	2.130E-05	0
24.04789195	0.0001296	0
31.71727497	0.0003270	0
36.39173156	0.0006157	0
38	0.001004	0.5833333
37.92654451	0.0010999	0.7980272
36.46691456	0.0014754	0.894547
31.71731052	0.0020510	0.9215546

Table.A.4 Abaqus Tension input

$\sigma_t$ ( MPa)	dt	$\epsilon_{t,in}$
2.896468154	0	0
2.418780964	0.164920574	0.00998258
1.941093774	0.329841148	0.019956585
1.463406583	0.494761722	0.02991362
0.55	0.810113569	0.039623675
0.6	0.801537679	0.049643748
0.574839792	0.811845215	0.0596194
0.544984342	0.792851166	0.044662386
0.515128893	0.822152751	0.069592229

Table A, 4 Input values for plastic behaviour of longitudinal reinforcement

Material type	True stress [MPa]	Plastic strain
Rebars	356.17	0
	591.6	0.1456
Structural steel	416.37	0
	562.6	0.457

## B. SEISMIC LOADING PROTOCL USED FOR THIS STUDY

Table B.1 step time versus amplitude

step time	Amplitude
0	0
1	7.5
2	0
3	-7.5
4	0
5	15
6	0
7	-15
8	0
9	22.5
10	0
11	-22.5
12	0
13	30
14	0
15	-30
16	0
17	60
18	0
19	-60
20	0
21	60
22	0
23	-60
24	0
25	60
26	0
27	-60
28	0
29	120
30	0
31	-120
32	0
33	120
34	0
35	-120
36	0
37	120
38	0
39	-120
40	0

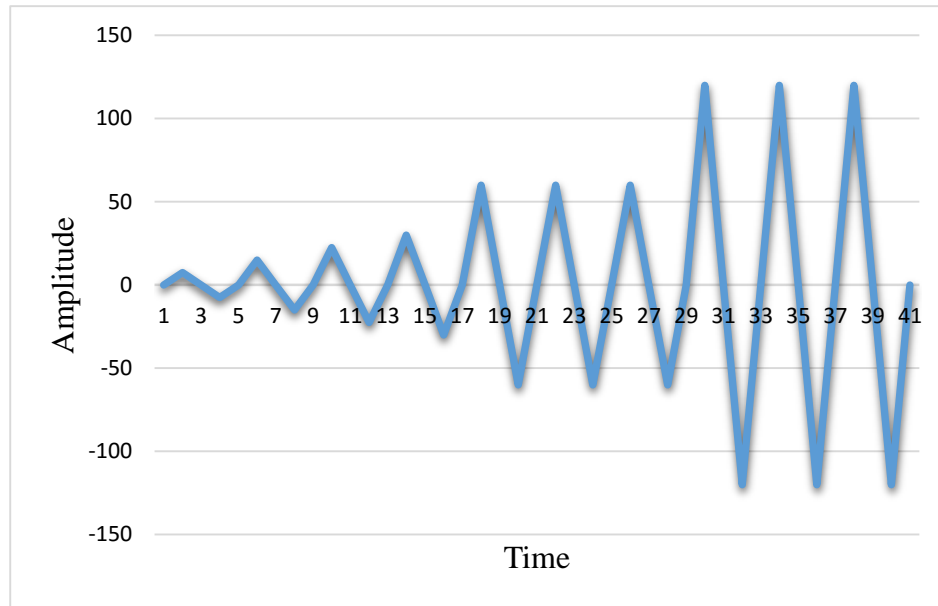
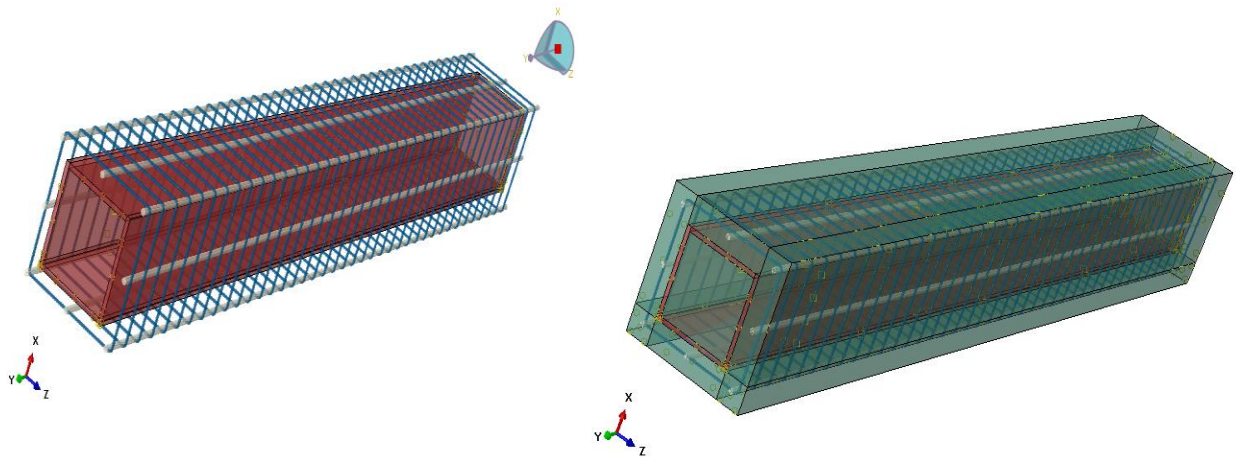
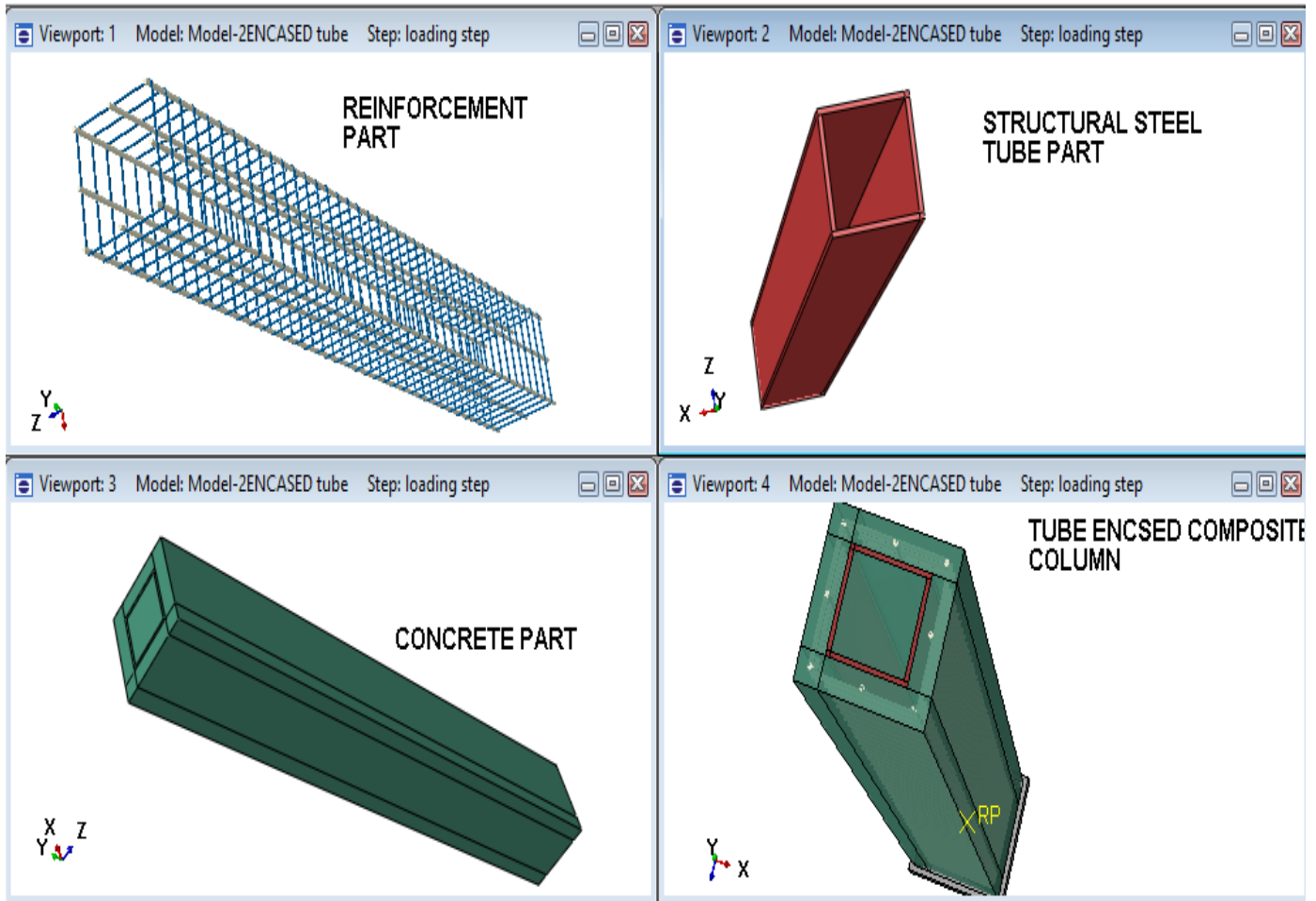
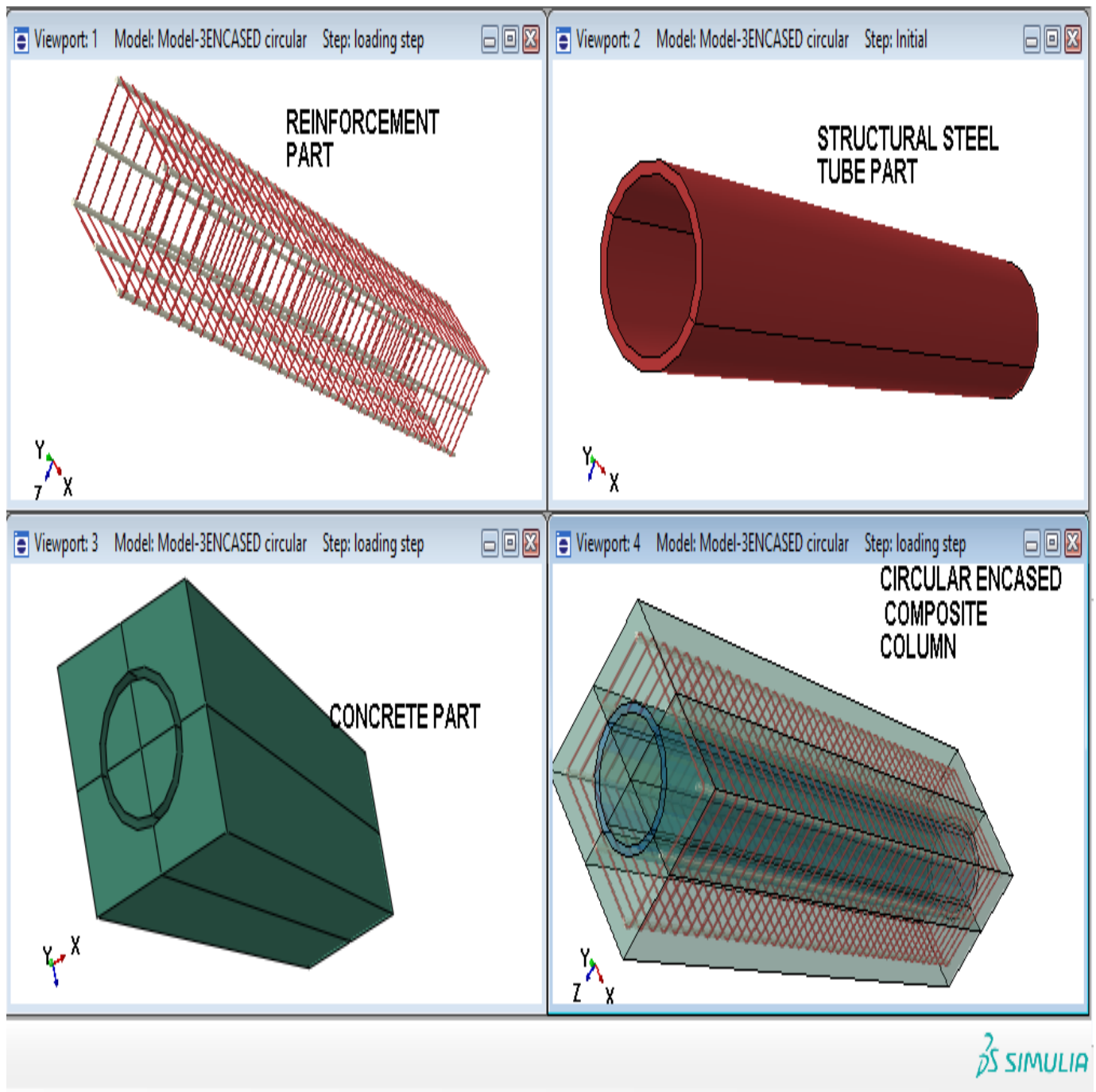


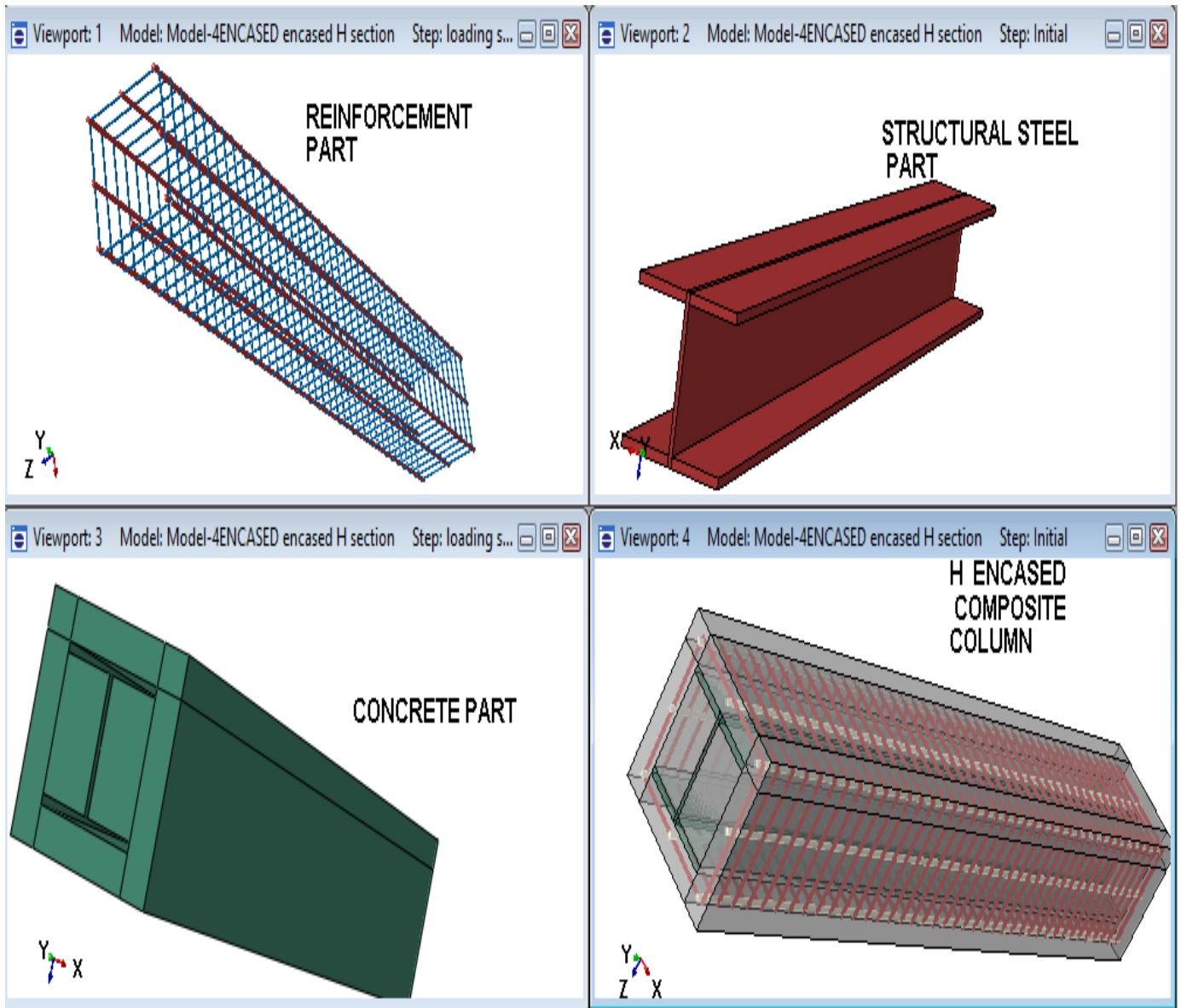
Figure B.2 loading protocol adopted under study

### C. MODEL OF COLUMN UNDER STUDY

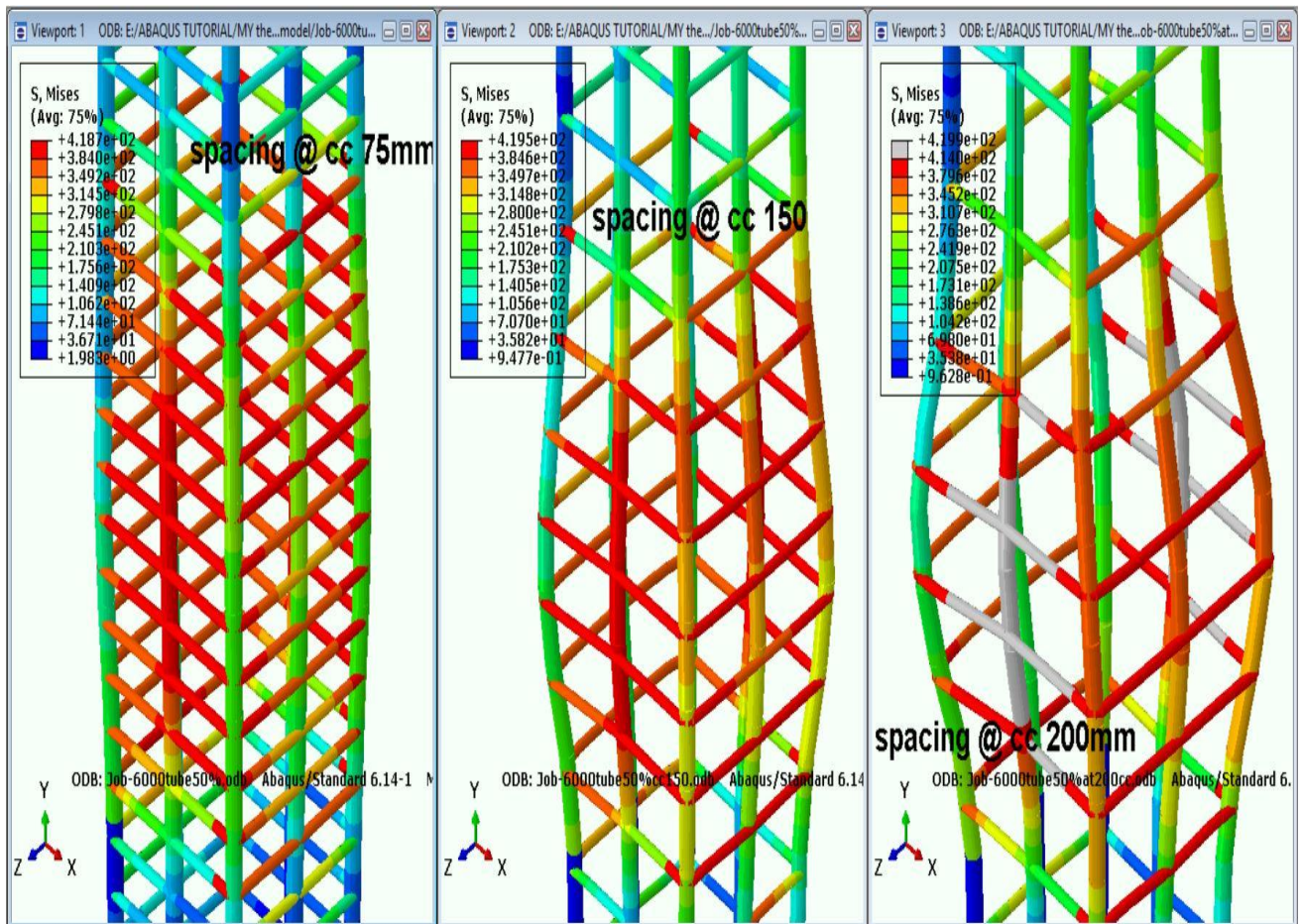
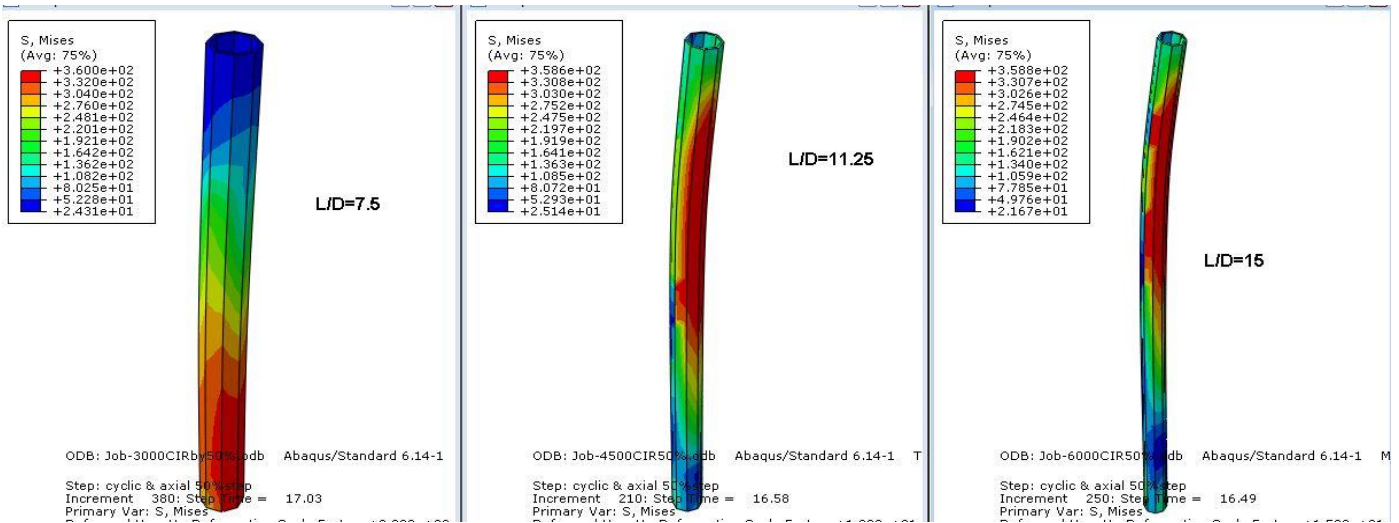




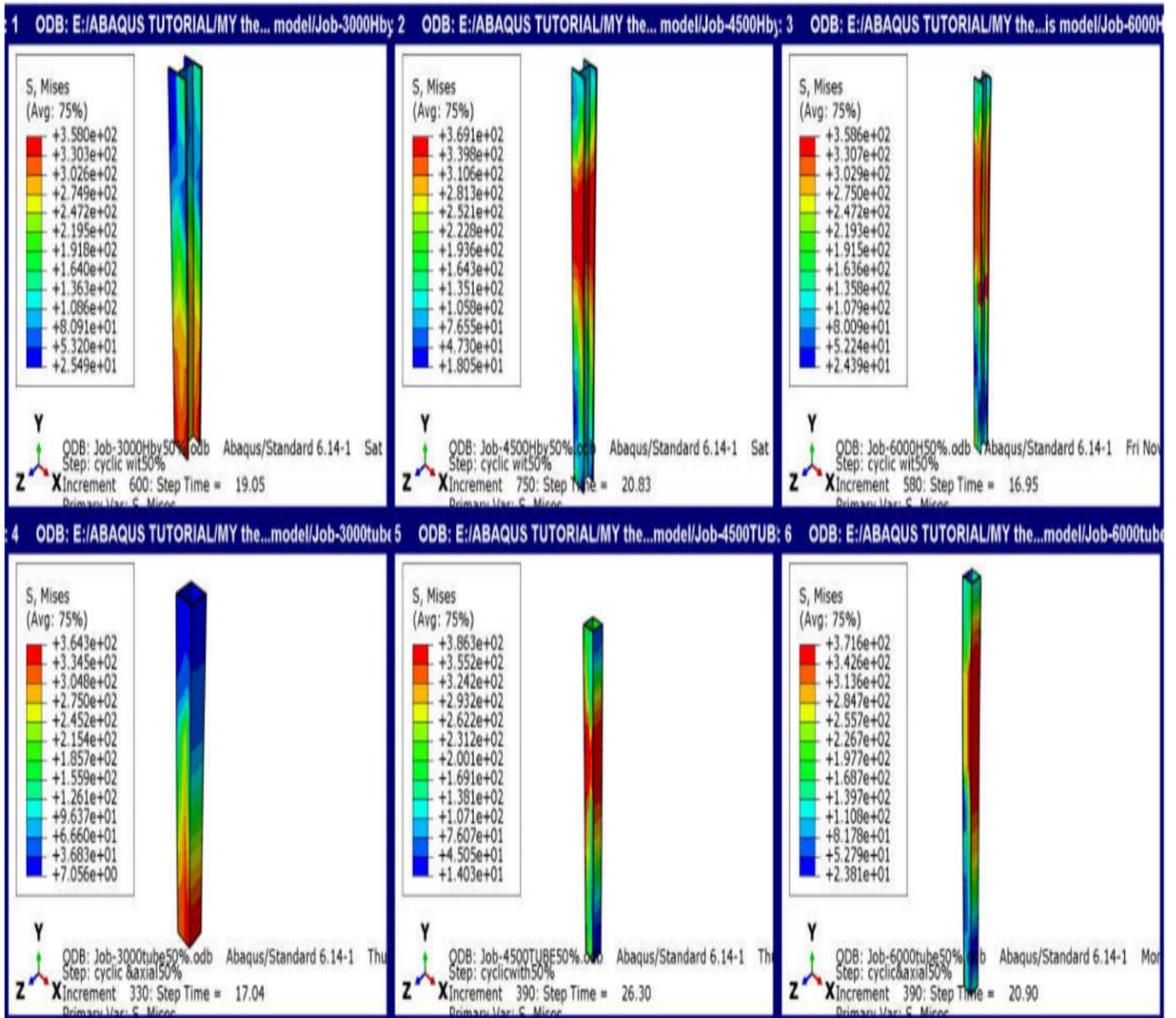


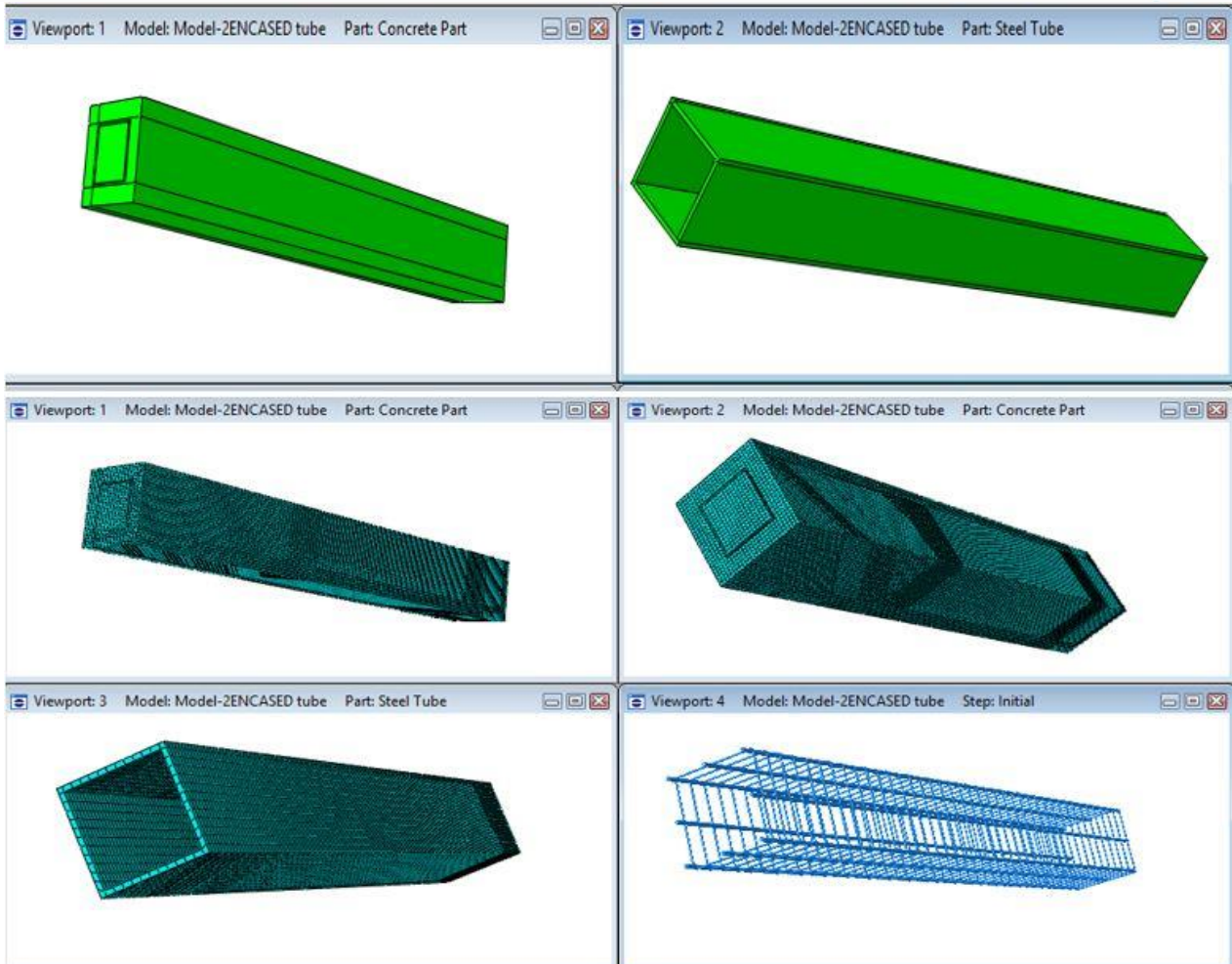
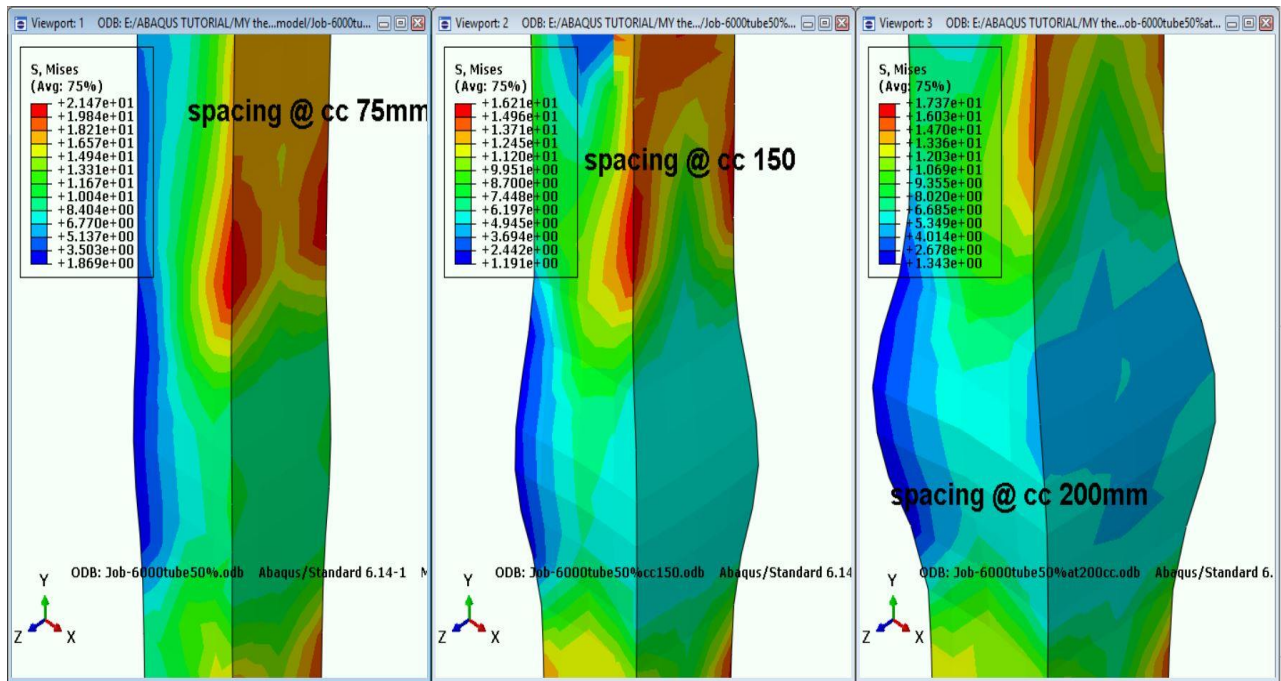


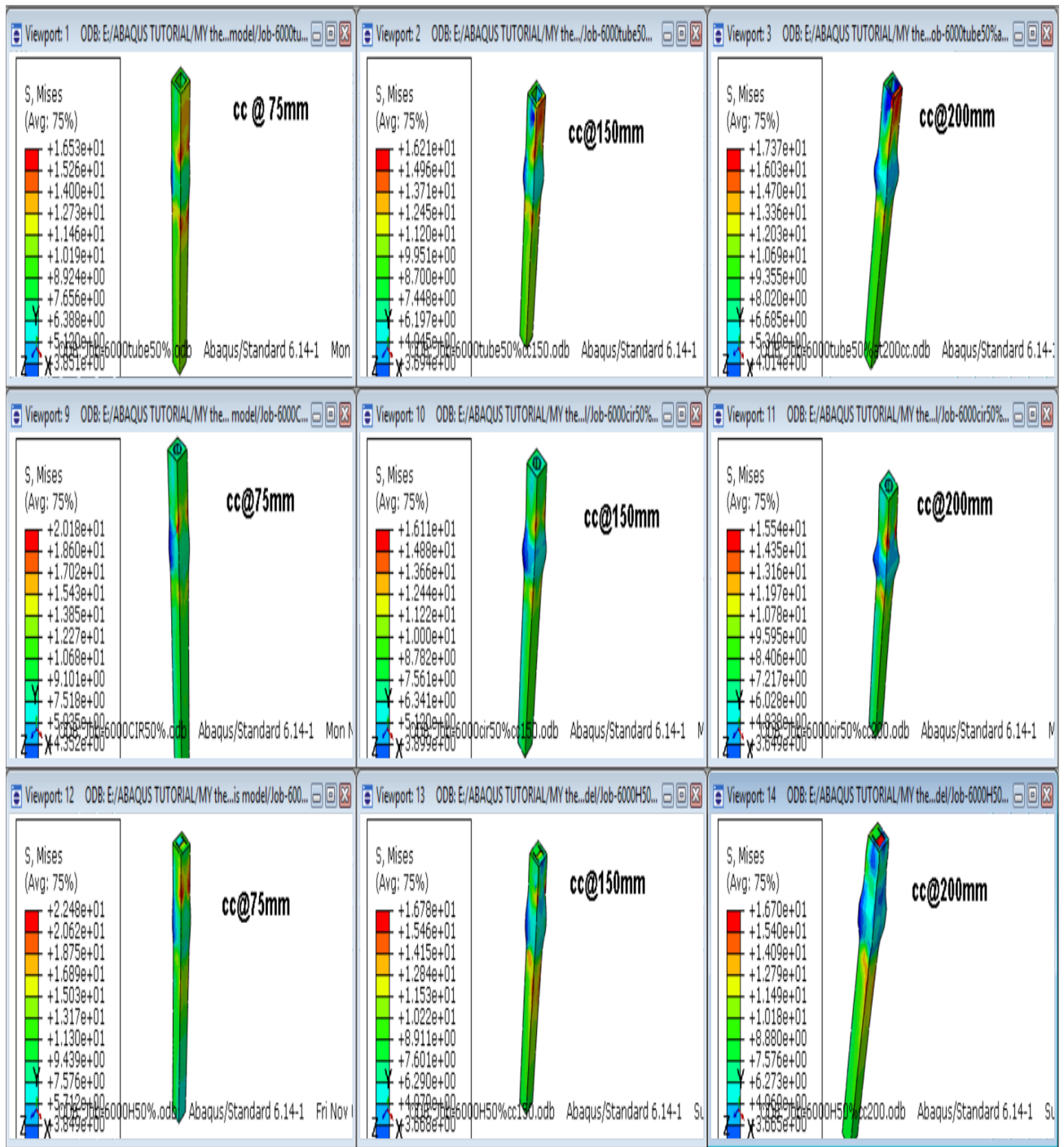
**D. OUT PUT OF ANALYSIS**











## E.ANALIYSIS OUT PUT FROM ABAQUS PROGRAM

Abaqus 6.14-1 Date 11-Nov-2019 Time 13:10:30  
For use by Supplied By SSQ under license from Dassault Systemes or its subsidiary.

The Abaqus Software is a product of:

Dassault Systemes Simulia Corp.  
Rising Sun Mills  
166 Valley Street  
Providence, RI 02909-2499, USA

The Abaqus Software is available only under license from Dassault Systemes or its subsidiary and may be used or reproduced only in accordance with the terms of such license.

On machine DESKTOP-ISBHC3V  
you are authorized to run  
Abaqus/Standard until 31-Dec-2055

Your site id is:

For assistance or any other information you may obtain contact information for your local office from the world wide web at:

<http://www.3ds.com/products/simulia/locations/>

```
*****
*
*          *****
*        * NOTICE *
*          *****
*
*          Abaqus 6.14-1
*
*        BUILD ID: 2014_06_04-15.11.02 134264
*
* Please make sure you are using release 6.14 manuals
* plus the notes accompanying this release.
*
*
*
*****
```

```
*Element, type=C3D8R
*Nset, nset="ASSEMBLY_outer concrete-1_outer conc set"
*Elset, elset="ASSEMBLY_outer concrete-1_outer conc set"
*Element, type=T3D2
*Nset, nset=ASSEMBLY_STTRUP-1-LIN-1-40-LIN-2-1__PICKEDSET3
*Elset, elset=ASSEMBLY_STTRUP-1-LIN-1-40-LIN-2-1__PICKEDSET3
*Element, type=T3D2
*Nset, nset=ASSEMBLY_STTRUP-1-LIN-1-40-LIN-3-1__PICKEDSET3
*Elset, elset=ASSEMBLY_STTRUP-1-LIN-1-40-LIN-3-1__PICKEDSET3
*Element, type=T3D2
*Nset, nset=ASSEMBLY_STTRUP-1-LIN-1-40-LIN-4-1__PICKEDSET3
*Elset, elset=ASSEMBLY_STTRUP-1-LIN-1-40-LIN-4-1__PICKEDSET3
*Element, type=T3D2
*Nset, nset=ASSEMBLY_STTRUP-1-LIN-1-40-LIN-5-1__PICKEDSET3
*Elset, elset=ASSEMBLY_STTRUP-1-LIN-1-40-LIN-5-1__PICKEDSET3
*Element, type=T3D2
*Nset, nset=ASSEMBLY_STTRUP-1-LIN-1-40-LIN-6-1__PICKEDSET3
*Elset, elset=ASSEMBLY_STTRUP-1-LIN-1-40-LIN-6-1__PICKEDSET3
*Element, type=T3D2
*Nset, nset=ASSEMBLY_STTRUP-1-LIN-1-40-LIN-7-1__PICKEDSET3
*Elset, elset=ASSEMBLY_STTRUP-1-LIN-1-40-LIN-7-1__PICKEDSET3
*Element, type=T3D2
*Nset, nset=ASSEMBLY_STTRUP-1-LIN-1-40-LIN-8-1__PICKEDSET3
*Elset, elset=ASSEMBLY_STTRUP-1-LIN-1-40-LIN-8-1__PICKEDSET3
*Element, type=T3D2
*Nset, nset=ASSEMBLY_STTRUP-1-LIN-1-40-LIN-9-1__PICKEDSET3
*Elset, elset=ASSEMBLY_STTRUP-1-LIN-1-40-LIN-9-1__PICKEDSET3
*Element, type=T3D2
*Nset, nset=ASSEMBLY_STTRUP-1-LIN-1-40-LIN-10-1__PICKEDSET3
*Elset, elset=ASSEMBLY_STTRUP-1-LIN-1-40-LIN-10-1__PICKEDSET3
*Element, type=T3D2
*Nset, nset=ASSEMBLY_STTRUP-1-LIN-1-40-LIN-11-1__PICKEDSET3
*Elset, elset=ASSEMBLY_STTRUP-1-LIN-1-40-LIN-11-1__PICKEDSET3
*Element, type=T3D2
*Nset, nset=ASSEMBLY_STTRUP-1-LIN-1-40-LIN-12-1__PICKEDSET3
*Elset, elset=ASSEMBLY_STTRUP-1-LIN-1-40-LIN-12-1__PICKEDSET3
*Element, type=T3D2
*Nset, nset=ASSEMBLY_STTRUP-1-LIN-1-40-LIN-13-1__PICKEDSET3
*Elset, elset=ASSEMBLY_STTRUP-1-LIN-1-40-LIN-13-1__PICKEDSET3
*Element, type=T3D2
*Nset, nset=ASSEMBLY_STTRUP-1-LIN-1-40-LIN-14-1__PICKEDSET3
*Elset, elset=ASSEMBLY_STTRUP-1-LIN-1-40-LIN-14-1__PICKEDSET3
*Element, type=T3D2
*Nset, nset=ASSEMBLY_STTRUP-1-LIN-1-40-LIN-15-1__PICKEDSET3
*Elset, elset=ASSEMBLY_STTRUP-1-LIN-1-40-LIN-15-1__PICKEDSET3
*Element, type=T3D2
*Nset, nset=ASSEMBLY_STTRUP-1-LIN-1-40-LIN-16-1__PICKEDSET3
*Elset, elset=ASSEMBLY_STTRUP-1-LIN-1-40-LIN-16-1__PICKEDSET3
```

PROBLEM SIZE

NUMBER OF ELEMENTS IS 7440  
NUMBER OF ELEMENTS DEFINED BY THE USER AND \*TIE 4880  
NUMBER OF INTERNAL ELEMENTS GENERATED FOR CONTACT 2560  
NUMBER OF NODES IS 11478  
NUMBER OF NODES DEFINED BY THE USER 6358  
NUMBER OF INTERNAL NODES GENERATED BY THE PROGRAM 5120  
TOTAL NUMBER OF VARIABLES IN THE MODEL 26964  
(DEGREES OF FREEDOM PLUS MAX NO. OF ANY LAGRANGE MULTIPLIER  
VARIABLES. INCLUDE \*PRINT,SOLVE=YES TO GET THE ACTUAL NUMBER.)

END OF USER INPUT PROCESSING

JOB TIME SUMMARY

USER TIME (SEC) = 1.4000  
SYSTEM TIME (SEC) = 0.40000  
TOTAL CPU TIME (SEC) = 1.8000  
WALLCLOCK TIME (SEC) = 5

Abaqus 6.14-1 Date 11-Nov-2019 Time 13:10:38  
For use by Supplied By SSQ under license from Dassault Systemes or its subsidiary.

STEP 1 INCREMENT 1  
TIME COMPLETED IN THIS STEP 0.00

STEP 1 STATIC ANALYSIS

AUTOMATIC TIME CONTROL WITH -

A SUGGESTED INITIAL TIME INCREMENT OF 5.000E-04  
AND A TOTAL TIME PERIOD OF 30.0  
THE MINIMUM TIME INCREMENT ALLOWED IS 2.000E-40  
THE MAXIMUM TIME INCREMENT ALLOWED IS 2.00

LINEAR EQUATION SOLVER TYPE DIRECT SPARSE

AUTOMATIC STABILIZATION WITH DAMPING FACTOR = 2.000E-04

LINEAR EQUATION SOLVER TYPE            DIRECT SPARSE  
 AUTOMATIC STABILIZATION WITH DAMPING FACTOR = 2.000E-04  
 LARGE DISPLACEMENT THEORY WILL BE USED  
 UNSYMMETRIC MATRIX STORAGE AND SOLUTION WILL BE USED

TOTAL MASS OF MODEL

2.809652

LOCATION OF THE CENTER OF MASS OF THE MODEL

-1.2789868E-13            -2999.815            1.0944929E-14

MOMENTS OF INERTIA ABOUT THE ORIGIN

I(XX)	I(YY)	I(ZZ)
3.3763849E+07	81470.82	3.3763770E+07

PRODUCTS OF INERTIA ABOUT THE ORIGIN

I(XY)	I(XZ)	I(YZ)
2.0097701E-11	1.8485213E-13	-3.7278625E-11

MOMENTS OF INERTIA ABOUT THE CENTER OF MASS

I(XX)	I(YY)	I(ZZ)
8480098.	81470.82	8480020.

PRODUCTS OF INERTIA ABOUT THE CENTER OF MASS

I(XY)	I(XZ)	I(YZ)
1.0980836E-09	1.8485213E-13	-1.2952727E-10

PRODUCTS OF INERTIA ABOUT THE CENTER OF MASS  
 I(XY)                      I(XZ)                      I(YZ)  
 1.0980836E-09            1.8485213E-13            -1.2952727E-10

M E M O R Y   E S T I M A T E

PROCESS	FLOATING PT OPERATIONS PER ITERATION	MINIMUM MEMORY REQUIRED (MB)	MEMORY TO MINIMIZE I/O (MB)
1	5.10E+009	26	160

NOTE:

- (1) SINCE ABAQUS DOES NOT PRE-ALLOCATE MEMORY AND ONLY ALLOCATES MEMORY AS NEEDED DURING THE ANALYSIS, THE MEMORY REQUIREMENT PRINTED HERE CAN ONLY BE VIEWED AS A GENERAL GUIDELINE BASED ON THE BEST KNOWLEDGE AVAILABLE AT THE BEGINNING OF A STEP BEFORE THE SOLUTION PROCESS HAS BEGUN.
- (2) THE ESTIMATE IS NORMALLY UPDATED AT THE BEGINNING OF EVERY STEP. IT IS THE MAXIMUM VALUE OF THE ESTIMATE FROM THE CURRENT STEP TO THE LAST STEP OF THE ANALYSIS, WITH UNSYMMETRIC SOLUTION TAKEN INTO ACCOUNT IF APPLICABLE.
- (3) SINCE THE ESTIMATE IS BASED ON THE ACTIVE DEGREES OF FREEDOM IN THE FIRST ITERATION OF THE CURRENT STEP, THE MEMORY ESTIMATE MIGHT BE SIGNIFICANTLY DIFFERENT THAN ACTUAL USAGE FOR PROBLEMS WITH SUBSTANTIAL CHANGES IN ACTIVE DEGREES OF FREEDOM BETWEEN STEPS (OR EVEN WITHIN THE SAME STEP). EXAMPLES ARE: PROBLEMS WITH SIGNIFICANT CONTACT CHANGES, PROBLEMS WITH MODEL CHANGE, PROBLEMS WITH BOTH STATIC STEP AND STEADY STATE DYNAMIC PROCEDURES WHERE ACOUSTIC ELEMENTS WILL ONLY BE ACTIVATED IN THE STEADY STATE DYNAMIC STEPS.
- (4) FOR MULTI-PROCESS EXECUTION, THE ESTIMATED VALUE OF FLOATING POINT OPERATIONS FOR EACH PROCESS IS BASED ON AN INITIAL SCHEDULING OF OPERATIONS AND MIGHT NOT REFLECT THE ACTUAL FLOATING POINT OPERATIONS COMPLETED ON EACH PROCESS. OPERATIONS ARE DYNAMICALLY BALANCED DURING EXECUTION, SO THE ACTUAL BALANCE OF OPERATIONS BETWEEN PROCESSES IS EXPECTED TO BE BETTER THAN THE ESTIMATE PRINTED HERE.
- (5) THE UPPER LIMIT OF MEMORY THAT CAN BE ALLOCATED BY ABAQUS WILL IN GENERAL DEPEND ON THE VALUE OF THE "MEMORY" PARAMETER AND THE AMOUNT OF PHYSICAL MEMORY AVAILABLE ON THE MACHINE. PLEASE SEE THE "ABAQUS ANALYSIS USER'S MANUAL" FOR MORE DETAILS. THE ACTUAL USAGE OF MEMORY AND OF DISK SPACE FOR SCRATCH DATA WILL DEPEND ON THIS UPPER LIMIT AS WELL AS THE MEMORY REQUIRED TO MINIMIZE I/O. IF THE MEMORY UPPER LIMIT IS GREATER THAN THE MEMORY REQUIRED TO MINIMIZE I/O, THEN THE ACTUAL MEMORY USAGE WILL BE CLOSE TO THE ESTIMATED "MEMORY TO MINIMIZE I/O" VALUE, AND THE SCRATCH DISK USAGE WILL BE CLOSE-TO-ZERO; OTHERWISE, THE ACTUAL MEMORY USED WILL BE CLOSE TO THE PREVIOUSLY MENTIONED MEMORY LIMIT, AND THE SCRATCH DISK USAGE WILL BE ROUGHLY PROPORTIONAL TO THE DIFFERENCE BETWEEN THE ESTIMATED "MEMORY TO MINIMIZE I/O" AND THE MEMORY UPPER LIMIT. HOWEVER ACCURATE ESTIMATE OF THE SCRATCH DISK SPACE IS NOT POSSIBLE.
- (6) USING "\*RESTART, WRITE" CAN GENERATE A LARGE AMOUNT OF DATA WRITTEN IN THE WORK DIRECTORY.

THE ANALYSIS HAS BEEN COMPLETED

---



Abaqus/Standard 6.14-1  
 SUMMARY OF JOB INFORMATION:  
 DATE 11-Nov-2019 TIME 13:10:50

STEP	INC	ATT	SEVERE DISCON ITERS	EQUIL ITERS	TOTAL ITERS	TOTAL TIME/ FREQ	STEP TIME/LPF	INC OF TIME/LPF	DOF MONITOR	IF RIKS
1	1	1	4	1	5	0.000500	0.000500	0.0005000		
1	2	1	3	0	3	0.00100	0.00100	0.0005000		
1	3	1	4	0	4	0.00175	0.00175	0.0007500		
1	4	1	3	0	3	0.00288	0.00288	0.001125		
1	5	1	3	0	3	0.00456	0.00456	0.001688		
1	6	1	3	0	3	0.00709	0.00709	0.002531		
1	7	1	3	1	4	0.0109	0.0109	0.003797		
1	8	1	3	0	3	0.0166	0.0166	0.005695		
1	9	1	2	1	3	0.0251	0.0251	0.008543		
1	10	1	4	0	4	0.0379	0.0379	0.01281		
1	11	1	3	0	3	0.0572	0.0572	0.01922		
1	12	1	3	0	3	0.0860	0.0860	0.02883		
1	13	1	3	0	3	0.129	0.129	0.04325		
1	14	1	3	0	3	0.194	0.194	0.06487		
1	15	1	3	1	4	0.291	0.291	0.09731		
1	16	1	3	0	3	0.437	0.437	0.1460		
1	17	1	4	1	5	0.656	0.656	0.2189		
1	18	1	3	1	4	0.985	0.985	0.3284		
1	19	1	7	0	7	1.48	1.48	0.4926		
1	20	1	8	1	9	2.22	2.22	0.7389		
1	21	1	8	0	8	3.32	3.32	1.108		
1	22	1U	9	0	9	3.32	3.32	1.663		
1	22	2	6	0	6	3.74	3.74	0.4157		
1	23	1	6	0	6	4.36	4.36	0.6235		
1	24	1	6	2	8	5.30	5.30	0.9352		
1	25	1	6	1	7	6.70	6.70	1.403		
1	26	1U	3	1	4	6.70	6.70	2.000		
1	26	2	6	1	7	7.20	7.20	0.5000		
1	27	1	5	1	6	7.95	7.95	0.7500		
1	28	1U	4	0	4	7.95	7.95	1.125		
1	28	2	4	1	5	8.23	8.23	0.2813		
1	29	1U	4	0	4	8.23	8.23	0.4219		
1	29	2U	4	0	4	8.23	8.23	0.1055		
1	29	3	5	2	7	8.26	8.26	0.02637		
1	30	1	13	1	14	8.30	8.30	0.03955		
1	31	1	1	1	2	8.33	8.33	0.02966		
1	32	1	2	1	3	8.36	8.36	0.02966		
1	33	1	3	0	3	8.40	8.40	0.04449		
1	34	1	3	0	3	8.47	8.47	0.06674		
1	35	1	2	1	3	8.57	8.57	0.1001		
1	36	1	5	0	5	8.72	8.72	0.1502		
1	37	1U	4	0	4	8.72	8.72	0.2253		
1	37	2	4	0	4	8.78	8.78	0.05631		
1	490	2	3	2	5	28.0	28.0	0.009806		
1	491	1	2	1	3	28.0	28.0	0.01471		
1	492	1	3	0	3	28.0	28.0	0.02206		
1	493	1	3	1	4	28.1	28.1	0.03309		
1	494	1	3	0	3	28.1	28.1	0.04964		
1	495	1	2	1	3	28.2	28.2	0.07446		
1	496	1	1	1	2	28.3	28.3	0.1117		
1	497	1	1	1	2	28.5	28.5	0.1675		
1	498	1	2	1	3	28.7	28.7	0.2513		
1	499	1	2	1	3	29.1	29.1	0.3770		
1	500	1	2	1	3	29.7	29.7	0.5655		
1	501	1	1	1	2	30.0	30.0	0.3269		

THE ANALYSIS HAS COMPLETED SUCCESSFULLY

1

Abaqus 6.14-1 Date 11-Nov-2019 Time 13:10:38  
 For use by Supplied By SSQ under license from Dassault Systemes or its subsidia

STEP 1 INCREMENT 1 STEP TIME 0.00

STEP 1 STATIC ANALYSIS

AUTOMATIC TIME CONTROL WITH -  
 A SUGGESTED INITIAL TIME INCREMENT OF 5.000E-04  
 AND A TOTAL TIME PERIOD OF 30.0  
 THE MINIMUM TIME INCREMENT ALLOWED IS 2.000E-40  
 THE MAXIMUM TIME INCREMENT ALLOWED IS 2.00

LINEAR EQUATION SOLVER TYPE DIRECT SPARSE

AUTOMATIC STABILIZATION WITH DAMPING FACTOR = 2.000E-04

I CONVERGENCE TOLERANCE PARAMETERS FOR FORCE

CRITERION FOR RESIDUAL FORCE FOR A NONLINEAR PROBLEM	5.000E-03
CRITERION FOR DISP. CORRECTION IN A NONLINEAR PROBLEM	1.000E-02
INITIAL VALUE OF TIME AVERAGE FORCE	1.000E-02
AVERAGE FORCE IS TIME AVERAGE FORCE	
ALTERNATE CRIT. FOR RESIDUAL FORCE FOR A NONLINEAR PROBLEM	2.000E-02
CRITERION FOR ZERO FORCE RELATIVE TO TIME AVRG. FORCE	1.000E-05
CRITERION FOR RESIDUAL FORCE WHEN THERE IS ZERO FLUX	1.000E-05
CRITERION FOR DISP. CORRECTION WHEN THERE IS ZERO FLUX	1.000E-03
CRITERION FOR RESIDUAL FORCE FOR A LINEAR INCREMENT	1.000E-08
FIELD CONVERSION RATIO	1.00
CRITERION FOR ZERO FORCE REL. TO TIME AVRG. MAX. FORCE	1.000E-05
CRITERION FOR ZERO DISP. RELATIVE TO CHARACTERISTIC LENGTH	1.000E-08

CONVERGENCE TOLERANCE PARAMETERS FOR MOMENT

CRITERION FOR RESIDUAL MOMENT FOR A NONLINEAR PROBLEM	5.000E-03
CRITERION FOR ROTATION CORRECTION IN A NONLINEAR PROBLEM	1.000E-02
INITIAL VALUE OF TIME AVERAGE MOMENT	1.000E-02
AVERAGE MOMENT IS TIME AVERAGE MOMENT	
ALTERNATE CRIT. FOR RESIDUAL MOMENT FOR A NONLINEAR PROBLEM	2.000E-02
CRITERION FOR ZERO MOMENT RELATIVE TO TIME AVRG. MOMENT	1.000E-05
CRITERION FOR RESIDUAL MOMENT WHEN THERE IS ZERO FLUX	1.000E-05
CRITERION FOR ROTATION CORRECTION WHEN THERE IS ZERO FLUX	1.000E-03

INCREMENT 1 STARTS. ATTEMPT NUMBER 1, TIME INCREMENT 5.000E-04

ASYNCHRONOUS TRACKING ELEMENT LOOP STARTED

INITIAL ELEMENT LOAD BALANCE

COMPUTE NODE	1	PROCESS	NUMBER OF ELEMENTS
		1	1024
		2	1040
		3	1024
		4	768
		5	1024
		6	768
		7	768
		8	1024

NUMBER OF EQUATIONS = 8286 NUMBER OF FLOATING PT. OPERATIONS = 5.10E+09

USING THE DIRECT SOLVER WITH 8 PROCESSORS

CHECK POINT START OF SOLVER

CHECK POINT END OF SOLVER

ELAPSED USER TIME (SEC) = 1.2000  
 ELAPSED SYSTEM TIME (SEC) = 0.10000  
 ELAPSED TOTAL CPU TIME (SEC) = 1.3000  
 ELAPSED WALLCLOCK TIME (SEC) = 0

ASYNCHRONOUS TRACKING ELEMENT LOOP STARTED

497 SEVERE DISCONTINUITIES OCCURRED DURING THIS ITERATION.  
 497 POINTS CHANGED FROM CLOSED TO OPEN

CONVERGENCE CHECKS FOR SEVERE DISCONTINUITY ITERATION 1

MAX. PENETRATION ERROR 160.753E-12 AT NODE OUTER CONCRETE-1.867 OF CONTACT  
 PAIR (ASSEMBLY\_INNER OF OUTRER CONC, ASSEMBLY\_OUTER OF TUB)  
 MAX. CONTACT FORCE ERROR -469.534 AT NODE OUTER CONCRETE-1.711 OF  
 CONTACT PAIR (ASSEMBLY\_INNER OF OUTRER CONC, ASSEMBLY\_OUTER OF TUB)  
 THE ESTIMATED CONTACT FORCE ERROR IS OUTSIDE OF CONVERGENCE TOLERANCES.

AVERAGE FORCE	3.48	TIME AVG. FORCE	3.48
LARGEST RESIDUAL FORCE	-790.	AT NODE	645 DOF 2

CONVERGENCE CHECKS FOR EQUILIBRIUM ITERATION 1

MAX. PENETRATION ERROR 51.9405E-12 AT NODE OUTER CONCRETE-1.640 OF CONTACT PAIR (ASSEMBLY\_INNER OF OUTRER CONC, ASSEMBLY\_OUTER OF TUB)  
 MAX. CONTACT FORCE ERROR 1.57537E-03 AT NODE OUTER CONCRETE-1.640 OF CONTACT PAIR (ASSEMBLY\_INNER OF OUTRER CONC, ASSEMBLY\_OUTER OF TUB)  
 THE CONTACT CONSTRAINTS HAVE CONVERGED.

AVERAGE FORCE	7.238E+03	TIME AVG. FORCE	6.854E+03
LARGEST RESIDUAL FORCE	7.338E-03	AT NODE	1405 DOF 2
INSTANCE: Steel Tube-1			
LARGEST INCREMENT OF DISP.	0.367	AT NODE	696 DOF 1
INSTANCE: outer concrete-1			
LARGEST CORRECTION TO DISP.	-2.978E-04	AT NODE	310 DOF 1
INSTANCE: outer concrete-1			
THE FORCE EQUILIBRIUM EQUATIONS HAVE CONVERGED			

AVERAGE MOMENT	0.00	TIME AVG. MOMENT	5.763E+05
		(FROM FORCE FIELD)	
LARGEST RESIDUAL MOMENT	-1.806E-02	AT NODE	1 DOF 6
INSTANCE:			
LARGEST INCREMENT OF ROTATION	2.279E-04	AT NODE	1 DOF 6
INSTANCE: {assembly node}			
LARGEST CORRECTION TO ROTATION	4.391E-11	AT NODE	1 DOF 6
INSTANCE: {assembly node}			
THERE IS ZERO MOMENT EVERYWHERE			

ITERATION SUMMARY FOR THE INCREMENT: 3 TOTAL ITERATIONS, OF WHICH  
 2 ARE SEVERE DISCONTINUITY ITERATIONS AND 1 ARE EQUILIBRIUM ITERATIONS.

TIME INCREMENT COMPLETED	0.565	FRACTION OF STEP COMPLETED	0.989
STEP TIME COMPLETED	29.7	TOTAL TIME COMPLETED	29.7

ASYNCHRONOUS OUTPUT DATABASE FRAME FLUSH STARTED

INCREMENT 501 STARTS. ATTEMPT NUMBER 1, TIME INCREMENT 0.327

ASYNCHRONOUS TRACKING ELEMENT LOOP STARTED

4 SEVERE DISCONTINUITIES OCCURRED DURING INCREMENT ATTEMPT INITIALIZATION.  
 4 POINTS CHANGED TO SLIPPING WITH NEGATIVE CPRESS

NUMBER OF EQUATIONS = 8286 NUMBER OF FLOATING PT. OPERATIONS = 3.24E+09

ASYNCHRONOUS TRACKING ELEMENT LOOP STARTED

40 SEVERE DISCONTINUITIES OCCURRED DURING THIS ITERATION.  
 22 POINTS CHANGED FROM OPEN TO CLOSED  
 8 POINTS CHANGED FROM CLOSED TO OPEN  
 10 POINTS CHANGED FROM SLIPPING TO STICKING

CONVERGENCE CHECKS FOR SEVERE DISCONTINUITY ITERATION 1

MAX. PENETRATION ERROR 269.363E-06 AT NODE OUTER CONCRETE-1.98 OF CONTACT PAIR (ASSEMBLY\_INNER OF OUTRER CONC, ASSEMBLY\_OUTER OF TUB)  
 MAX. CONTACT FORCE ERROR 4.08497E+03 AT NODE OUTER CONCRETE-1.98 OF CONTACT PAIR (ASSEMBLY\_INNER OF OUTRER CONC, ASSEMBLY\_OUTER OF TUB)  
 THE CONTACT CONSTRAINT ERRORS ARE WITHIN THE TOLERANCES.

AVERAGE FORCE	7.250E+03	TIME AVG. FORCE	6.854E+03
LARGEST RESIDUAL FORCE	-1.295E+03	AT NODE	1397 DOF 1
INSTANCE: Steel Tube-1			
LARGEST INCREMENT OF DISP.	0.367	AT NODE	696 DOF 1
INSTANCE: outer concrete-1			
LARGEST CORRECTION TO DISP.	-0.310	AT NODE	696 DOF 1
INSTANCE: outer concrete-1			
FORCE EQUILIBRIUM NOT ACHIEVED WITHIN TOLERANCE.			

AVERAGE MOMENT	0.00	TIME AVG. MOMENT	5.763E+05
		(FROM FORCE	FIELD)
LARGEST RESIDUAL MOMENT	-507.	AT NODE	1 DOF 6
INSTANCE:			
LARGEST INCREMENT OF ROTATION	2.279E-04	AT NODE	1 DOF 6
INSTANCE: {assembly node}			
LARGEST CORRECTION TO ROTATION	-1.936E-04	AT NODE	1 DOF 6
INSTANCE: {assembly node}			
THE MOMENT IS ZERO EVERYWHERE BUT THE MOMENT RESIDUAL OR THE ROTATION CORRECTION IS NON-ZERO			

NUMBER OF EQUATIONS = 8286 NUMBER OF FLOATING PT. OPERATIONS = 3.24E+09

USING THE DIRECT SOLVER WITH 8 PROCESSORS

CHECK POINT START OF SOLVER

CHECK POINT END OF SOLVER

ELAPSED USER TIME (SEC)	=	0.80000
ELAPSED SYSTEM TIME (SEC)	=	0.10000
ELAPSED TOTAL CPU TIME (SEC)	=	0.90000
ELAPSED WALLCLOCK TIME (SEC)	=	0

ASYNCHRONOUS TRACKING ELEMENT LOOP STARTED

CONVERGENCE CHECKS FOR EQUILIBRIUM ITERATION 1

THE CONTACT CONSTRAINTS HAVE CONVERGED.

AVERAGE FORCE	7.239E+03	TIME AVG. FORCE	6.855E+03
LARGEST RESIDUAL FORCE	-0.802	AT NODE	48 DOF 3
INSTANCE: outer concrete-1			
LARGEST INCREMENT OF DISP.	0.142	AT NODE	696 DOF 1
INSTANCE: outer concrete-1			
LARGEST CORRECTION TO DISP.	1.706E-03	AT NODE	277 DOF 1
INSTANCE: outer concrete-1			
ESTIMATE OF DISP. CORRECTION	8.172E-07		
FORCE EQUILIB. ACCEPTED BASED ON SMALL RESIDUAL AND ESTIMATED CORRECTION			
AVERAGE MOMENT	0.00	TIME AVG. MOMENT	5.764E+05
		(FROM FORCE FIELD)	
LARGEST RESIDUAL MOMENT	2.03	AT NODE	1 DOF 6
INSTANCE:			
LARGEST INCREMENT OF ROTATION	8.848E-05	AT NODE	1 DOF 6
INSTANCE: {assembly node}			
LARGEST CORRECTION TO ROTATION	-1.980E-08	AT NODE	1 DOF 6
INSTANCE: {assembly node}			
THERE IS ZERO MOMENT EVERYWHERE			

ITERATION SUMMARY FOR THE INCREMENT: 2 TOTAL ITERATIONS, OF WHICH  
1 ARE SEVERE DISCONTINUITY ITERATIONS AND 1 ARE EQUILIBRIUM ITERATIONS.

TIME INCREMENT COMPLETED	0.327	FRACTION OF STEP COMPLETED	1.00
STEP TIME COMPLETED	30.0	TOTAL TIME COMPLETED	30.0
MAX. PENETRATION ERROR 75.2279E-06 AT NODE OUTER CONCRETE-1.48 OF CONTACT PAIR (ASSEMBLY_INNER OF OUTRER CONC, ASSEMBLY_OUTER OF TUB)			
MAX. CONTACT FORCE ERROR 1.71176E+03 AT NODE OUTER CONCRETE-1.48 OF CONTACT PAIR (ASSEMBLY_INNER OF OUTRER CONC, ASSEMBLY_OUTER OF TUB)			
MAX. PENETRATION ERROR 3.30799E-09 AT NODE OUTER CONCRETE-1.661 OF CONTACT PAIR (ASSEMBLY_INNER OF OUTRER CONC, ASSEMBLY_OUTER OF TUB)			
MAX. CONTACT FORCE ERROR 100.105E-03 AT NODE OUTER CONCRETE-1.661 OF CONTACT PAIR (ASSEMBLY_INNER OF OUTRER CONC, ASSEMBLY_OUTER OF TUB)			

THE ANALYSIS HAS BEEN COMPLETED

ASYNCHRONOUS TRACKING ELEMENT LOOP STARTED

CONVERGENCE CHECKS FOR EQUILIBRIUM ITERATION 1

THE CONTACT CONSTRAINTS HAVE CONVERGED.

AVERAGE FORCE	7.239E+03	TIME AVG. FORCE	6.855E+03
LARGEST RESIDUAL FORCE	-0.802	AT NODE	48 DOF 3
INSTANCE: outer concrete-1			
LARGEST INCREMENT OF DISP.	0.142	AT NODE	696 DOF 1
INSTANCE: outer concrete-1			
LARGEST CORRECTION TO DISP.	1.706E-03	AT NODE	277 DOF 1
INSTANCE: outer concrete-1			
ESTIMATE OF DISP. CORRECTION	8.172E-07		
FORCE EQUILIB. ACCEPTED BASED ON SMALL RESIDUAL AND ESTIMATED CORRECTION			
AVERAGE MOMENT	0.00	TIME AVG. MOMENT	5.764E+05
		(FROM FORCE FIELD)	
LARGEST RESIDUAL MOMENT	2.03	AT NODE	1 DOF 6
INSTANCE:			
LARGEST INCREMENT OF ROTATION	8.848E-05	AT NODE	1 DOF 6
INSTANCE: {assembly node}			
LARGEST CORRECTION TO ROTATION	-1.980E-08	AT NODE	1 DOF 6
INSTANCE: {assembly node}			
THERE IS ZERO MOMENT EVERYWHERE			

ITERATION SUMMARY FOR THE INCREMENT: 2 TOTAL ITERATIONS, OF WHICH  
1 ARE SEVERE DISCONTINUITY ITERATIONS AND 1 ARE EQUILIBRIUM ITERATIONS.

TIME INCREMENT COMPLETED	0.327	FRACTION OF STEP COMPLETED	1.00
STEP TIME COMPLETED	30.0	TOTAL TIME COMPLETED	30.0
MAX. PENETRATION ERROR 75.2279E-06 AT NODE OUTER CONCRETE-1.48 OF CONTACT PAIR (ASSEMBLY_INNER OF OUTRER CONC,ASSEMBLY_OUTER OF TUB)			
MAX. CONTACT FORCE ERROR 1.71176E+03 AT NODE OUTER CONCRETE-1.48 OF CONTACT PAIR (ASSEMBLY_INNER OF OUTRER CONC,ASSEMBLY_OUTER OF TUB)			
MAX. PENETRATION ERROR 3.30799E-09 AT NODE OUTER CONCRETE-1.661 OF CONTACT PAIR (ASSEMBLY_INNER OF OUTRER CONC,ASSEMBLY_OUTER OF TUB)			
MAX. CONTACT FORCE ERROR 100.105E-03 AT NODE OUTER CONCRETE-1.661 OF CONTACT PAIR (ASSEMBLY_INNER OF OUTRER CONC,ASSEMBLY_OUTER OF TUB)			

THE ANALYSIS HAS BEEN COMPLETED